# Identification of Novel Small Molecules Targeting the Protease Activity of Separase

Doctoral thesis for obtaining the academic degree

Doctor of Natural Sciences (Dr. rer. nat.)

submitted by

Lars Henschke

at the

Universität Konstanz

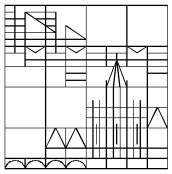

Faculty of Sciences

Department of Biology

Konstanz, 2022

Date of the oral examination: 24.03.2022

1. Reviewer: Prof. Dr. Thomas Mayer

2. Reviewer: Prof. Dr. Martin Scheffner

*This thesis is dedicated to*
*my grandma and my parents.*

# Table of Contents

# 1. Abstract

During early mitosis replicated chromosomes are entrapped by the ring-shaped protein complex cohesin. Separation of chromosomes in anaphase of mitosis is an essential step in cell division and is triggered by the large cysteine protease separase. Proteolytic cleavage of the Rad21 subunit of cohesin by separase resolves sister chromatid cohesion and initiates anaphase onset. Deregulated separase activity is associated with an abnormal number of chromosomes, termed aneuploidy, that is known to be a hallmark of most human cancers. In fact, separase is highly overexpressed in a number of solid cancers, making it an attractive chemotherapeutic target. In order to identify novel small molecules capable of inhibiting separase, we established a cell-based high-throughput assay with a known fluorescent activity probe to quantify separase activity in its complex cellular environment. Screening of 51 009 compounds for separase inhibitors identified 495 small molecules that efficiently reduced the cleavage of the separase sensor. Further *in vitro* assays confirmed that five of the identified compounds efficiently inhibited reconstituted separase, while not affecting caspase-1, a protease that is structurally related to separase. These five small molecules were named separase inhibiting compounds (SIC1-SIC5).

However, incubation of SICs with HeLa cells failed to induce any separase inhibition phenotypes seen in knockdown experiments. Titration of separase levels by RNAi revealed that minor amounts of separase in HeLa cells are sufficient for error-free chromosome separation during mitosis. Hence, small molecule inhibitors would have to bind nearly the entire pool of separase in cells to trigger segregation errors during mitotic exit. Cells with reduced separase levels displayed severe chromosome segregation defects upon treatment with SIC1, SIC3 and SIC5, confirming that the identified compounds are bioactive in cancer cells. Structure−activity relationship studies of the most potent and promising inhibitor SIC5 successfully yielded the optimized and more potent derivate SIC5-6.

Additionally we found that a truncation of the last three amino acids of the c-terminal end of separase results in the complete loss of catalytic activity *in vitro*.

Overall, this study demonstrates the feasibility of identifying separase-specific inhibitors, which serve as promising lead compounds for the development of clinically relevant separase inhibiting drugs.

# 2. Zusammenfassung

Während früher Mitose sind replizierte Chromosomen vom ringförmigen Proteinkomplex Cohesin umschlossen. Trennung der Chromosomen in Anaphase von Mitose ist ein essenzieller Schritt der Zellteilung und wird von der Cysteinprotease Separase eingeleitet. Die proteolytische Spaltung der Rad21-Untereinheit des Cohesinkomplexes löst die Schwesterchromatidkohäsion und initiiert den Beginn der Anaphase. Unregulierte Separaseaktivität ist mit abnormaler Chromosomenanzahl, sogenannte Aneuploidie, assoziiert und als Kennzeichen vieler humaner Krebsarten bekannt. Tatsächlich ist Separase in mehreren soliden Tumoren höchst überexprimiert, was es zu einem attraktiven chemotherapeutischen Target macht. Um neue niedermolekulare Verbindungen, sogenannte Small Molecules, zu identifizieren, welche in der Lage sind Separase zu inhibieren, haben wir einen zellbasierten Hochdurchsatz Assay etabliert, in welchem mit Hilfe eines fluoreszenten Sensors die Proteaseaktivität von Separase direkt in der komplexen zellulären Umgebung quantifiziert werden kann. Das Screening von 51 009 chemischen Verbindungen identifizierte 495 niedermolekulare Verbindungen, welche die Spaltung des Separasesensors stark reduzierte. Weitere Experimente *in vitro* bestätigten, dass fünf der identifizierten Verbindungen effizient rekonstituierte Separase inhibierten, jedoch keine Wirkung auf Caspase-1 zeigten, welche eine strukturähnliche Protease ist. Diese fünf Verbindungen wurden "Separase inhibierende Verbindungen" (engl. separase inhibiting compounds, SIC1-SIC5) genannt.

Allerdings blieb bei der Inkubation der SICs mit HeLa-Zellen der erwartete Phänotyp, wie er bei einer Separasedepletion zu sehen ist, aus. Die Titration der Separasemenge mittels RNAi zeigte, dass auch sehr geringe Mengen von Separase in HeLa-Zellen ausreichen um eine fehlerfreie Chromosomentrennung in Mitose zu ermöglichen. Folglich müssten die Inhibitoren fast an die gesamte Population von Separase in Zellen binden um Segregationsfehler am Ende der Mitose zu verursachen. Zellen mit einem reduzierten Separaselevel zeigten hingegen starke Fehler bei der Chromosomensegregation nach Behandlung mit SIC1, SIC3 und SIC5, was bestätigt, dass die identifizierten Verbindungen in Krebszellen aktiv sind. Struktur/Wirkungs-Beziehung des vielversprechendsten Inhibitors SIC5 führte zum verbesserten und potenteren Derivat SIC5-6.

Des Weiteren wurde entdeckt, dass eine Verkürzung um drei Aminosäuren am C-terminalen Ende von Separase zu einem vollständigen Aktivitätsverlust *in vitro* führt.

Zusammenfassend demonstriert diese Studie die erfolgreiche Identifizierung Separase-spezifischer Inhibitoren, welche als vielversprechende Leitstruktur für die Entwicklung von Separase-inhibierenden Medikamenten mit einer klinischen Relevanz dienen könnte.

# 3. Introduction

## 3.1 Small Molecule Inhibitors

### 3.1.1 Origins

Treatment of human deceases is in most cases based on pharmaceutical drugs - chemical small molecules. It is more than a century ago, that the groundbreaking discovery to use chemical compounds to treat human deceases has created a novel field of medicinal and biological research. Paul Ehrlich's idea that a chemical compound binds specifically to a cellular target originated in his early work in histology. Using chemical dyes to stain specific cellular tissues in a histological sample, based on the dye's chemical scaffold, inspired his theory about "magic bullets" that uses chemical compounds to target specific decease-causing bacteria while not affecting cells of the host (Kaufmann, 2008; Tan and Grimes, 2010). Paul Ehrlich collaborated with the chemist Alfred Bertheim, who synthesized a derivative library based on arsanilic acid and eventually yielded Salvarsan, a small molecule that was used against malaria and syphilis (Strebhardt and Ullrich, 2008; Williams, 2009). Over the last century the drug-based approach using small molecule "bullets" has vastly improved and has created the pharmaceutical industry, that develops with state of the art technology specific and effective drugs against most of present-day deceases and pathogens.

### 3.1.2 Application in Biological Research

But small molecules are not solely applied in medicinal treatments of deceases, they are additionally of great interest in basic research in molecular biology, where they supplement the molecular toolbox of scientists to allow easy manipulation of a molecular target, such as regulating enzyme activity, abolishing or initiating protein-protein interaction or even trigger the degradation of the target protein (Chen and Lampson, 2021; Schneider-Poetsch and Yoshida, 2018; Schreiber, 2019).

In order to answer a biological question, a common scientific approach is to remove a protein of interest (POI) by knockout or knockdown of the corresponding gene or create an excess of the POI by its overexpression and subsequently draw a conclusion based on the interpretation of the resulting phenotype (Chen and Lampson, 2021). Although this approach has allowed scientists in molecular biology to reveal complex regulatory and functional processes in biological systems and recent advances in genome editing using CRISPR/Cas has widened the available tools in this field of research, there are limitations to these classical methods such as temporal restrictions. For instance, the investigation of biological processes that only take a few

minutes but the efficient depletion of the involved POIs, using for instance RNA interference, takes time in the order of days and perturbs additional functions of the POI that can lead to artifacts which may mask the original phenotype (Chen and Lampson, 2021; O'Connor et al., 2011). A potent small molecule acts within minutes, allowing a high temporal control of the experimental setup and to specifically address an individual feature of a POI, e.g. with the chemical approach it is possible to target the enzymatic activity without affecting other non-catalytic protein-protein interactions or vice versa. The combination of multiple compounds in one experimental setup enables the manipulation of several targets via an easy and controllable method (Schreiber, 2019). For instance during investigation of rapid mitotic processes in cell cycle research, small molecule inhibitors are well-established to synchronize cells in specific phases (Teusel et al., 2018).

### 3.1.3 Characteristics of Small Molecule Compounds

In modern drug discovery a typical small molecule is defined with Lipinski's rule of five, which means it has a molecular weight of less than 500 Da, has not more than five hydrogen bond donors, has not more than 10 hydrogen bond acceptors and has a octanol-water partition coefficient of less than five. The rule of five was established by Christopher Lipinski and is a rule of thumb to crudely estimate the likeliness of a chemical compound to be suitable for oral administration and therefore how promising a potential drug candidate is for pharmaceutical drug development (Lipinski et al., 2001). This class of molecules is not an artificial creation of mankind because next to nature's huge macromolecules polysaccharides, nucleic acids, proteins or lipids, there are also naturally occurring small molecules that are indispensable for fully functional biological systems with their complex, dynamic and adaptive features that have evolved over time. The "central dogma of molecular biology" describes the transfer of information encoded on DNA via RNA to eventually form proteins as the functional effector of this information flux. But for a complete and comprehensive picture of our understanding of biological life, small molecules play an essential role in many molecular processes. They act as second messengers between proteins, as ligands to open or close transmembrane receptors, as energy transfer molecules, as intercellular signal molecules or they bind specific DNA sequences to upregulate or downregulate the transcription of a gene, just to name a few examples (Schneider-Poetsch and Yoshida, 2018; Schreiber, 2005). Hence, it is therefore not surprising that scientists have tried to mimic known small molecules to control biological processes or to find new chemical compounds - new magic bullets - to alter and control specific biological functions.

Using chemical compounds to study biological systems is a research field called chemical genetics and is based on the assumption that all proteins can be targeted by small molecules. An analysis to find potential targets in the human genome which are associated with deceases estimated in 2002 that about 500 genes are druggable by compounds (Hopkins and Groom, 2002). Compared to the total of 20 000 to 25 000 protein-coding genes, this number is very low but limited structural information of proteins and restriction of the analysis to genes with similarities to targets with known small molecule binding partners were responsible for this small estimation. More recent studies estimate an increased number of potential targets but still only predict a fraction of the entire protein-coding genes to be druggable (Finan et al., 2017). The assumption to be able to predict potential binding sites for new small molecules are probably the main reason for these low estimations.

### 3.1.4 Identification of New Small Molecules

The most established and conventional method to identify novel small molecules is via a high-throughput screen (HTS). Here, a vast number of chemical compounds, that covers as much chemical space as possible, is tested in a biological assay to eventually identify an active molecule that satisfies the expectations of the biological setup, for instance the inhibition of an enzymatic activity (O'Connor et al., 2011). One can compare this approach with the brute-force method to open a combination lock, where all possible combinations are tried until the lock eventually opens whereas in a HTS only a fraction of all possible combinations, which would be the entire chemical space, is tested, hence there is no guarantee to find the desired molecule - the magic bullet - for the biological question at hand. Therefor the quality of the compound library is vital and contributes hugely to the success of the HTS. The coverage of the chemical space is one aspect that is important when creating a diverse compound collection. The complete chemical space of carbon-based small molecules is estimated to contain $10^{60}$ molecules. Current HTS test between $10^5$ compounds in academia and more than $10^6$ compounds in pharmaceutical industry and although this number will most likely further increase in the following years, it still remains only an almost insignificantly tiny fraction of the chemical space and highlights that the quality of the compounds is far more important than the sheer size of the library (Dahlin and Walters, 2014; Dandapani et al., 2012; Kawasumi and Nghiem, 2007; O'Connor et al., 2011). Commercially available libraries are optimized and do not contain problematic compounds such as highly reactive small molecules that most likely would be unspecific and would yield false positive hits.

The classical genetic approach either starts with inducing a random mutation of a gene that results in the desired phenotype and subsequently this mutated gene is identified or one defined gene is mutated and the resulting phenotype offers conclusions about the biological context of this gene of interest. The first principle is called "forward genetics", where a hypothesis is generated based on the occurring phenotype and the second principle is called "reverse genetics", where a postulated hypothesis is validated by manipulating a known gene. In analogy to this, chemical genetics can be divided in a forward approach with a phenotype-based assay and subsequent identification of the molecular target and a reverse approach, where a small molecule compound for a defined target is to be found and in a subsequent validation the resulting phenotype can be observed (Kawasumi and Nghiem, 2007).

#### 3.1.4.1 Reverse Chemical Genetics

In the reverse screening setup the target protein is often purified and tested against the compound library in an *in vitro* setup to select compounds that modulate a specific feature of the POI. The readout is typically based on a fluorescent signal to allow fast and automated analysis, e.g. a fluorescent substrate that gains or loses intensity when being processed by the enzyme of interest or fluorescently labelled proteins of a multi-protein complex to quantify protein-protein interactions via FRET or fluorescence polarization techniques. To provide sufficient quantity of the purified protein in its native structural fold can be challenging, if the target is a complex multi-subunit protein complex or has unstable and aggregation-prone properties. Additionally it has to be considered, that in a reconstituted *in vitro* setting, which usually is not able to fully mimic the complex native environment of the target protein, the reverse approach can result in false positives or miss false negatives (Kawasumi and Nghiem, 2007; O'Connor et al., 2011; Stockwell, 2000). For validation of the identified compounds, a secondary assay determines if the identified small molecules are active in a different assay setup. Here, typically an orthogonal system is used to remove false positive hits, which in the primary assay rather targeted the assay setup than the POI, for instance a target-independent change in fluorescence intensity due to autofluorescence or a shift in pH that leads to aggregation of the POI. Cell-based secondary assays reveal if compounds are cell-permeable or are cytotoxic. Cell-based (reverse) HTS setups already select for non-toxic and cell-permeable compounds but also identify more false positive hits, since in cells compounds can also act upstream in the regulatory pathway of the POI instead of binding directly to the desired target. An orthogonal secondary assay with the purified POI is able to eliminate these false positive hits (Thorne et al., 2010).

### 3.1.4.2 Forward Chemical Genetics

In forward chemical genetics the primary assay is set up with a more complex biological system, usually a human cell line or a model organism such as yeast (*S. cerevisiae*), worms (*C. elegans*) or zebrafish is used and active compounds are selected by a specific but more global phenotype that is triggered, e.g. the arrest of cells in a particular cell cycle phase, induction or blocking of cell differentiation or initiation of apoptosis. Feasible readouts can be for instance a microscopy-based approach or a whole-cell immunodetection assay (cytoblot assay) (Stockwell et al., 1999). In a secondary assay the molecular target of the active compound has to be identified. A possible approach for this question is to covalently tether the active compound to a solid matrix, e.g. beads, and to analyze via mass spectrometry which proteins from a cell lysate bind to the lead compound. Further down the line, the suspected target protein can be validated by classical genetic approaches to reproduce the observed phenotype of the primary assay (Rix and Superti-Furga, 2009).

After the successful validation of the identified active small molecules, the chemical space around the lead compound is explored, which means a number of chemically similar derivatives are tested to improve the compounds potency. This will also reveal information about the structure-activity-relationship (SAR) of the identified molecule, i.e. which moieties of the compound are essential for its biological activity. Additionally, this allows to optimize properties such as specificity, cell-permeability or solubility (Dandapani et al., 2012).

## 3.2 Eukaryotic Cell Division Cycle

The perseverance of life depends on cell division. The fact that a new cell can only be created by duplication of an existing cell implicates that all life on earth - from single celled organisms to complex multi-cellular organisms such as mammals - has evolved from a single cell at the beginning of life on earth over three billion years ago (Theobald, 2010). Cells replicate in two major steps, by duplication of all cellular components and subsequent distribution to the two emerging daughter cells. Humans, as a multicellular species, evolve from a single fertilized egg through a vast number of cell divisions to a functional organism that consists of differentiated cell populations with individual and specific purpose and function and the mature adult body requires cell division to replenish dead cells (Morgan, 2007).

One of the most crucial objectives of eukaryotic cell division is to maintain the genetic stability of an organism or a species, i.e. assuring that the daughter cells have the identical genetic information as the mother cell. To realize that, first the genome is duplicated in S phase

(synthesis phase) and subsequently distributed in M phase (mitotic phase) to the two daughter cells (Figure 1). Additionally there are two gap phases, one before S phase (G1) and one before M phase (G2) where cells replenish other cell components such as mitochondria, cytosolic vesicles or nucleotides and prepare for the following cell cycle phase. To maintain a constant

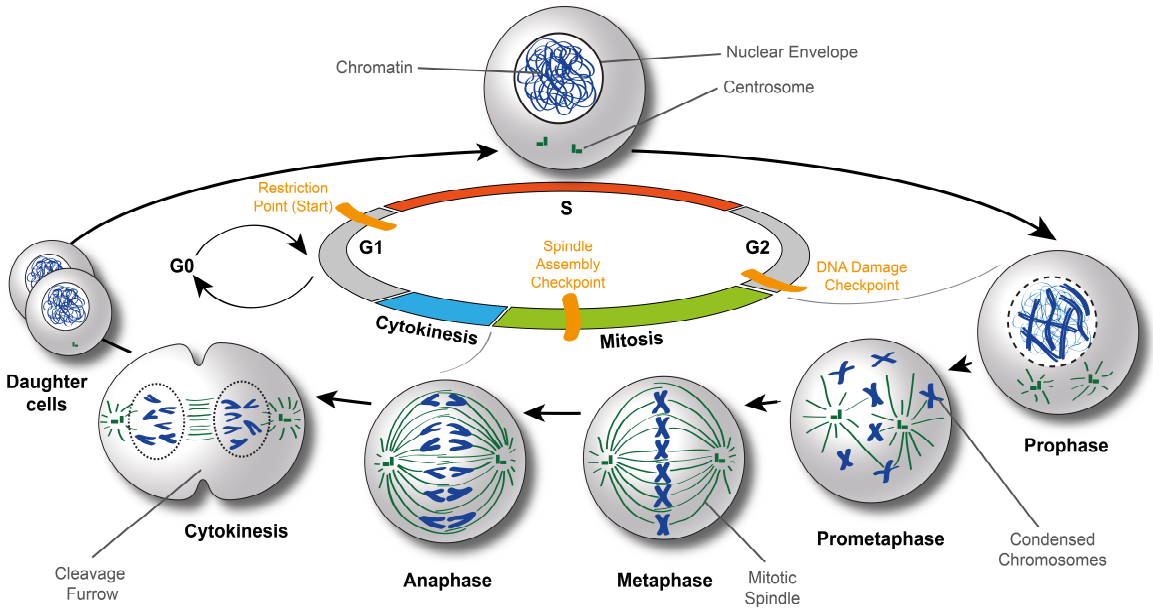


**Figure 1: The eukaryotic cell cycle.** The eukaryotic cell cycle is divided in G1 phase, S phase, G2 phase and M phase. In S phase the genome is duplicated and in M phase segregated in the emerging daughter cells. There are three cell cycle checkpoints: the restriction point, the DNA damage checkpoint and the spindle assembly checkpoint (all marked in orange). Mitosis is divided in Prophase, Prometaphase, Metaphase and Anaphase with subsequently is followed by cytokinesis. (Modified from Morgan, 2007)

cell size, cells have to grow during these gap phases as well. When cells stop to proliferate, they can exit the cell cycle and enter a senescent state (G0). G1, S and G2 phase are often collectively referred to as interphase and take up to 23 hours. M phase takes less than an hour and triggers major rearrangements of the cellular structure, which is a beautiful process that can be easily observed through a simple brightfield microscope. Based on these morphological changes, M phase can be further categorized in five mitotic stages. At mitotic entry, in *prophase*, DNA starts to be organized in condensed superstructures as chromosomes, where the two identical copies of each chromosome are paired together. The nuclear envelope is disassembled and allows the mitotic spindle to align the pairs of sister chromatids at the equatorial plain of the cell in *metaphase*. After all sister chromatids have been successfully aligned, the two sets of chromosomes are segregated to the opposite cell poles in *anaphase.* In *telophase* the mitotic spindle disassembles and the nuclear envelope reestablishes while the chromosomes decondense, which completes the nuclear division. During the following *cytokinesis* a contractile ring pinches off the two daughter cells and concludes M phase with two separate, independent and identical daughter cells (Morgan 2007; Molecular Biology of the Cell, 2015).

During this highly complex process there are a number of potential obstacles that have to be controlled to ensure an accurate cell duplication.

### 3.2.1 Unidirectionality of the Cell Cycle due to Cdk-Cyclin Complexes

An elaborate and sophisticated network of control mechanisms has evolved to monitor and drive cell cycle events to occur in the correct order. Compared with a mechanical watch, which due to its internal engineering and arrangement of gears in its clockwork only turns its clock hands in one direction, cells can also proceed only in one direction. One of the central elements of this cell cycle control system is a family of cyclin-dependent kinases (Cdks) that by phosphorylation changes the enzymatic activity, localization or the interactome of their substrates. The activity of these kinases is controlled by binding of specific regulatory proteins, so called cyclins, that activate the otherwise inactive Cdk subunit. The individual cyclins each catalyze the phosphorylation of specific cell cycle-dependent substrates and eventually trigger the expression of the following cyclin. The irreversible degradation of the cyclins by the Ubiquitin-Proteasome-System results in the oscillation of transient activity of the corresponding Cdk-Cyclin complexes and ensure the unidirectionality of events (Bardin and Amon, 2001; Morgan, 1997; Novak et al., 2007). In contrast to the watch analogy, cell cycle control does not proceed stubbornly in defined time intervals but instead still allows the cell, at crucial transition events, to wait until previous processes are completed or potential problems have been solved. These transition points are called checkpoints (Hartwell and Weinert, 1989).

### 3.2.2 Checkpoints Control Progression at Key Transition Events

There are three major checkpoints in eukaryotic cells that monitor the accurate cell cycle progression (Barnum and O'Connell, 2014). The first transition is the G1/S checkpoint or Start checkpoint. Only if internal and external conditions are optimal for proliferation, cells enter a new replication cycle. The G1/S checkpoint is a *point-of-no-return* after which cells commit to a full replication cycle and start with expressing G1/S and S phase cyclins that will initiate DNA replication. The subsequent G2/M checkpoint verifies that the replication is completed and the duplicated genome has no DNA damage. The third checkpoint is the spindle assembly checkpoint (SAC) (Musacchio, 2015), which verifies that at the end of metaphase all chromosomes are attached to the mitotic spindle and are aligned at the equatorial plain of the cell before sister chromatids are separated in anaphase. If the segregation of the sister

chromatids happens prematurely, the resulting daughter cells become aneuploid, i.e. become cells with an abnormal number of chromosomes, which is a hallmark of cancer.

### 3.2.3 Spindle Assembly Checkpoint (SAC)

As mentioned in a previous section, the beautiful process of chromosome alignment and segregation can be followed with a simple brightfield microscope. It can be observed that cells do not proceed to anaphase, while chromosomes are not aligned at the metaphase plate - even if it is only one single lagging chromosome. The resulting conclusion was the existence of a checkpoint with two features: a sensory mechanism that checks the alignment status of the chromosomes and an effector mechanism that halts the cell in metaphase until the sensory mechanism is satisfied (Musacchio, 2015). In order to correctly align all chromosomes at the metaphase plate, chromosomes have to be bi-polarly attached to the mitotic spindle, i.e. each sister chromatid is connected to the opposite spindle pole and monotelic or syntelic attachments have to be corrected. There is evidence that the sensory mechanism of the SAC is based on tension at the kinetochores, that is exclusively created in a bi-polar amphitelic attachment status (Chen et al., 2021). Aurora B is part of the chromosomal passenger complex (CPC), which is located at the inner part of the kinetochore. Among Aurora B's substrates is the Knl1-Mis12-Ndc80 complex (KMN network) on the outer part of the kinetochore. Here, CH domain phosphorylation of Ndc80 recruits the kinase Mps1, which subsequently phosphorylates MELT repeats (Met-Glu-Leu-Thr motif) on Knl1. These phosphorylated motifs on Knl1 act as assembly platforms for the mitotic checkpoint complex (MCC), which is the effector of the SAC and is composed of Mad2, Bub1, BubR1 and Cdc20. The incorporation of the APC/C coactivator Cdc20 in the MCC prevents the activation of the E3 ligase and consequently prevents anaphase onset. Upon bi-polar attachment, the kinetochore complex is stretched and Aurora B on the inner part of the kinetochore can no longer reach the KMN network on the outer part of the kinetochore, resulting in the inactivation of the SAC, the disassembly of the MCC and APC/C activation. The degradation of cyclin B and securin initiates anaphase onset (Lara-Gonzalez et al., 2012; Musacchio, 2015).

### 3.2.4 Chromosomal Organization of Genomic DNA

Segregation of the duplicated genome in mitosis is a complex task and requires the formation of condensed mitotic chromosomes. Stretched out to a single thread, the human genome has a length of more than 2 m. Hence, the error-free segregation of two copies of randomly packed

and intertwined sister DNA coils during M-phase is not possible and therefor the organization of the genetic information in condensed mitotic chromosomes is vital for a successful cell division in eukaryotic cells (Maeshima and Eltsov, 2008; Piovesan et al., 2019). However, additional to the organization of genomic DNA in tightly packed chromosomes, the close arrangement of the two sister chromatids that holds them together until they are separated in anaphase is a prerequisite for their alignment at the equatorial plain in metaphase. The mechanism behind this phenomenon is called cohesion.

### 3.2.5 Sister Chromatid Cohesion by Cohesin

Cohesion between sister chromatids is facilitated by the multi-subunit ring complex called cohesin, that physically embraces both sister DNA strands of a chromosome (Haarhuis et al., 2014). The ring complex consists of two structural maintenance of chromosomes subunits (Smc1 and Smc3) and a sister chromatid cohesin 1 subunit (Scc1; or Rad21 in humans) (Haering et al., 2008; Nasmyth and Haering, 2009). Smc1 and Smc3 are long, rod-shaped coiled-coil proteins that interact with each other at their hinge domain. C- and N-terminus form a head domain, which are ATPase domains that are similar to ATPase domains of ATP binding cassette transporters (ABC-like transporters). The kleisin subunit Rad21 interacts with the head domains of both Smc1 and Smc3, completing and closing the tripartite ring structure (Haarhuis et al., 2014).

#### 3.2.5.1 Loading of Cohesin onto DNA

Loading of cohesin to chromatin starts in telophase and is a steady-state of loading DNA into the ring structure and release of it (Figure 2). Although cohesin was shown to associate with naked DNA *in vitro* without the opening of the ring structure, the topological loading where cohesin physically encircles the DNA strand is catalyzed by the loading complex Scc2-Scc4 (Gutierrez-Escribano et al., 2019; Kanke et al., 2016). DNA is loaded through the interphase between Smc1 and Smc3 at their hinge domain and requires ATP hydrolysis (Gruber et al., 2006). The antagonist of this process is Wapl, a cohesin binding protein that opens the interphase between Scc1 and Rad21 allowing the release of the ring complex from DNA (Huis in 't Veld et al., 2014). This equilibrium of loading and release comes to a halt when Smc3 is acetylated at the ATPase domain via the acetyltransferases Eco1/2 starting in S-phase. Acetylated Smc3 then recruits Sororin, another cohesin binding protein, which prevents Wapl

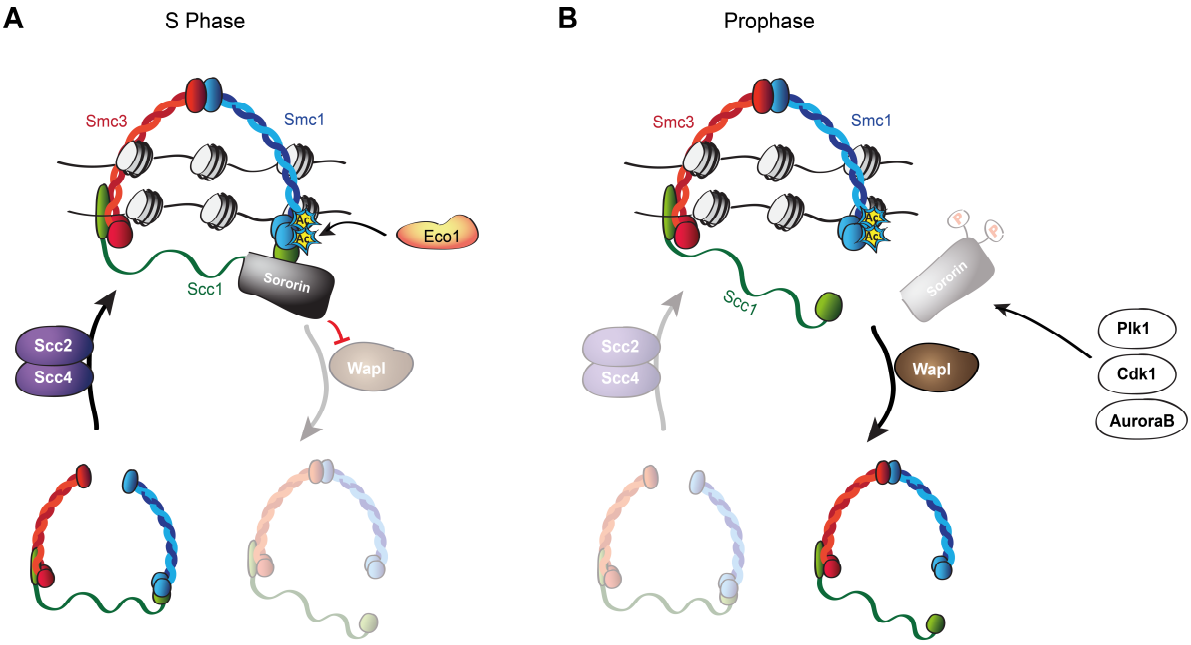


**Figure 2: Cycle of DNA Entrapment and Release by Cohesin Ring. (A)** The loading onto DNA is stabilized, when Eco1 acetylates Smc3, this allows the recruitment of Sororin, which locks cohesin in a closed state and is insensitive to Wapl.**(B)** In Prophase, cohesin rings start to be unlocked along chromosome arms. This process begins by phosphorylation of Sororin, which leads to dissociation of Sororin from cohesin and allows Wapl to bind and open the exit gate. (Modified from Haarhuis et al., 2014)

from binding and as a consequence confines cohesin in a DNA-loaded state (Figure 2A). Since the involved acetyltransferase has been shown to bind multiple factors of the DNA replication machinery, it offers speculations on the regulation of co-entrapping specifically sister DNA strands, however this process is still not fully understood (Chan et al., 2012; Haarhuis et al., 2014).

### 3.2.5.2 Cohesin Removal

At the entry into mitosis the majority of cohesin rings are locked in a DNA-entrapping conformation, resulting in sister chromatids that are cohesed along the entire length of their arms. The mode of cohesin removal from chromosomes is a two-step process that occurs consecutively (Figure 2B). First, during the so-called prophase pathway, mitotic phosphorylation of Sororin via Cdk1, Plk1 or Aurora B leads to dissociation of Sororin from Smc3 that again allows Wapl to bind and open cohesin. At the kinetochores, these mitotic phosphorylations on Sororin are locally antagonized by the phosphatase PP2A-B56, that protects the centromeric pool of cohesin from the prophase pathway and results in the typical X-shape of late mitotic chromosomes. At the end of metaphase, the remaining centromeric

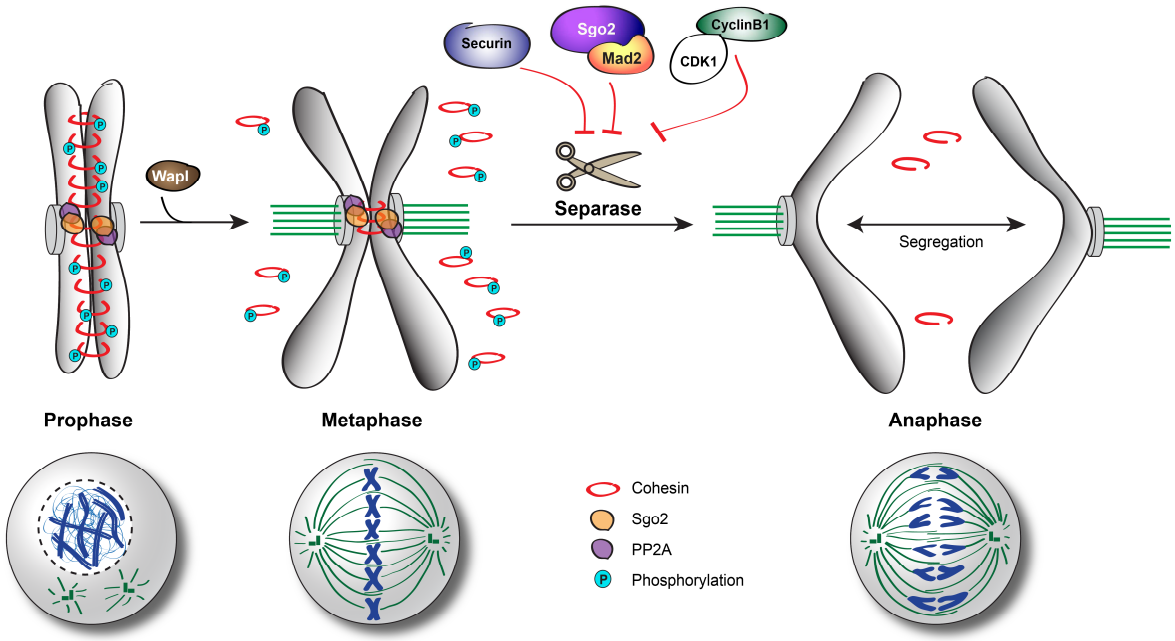


**Figure 3: Cohesin's two-step removal from chromosomes.** Cohesin stably co-entrap the sister chromatids from G2 until the entry of mitosis. Then phosphorylation by Cdk1, Plk1 and AuroraB allows Wapl to remove cohesin from chromosome arms. The centromeric population of cohesin is protected by Sgo2, which recruits PP2A that counteracts the phosphorylation and keeps centromeric cohesin in a locked state. The second step of cohesin removal is removed by separase which proteolytically cleaves the Rad21 subunit of cohesin. Until Anaphase onset, separase is inhibited by binding of Securin, Cdk1-cyclin B1 and Sgo2-Mad2. After all chromosomes are aligned, securin and cyclin B are degraded and Sgo2-Mad2 is removed from separase, activating the final trigger of anaphase, which leads to chromosome segregation. (modified from Haarhuis et al., 2014)

population of cohesin is removed in a final wave via a proteolytic cleavage of the Rad21 subunit causing the complete separation of all sister chromatids and triggers anaphase onset. The enzyme that catalyzes this process is separase (Buheitel and Stemmann, 2013; Haarhuis et al., 2014; Waizenegger et al., 2000).

## 3.3 Separase

### 3.3.1 Structure

More than two decades ago, the enzyme that cleaves the cohesin ring at metaphase to anaphase transition was first identified in yeast (Ciosk et al., 1998) and one year later Uhlmann and colleagues identified the human ortholog - Separase (Uhlmann et al., 1999). Separase is a cysteine protease with a size of 2120 amino acids of the human ortholog. Due to its aggregation-prone nature, obtaining high-resolution structural information was a great challenge. Based on low-resolution electron microscopy data and the combination with computational modelling of known crystal structures of proteins with similar sequence domains, the first structural model was proposed. This triangular, bi-lobal whale-shaped model consisted of an N-terminal tail and

trunk domain and a C-terminal head domain. Tail and trunk segments contain several superhelical Armadillo (ARM)/HEAT repeats and are connected to the catalytic head domain via an unstructured region. The catalytic head domain consists of two protease domains, an active protease fold and an inactive pseudo protease fold, that both share similarities with caspases. (Viadiu et al., 2005; Winter et al., 2015). In 2016, the first high-resolution crystal structure of the protease domain of separase from the fungus *Chaetomium thermophilum* was solved (Lin et al., 2016). High-resolution structural information from *S. cerevisiae* (yeast), *C. elegans* and finally human separase followed (Boland et al., 2017; Luo and Tong, 2017; Yu et al., 2021). Whereas the the N-terminal domain is highly variable in sequence and length across

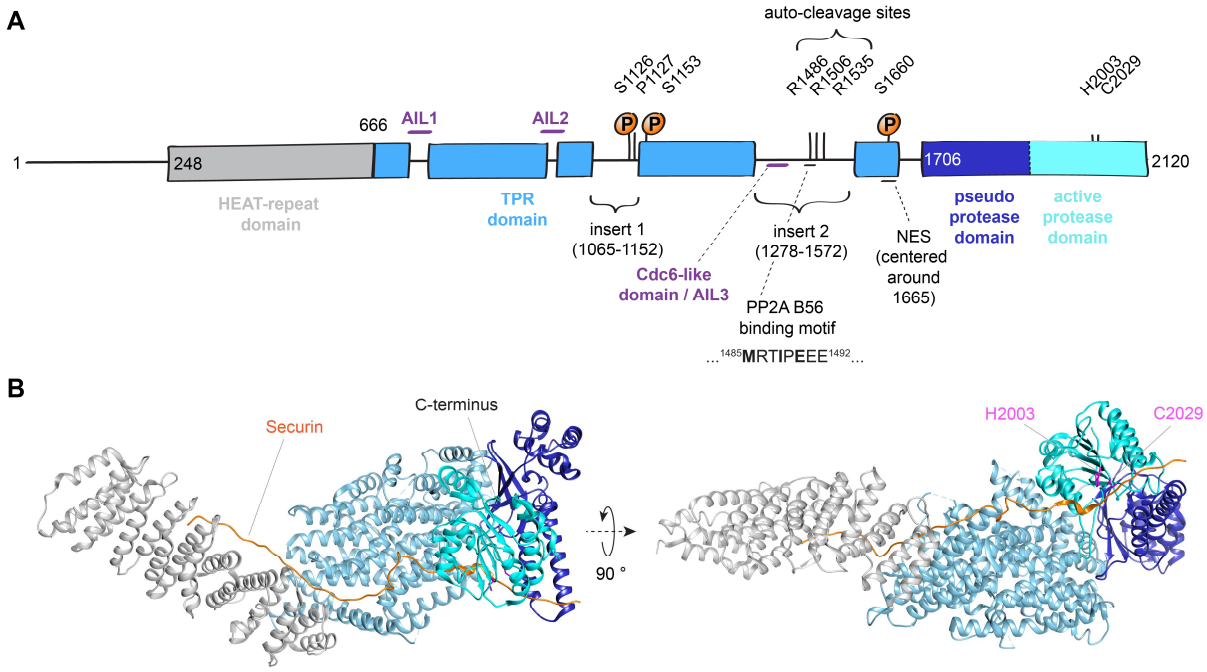


**Figure 4: Domain organization of humans separase. (A)** Diagram of human separase, with structured regions as blocks and flexible loop regions as solid line (insert 1 & insert 2). Labelled are a selection of phosphorylations sites that are essential for this study and further features for regulation and catalytic activity of the protease. **(B)** Two views of the overall structure of the human separase-securin complex (PDB file 7NJ1); the separase domains are colored as in (A)

species, the C-terminal protease domain shows some sequence conservation and houses the active site cysteine and histidine of the catalytic dyad (Figure 4). Separase substrates are cleaved after an arginine with the minimal consensus motif ExxR (Hauf et al., 2001; Uhlmann et al., 1999; Uhlmann et al., 2000). The motif was extended to have an acidic or phosphorylated residue two positions upstream of the ExxR (Alexandru et al., 2001; Hauf et al., 2005; Hauf et al., 2001; Lin et al., 2016) and an additional LPE motif, which is located downstream of the cleavage site of separase substrates (Rosen et al., 2019). Because there is still only a hand full

of substrates known, additional and more complex substrate binding motifs have not been identified.

### 3.3.2 Known Functions of Separase

Besides its essential function in chromosome segregation in mitosis and meiosis where separase cleaves the mitotic kleisin subunit Rad21/Scc1/Mcd1 or the meiotic homolog Rec8, the protease is also involved in a number of other segregation independent processes. It has been shown that separase activity is required for DNA damage repair in yeast and is activated in human cells in interphase to locally remove cohesin from DNA and to facilitate homology directed repair of double-strand breaks (Hellmuth et al., 2018; McAleenan et al., 2013; Nagao et al., 2004). Separase is also involved in the regulation of the centriole duplication cycle. Centrosomes, the main microtubule organization centers with centrioles at their core, have to duplicate with each cell division to maintain the constant number of two in each cell. During the licensing step of centriole duplication, separase cleaves pericentrin B and centrosomal cohesin to enable centriole disengagement (Lee and Rhee, 2012; Matsuo et al., 2012; Nakamura et al., 2009; Schockel et al., 2011; Tsou et al., 2009). Most recently it was shown that separase is able to cleave phosphorylated Mcl-1, an anti-apoptotic protein at the mitochondrial outer membrane (MOM) that is turned into a pro-apoptotic factor upon cleavage by separase and results in pore formation in the MOM. Because Mcl-1 is dephosphorylated until anaphase onset, this mechanism is thought to be a failsafe mechanism for premature separase activation that kills cells with an insufficient separase regulation (Hellmuth and Stemmann, 2020).

Other functional roles of separase include the cleavage of Meikin, a meiosis-specific kinetochore protein that is involved in proper chromosome alignment during meiosis II (Maier et al., 2021), membrane trafficking and cytokinesis in *C. elegans* where separase is recruited to vesicle membranes of meiosis specific cortical granules (Bai and Bembenek, 2017; Bembenek et al., 2007; Bembenek et al., 2010), spindle organization in yeast late mitosis, where cleavage of Slk19 stabilizes the anaphase spindle (Sullivan et al., 2001), inhibition of PP2A by directly binding to the Cdc55 regulatory subunit in yeast and initiating mitotic exit (Queralt et al., 2006) and the inhibition of the Cdk1-cyclinB1-Cks1 complex via inhibitory binding (Gorr et al., 2005; Yu et al., 2021) which will be explained in more detail in chapter 1.3.3.2 as this interaction is essential for separase regulation as well.

### 3.3.3 Regulation of Separase Activity

Proteolytic cleavage of the cohesin ring is irreversible and therefor has to be tightly regulated since premature chromosome separation has catastrophic consequences. To keep separase in check, three currently known regulatory mechanisms have evolved over time to establish redundancy for this crucial inhibition: inhibitory binding of securin, inhibitory binding of Cdk1-cyclinB1-Cks1 and inhibitory binding of the Shugoshin2-Mad2 complex (Figure 3).

#### 3.3.3.1 Inhibition by Securin

Until anaphase onset, separase is inhibited by securin, that binds separase in an extended and antiparallel manner to both C- and N-terminal domains of the protease. Securin associates already to nascent separase and is thought to be an inhibitory chaperone because securin-free separase was shown to be more aggregation-prone than securin-bound separase (Boland et al., 2017; Hellmuth et al., 2015a; Luo and Tong, 2017). Securin is an intrinsically disordered protein and is assumed to be mutually stabilized by binding to separase (Csizmok et al., 2008; Sanchez-Puig et al., 2005). Besides the role as a chaperone, securin inhibits separase via a pseudo substrate motif (in human $^{113}$EI**E**KF**F**$^{118}$) that resembles the minimal consensus motif with a hydrophobic Phe118 at the P1 position and as a consequence cannot be cleaved. Mutation of this hydrophobic site to an arginine, turns securin into a cleavable substrate (Lin et al., 2016; Nagao and Yanagida, 2006). The LPE motif ($^{130}$LPE$^{132}$) and the NXLXΦE motif ($^{121}$NPLDFE$^{126}$) are two additional binding motifs that were identified on securin that can also be found on substrates and hence perturb substrate binding to the protease (Yu et al., 2021). At anaphase onset, securin is targeted to the APC/C by its N-terminal KEN- and D-box and subsequently degraded via the proteasome, which is assumed to peel off securin from separase (Ciosk et al., 1998; Kumada et al., 1998; Zou et al., 1999). Non-separase associated securin was found to be degraded earlier than separase-associated securin (Shindo et al., 2012). This preference is due to phosphorylation at Ser31, Thr66, Ser87 and Ser89, which turns phosphorylated securin into a better substrate for the APC/C. PP2A-B56 is the counteracting phosphatase that, recruited to separase, keeps separase-bound securin dephosphorylated as a hyperphosphorylation of these four Ser/Thr sites was observed when binding of PP2A to separase was abolished (Hellmuth et al., 2014).

### 3.3.3.2 Regulation by Cdk1-Cycblin B1-Cks1

Although the major inhibitory regulation of separase is mediated by securin, it was shown that yeast cells still segregate their sister chromatids with normal kinetics in the absence of securin (Alexandru et al., 1999). The fact that human HCT116 cells with securin knocked out, even when arrested in metaphase, do not show a premature loss of sister chromatid cohesion (Jallepalli et al., 2001) and securin knockout mice are viable (Mei et al., 2001; Wang et al., 2001) strongly suggested additional inhibitory regulatory mechanisms towards separase. And indeed, it was first shown in *Xenopus laevis* egg extract that non-degradable cyclin B1, that was expected to block meiotic exit, additionally abolished sister chromatid separation at high concentrations through inhibition of separase activity. This inhibitory binding is dependent on the kinase activity of Cdk1 and the phosphorylation of Ser1126, Thr1346 and Ser1399 (Boos et al., 2008; Gorr et al., 2005; Stemmann et al., 2001). In the same way as securin, this inhibition is removed at anaphase onset by APC/C-mediated ubiquitination and proteasomal degradation of cyclinB1.

The cunning molecular mechanism behind this regulation was recently described in great detail by the group of Andreas Boland (Yu et al., 2021). In human cells, the binding of the Cdk1-Cyclin B1-Cks1 (CCC) complex is dependent on phosphorylation of Ser1126, which is phosphorylated by Cdk1. In contrast to securin, that itself harbors at least three critical binding motifs in its sequence, the binding of the CCC complex, leads to structural rearrangements in separase that then allows three auto-inhibitory loops (AIL1-3) of separase to block crucial substrate binding pockets in a similar fashion as securin does. Residues Ser1396 and Asn1394 bind in a reverse orientation to the P6 and P4 position at the catalytic pocket. Additionally the $^{715}$NDLNYE$^{720}$ motif on AIL1, that matches the NXLXΦE motif of Rad21 and securin, binds to the same cleft between the TPR-like domain and the protease domain on separase as securin does. AIL2 binds to a small hydrophobic channel of separase, which on securin binds C-terminal to the LPE motif. The LPE-motif binding site is not occupied in CCC complex bound state. Because the inhibition by securin and the CCC complex result in the occupation of the same binding sites on separase, their mode of action is mutually exclusive, which means that CCC can only associate with separase after securin has been removed.

Interestingly, the association of the CCC complex with separase leads to its own inhibition (Gorr et al., 2005). Cdc6 is an ATPase that was shown to inhibit Cdk1 (Bueno and Russell, 1992). The AIL3 of separase harbors a Cdc6-like domain (CLD), that binds to Cdk1 of the CCC complex and inhibits the kinase activity. Phosphorylated Ser1126 on AIL3 binds to a phosphate binding site on cyclin B1 and mutation of Ser1126 to alanine (named separase$^{PM2}$) abolishes Cdk1-cyclin B1-mediated inhibition of separase (Boos et al., 2008; Gorr et al., 2005; Yu et al., 2021).

Overexpression of separase$^{PM2}$ in HeLa cells leads to premature sister chromatid separation (Holland and Taylor, 2006) whereas in mouse embryonic stem cells, where one allele was mutated (separase$^{+/S1121A}$), only a minor premature activation was observed after a prolonged prometaphase arrest (Huang et al., 2005). The regulation of separase by the CCC complex is therefore thought to inhibit the exceeding pool of separase that cannot be covered by securin.

#### 3.3.3.3 Separase Self-Cleavage

Besides the already mentioned substrates of this protease, separase also cleaves itself. Human separase has three auto-cleavage sites (Arg1486, Arg1506 and Arg1535) and only mutation of all three residues to alanine abolishes self-cleavage. Although all three sites are conserved in vertebrates, they are not essential for catalytic activity, since mutation of all three sites still allows cleavage of Rad21 *in vitro* (Chestukhin et al., 2003; Waizenegger et al., 2002; Zou et al., 2002). The majority of this auto-cleavage process happens intramolecular due to the fact that ectopic co-expression of catalytic inactive separase$^{CS}$, where the active site cysteine was mutated to a serine, together with ectopic separase$^{WT}$ in HEK293 cells mainly resulted in cleavage of ectopic separase$^{WT}$ and barely showed any cleavage fragments of ectopic separase$^{CS}$ (Zou et al., 2002). All cleavage sites are located on an unstructured loop in the TPR-like domain (insert 2), which is long enough to fold back and reach the catalytic site to allow an intramolecular cleavage (Boland et al., 2017; Yu et al., 2021). The two resulting fragments stay stably associated with each other and do not show a reduction of the proteolytic activity *in vitro* (Boland et al., 2017; Zou et al., 2002). However, human HCT116 cells with five of the six cleavage sites (considering both alleles) mutated, showed a delay in G2/M transition and problems with bipolar chromosome alignment (Papi et al., 2005). Auto-cleavage of separase abrogates its association with PP2A, which binds to a 55 amino acid long stretch directly N-terminal to the self-cleavage sites and to a short linear PP2A-B56 binding motif directly at the second auto-cleavage site (Hertz et al., 2016; Holland et al., 2007). However, it still remains elusive how this primarily intramolecular self-cleavage positively contributes to cell cycle progression in G2 and M phase.

#### 1.3.3.4 Additional Regulatory Mechanisms

In studies with double mutant separase variants, that cannot be maintained by securin or the CCC complex, the protease was only prematurely activated after a prolonged mitotic arrest and in contrast was not prematurely activated in interphase cells (Huang et al., 2005). This hint for

an additional regulatory mechanism motivated Stemmann and colleagues to identify the inhibitory Shugoshin2-Mad2 complex (Hellmuth et al., 2020). It was shown that Shugoshin2 can be co-immunoprecipitated with separase from HeLa, Hek293 and HCT116 cells and the Shugoshin2-associated separase population is greater than pool of separase-CCC complex in prometaphase-arrested cells. Shugoshin2, like securin, has a pseudosubstrate motif that, when mutated, can be cleaved by active separase. This motif is thought to bind to the catalytic site but the lack of structural information for this complex makes this regulatory mechanism an interesting topic for current research.

The phospho-specific peptidyl prolyl cis/trans isomerase Pin1 converts *trans*-separase at the $^{1126}$SP$^{1127}$ peptide bond into its *cis*-isomer (Hellmuth et al., 2015b). This isomerization happens exclusively to securin-free separase and is dependent on phosphorylation of Ser1126 and Ser1153. The resulting *cis*-isoform is resistant against securin rebinding and has been shown in HeLa cells to be a prerequisite for binding to cyclin B1 (Hellmuth et al., 2015b). However, in another study the *in vitro* assembly of the separase-Cdk1-Cyclin B1-Cks1 complex is Pin1-independent (Yu et al., 2021). Free and uninhibited *cis*-separase is more aggregation-prone and leads to a quick inactivation of the protease, which is thought to be important for an efficient cohesin reloading in G1 (Hellmuth et al., 2015b).

Separase is located in the cytosol of undamaged human cells, due to a nuclear export signal (NES) at residues 1651 to 1661. Triggered by DNA damage, ATM kinase phosphorylates Ser1660 and thereby inactivating the NES, facilitating nuclear localization of separase in interphase to DNA double strand breaks. Additionally, the arginine methylation of an RG-motif centered around position 1426 and the SUMOylation of Lys1034 positively regulate separase's involvement in DNA damage repair (Hellmuth et al., 2018; Sun et al., 2006). As it is a DNA-binding protein, separase is recruited to mitotic chromosomes after nuclear envelope breakdown. However, the association do DNA or chromatin does not alter the proteolytic activity *in vitro* (Sun et al., 2009).

### 3.3.4 Misregulated Separase Activity

The fact that separase's catalytic outcome is irreversible leads to dramatic consequences for genome stability of a cell, in case of separase malfunction due to premature activation or lack of activity. Separase depletion perturbs sister chromatid separation and as a consequence causes cells to start cytokinesis with cohesed sister chromatids where cleavage furrow ingression constricts the chromosome masses with severe DNA bridges. This phenotype was named cell untimely torn (cut) and was first described in *S. pombe*. Eventually, cytokinesis fails, the

daughter cells refuse and a multinucleated cell with an abstract multilobed nucleus forms (Chestukhin et al., 2003; Hirano et al., 1986). Separase knockout causes embryonic lethality and knockout of one allele leads to severe developmental defects in mice (Wirth et al., 2006). Artificially prolonged cohesion of sister chromatids by expression of a non-cleavable kleisin subunit or a non-degradable securin results in a phenotype that displays the same segregation errors during mitotic exit as can be observed in separase depletion experiments (Hauf et al., 2001; Zur and Brandeis, 2001).

When activated too early, for instance by expression of the CCC binding mutant in HeLa cells or in a mouse model, sister chromatids separate prematurely and cells arrest in prometaphase due to activation of the spindle assembly checkpoint (Holland and Taylor, 2006; Xu et al., 2011). In mouse mammary epithelial cells, with p53 knocked out, separase expression was elevated and reciprocal overexpression of separase in mouse mammary epithelial cells induced segregation errors and developed aneuploidy and tumor formation (Pati, 2008; Pati et al., 2004; Zhang et al., 2008). These findings strongly suggest separase to be an oncogene and indeed, by comparing a number of human tumor tissues with the corresponding non-transformed tissue has revealed that in osteosarcoma, colorectal, breast and prostate cancer tissue separase is overexpressed and correlates with the occurrence of relapse, metastasis and overall survival in breast and prostate cancer patients (Meyer et al., 2009). The same study showed that in transformed tissue, the CD clan protease is mislocalized to the nucleus throughout the cell cycle. Based on these data, separase might make a promising target for pharmacological treatment in cancer therapy and consequently a potent small molecule inhibitor for separase is of great interest.

### 3.3.5 Aim of this study

The molecular toolkit to manipulate separase activity is currently extremely limited. Uhlmann and colleagues engineered a small inhibitory peptide that consists of a hexapeptide SVEQGR resembling the cleavage site of yeast Scc1 but has a reactive acyloxymethyl ketone as a "war head" at the cleavage site arginine, which reacts covalently with the active site cysteine of the protease. This inhibitor was only effective in cell-free experiments like *Xenopus laevis* egg extract but would not be suitable for cell-based experiments (Uhlmann et al., 2000). The research group of Debananda Pati identified the first small molecule inhibitor, Sepin-1, that is thought to inhibit separase in a non-competitive mode of action. *In vitro* assays showed effective reduction of separase's proteolytic activity and cell lines with high separase levels were more sensitive towards this compound, suggesting a separase-dependent correlation. Xenograft

experiments revealed that Sepin-1 reduced tumor size in mice that were treated with Sepin-1 orally and therefor support the idea that separase is a potential target for future cancer therapeutics (Zhang et al., 2014). Unfortunately, follow up studies revealed that Sepin-1 also acts on FoxM1, a transcription factor for a number of cell cycle regulating genes such as Plk1 and Cdk1 and therefor most likely does not reduce tumor growth solely by inhibition of separase but rather perturbs proliferation in a more general manner (Zhang and Pati, 2018).

The aim of this work was to identify a novel small molecule inhibitor for separase via a high-throughput screening approach, which is potent enough to inhibit separase activity in cells. If successful, chemical inhibition of separase is of great interest and will have a broad field of application, reaching from basic research to possibly drug development for cancer therapy.

# 4. Results

The aim of this study was to identify potent and cell permeable small molecules that selectively inhibit separase. To realize this, a high-throughput screening (HTS) approach was chosen, during which 51 009 potentially active compounds of a pharmacophore small molecule library were tested in a cell-based experimental setup.

## 4.1 Development of the High-Throughput Screening Setup

Due to the fast aggregating nature of active and securin-free separase in a reconstituted system (Hellmuth et al., 2015a), a cell-based high-throughput screening approach was established to identify new small molecule separase inhibitors. This approach would allow to search for cell-permeable and non-cytotoxic compounds. A known separase activity probe (Shindo et al., 2012) was used to quantify the proteolytic activity of separase in cells. This activity probe is a fusion

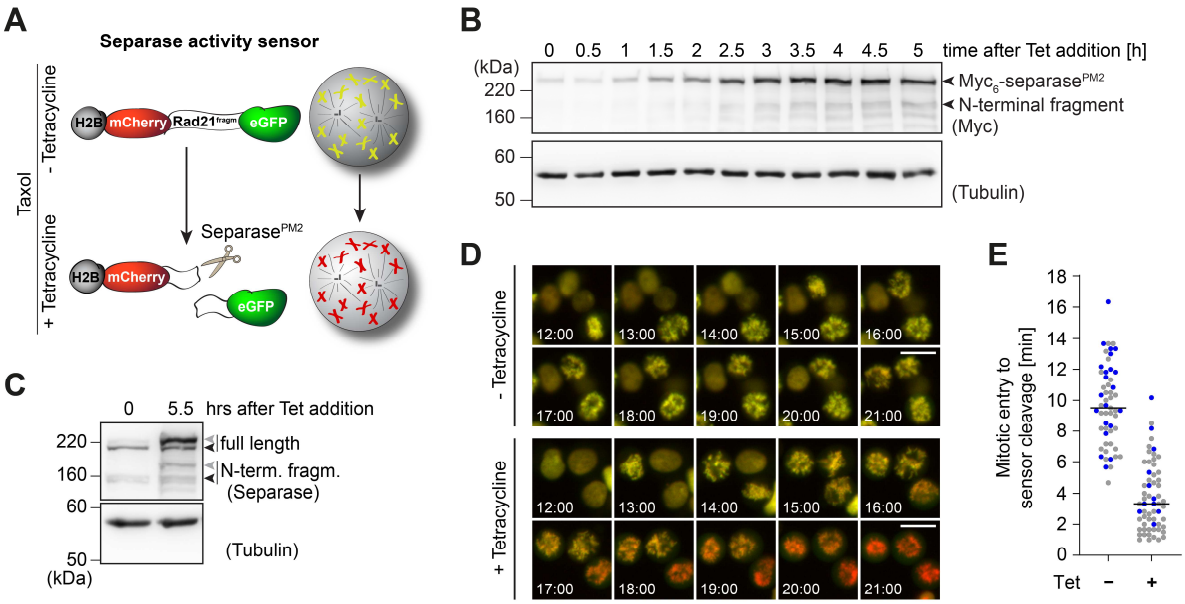


**Figure 5: HEK293T cells for high-throughput assay. (A)** Schematic representation of separase activity sensor and expected merge color of prometaphase arrested screening cells. Upon addition of tetracycline (Tet) the sensor construct is cleaved by separase$^{PM2}$ in prometaphase arrested cells. **(B)** Western blot of time course of separase$^{PM2}$ induction in HEKL293T cells. Time stamps relative to tetracycline addition. **(C)** Western blot of HEK293T cells before and 5.5 hrs after tetracycline addition; detected are endogenous (black arrow head) and exogenous separase (grey arrow head). **(D)** Exemplary images of live-cell experiment. Thymidine-synchronized HEK293T cells were arrested with taxol (230 nM) in prometaphase with or without overexpression of separase$^{PM2}$, time stamp relative to release from thymidine, scale bar 20 µm. (E) Quantification of duration from mitotic entry to sensor cleavage as shown in (D); blue dots indicate cells that showed no sensor cleavage before the end of the experiment.

protein consisting of two fluorophores (eGFP and mCherry) that are linked by a fragment of human Rad21 (aa128-268) containing a cleavage site for separase right after Arg172. Histone H2B N-terminal to mCherry facilitates localization of the activity sensor to chromatin (Figure 5A). Thus, in the absence of separase activity mCherry and eGFP co-localize to chromatin, resulting in a yellow merge color. Upon separase-dependent cleavage, the eGFP-containing fragment dissociates from chromatin and is degraded, which leads to a change in color from yellow to red in the merged pseudo-color image (Figure 5A). The pseudo-color is quantified via the Hue value, which is a numerical representation of the full color spectrum and independent of brightness. Therefor it is an ideal readout for sensor cleavage and is not susceptible to variations of the sensor's expression level.

Separase activity is regulated by the association of the inhibitory proteins securin and cyclin B1, both of which are degraded in an APC/C-dependent manner after the satisfaction of the SAC. Thus, compounds triggering SAC activation, e.g. microtubule-targeting drugs or compounds that prevent the inactivation of the SAC, would score in our cell-based assay as separase inhibitors. To select compounds that directly affect separase activity, rather than acting upstream of the SAC, we overexpressed the previously described separase$^{PM2}$ variant (S1126A) that cannot bind cyclin B1 (Stemmann et al., 2001). The activity of separase$^{PM2}$ was now primarily inhibited by securin. Compared to endogenous separase, the mutant protease was overexpressed three-fold on protein level (Figure 5C) and the maximal expression levels were reached four hours after induction with tetracycline (Figure 5B). The overexpressed separase$^{PM2}$ should exceed the available pool of securin and thus, the activity of separase$^{PM2}$ should be independent of the SAC-controlled degradation of securin via the APC/C. To validate this setup, we arrested HEK293T screening cells in prometaphase with taxol, where endogenous separase is inactive, and induced separase$^{PM2}$ expression or not. Time lapse microscopy analysis revealed that in cells with tetracycline-induced separase$^{PM2}$ overexpression, the activity sensor was efficiently cleaved 3.5 hours after entry in mitosis, whereas control cells without separase$^{PM2}$ expression did only show sensor cleavage very late at 9.5 hours after mitotic entry or not all (Figure 5D-E). This validated the assay setup to be suitable to identify small molecule inhibitors, that act directly on the target protease.

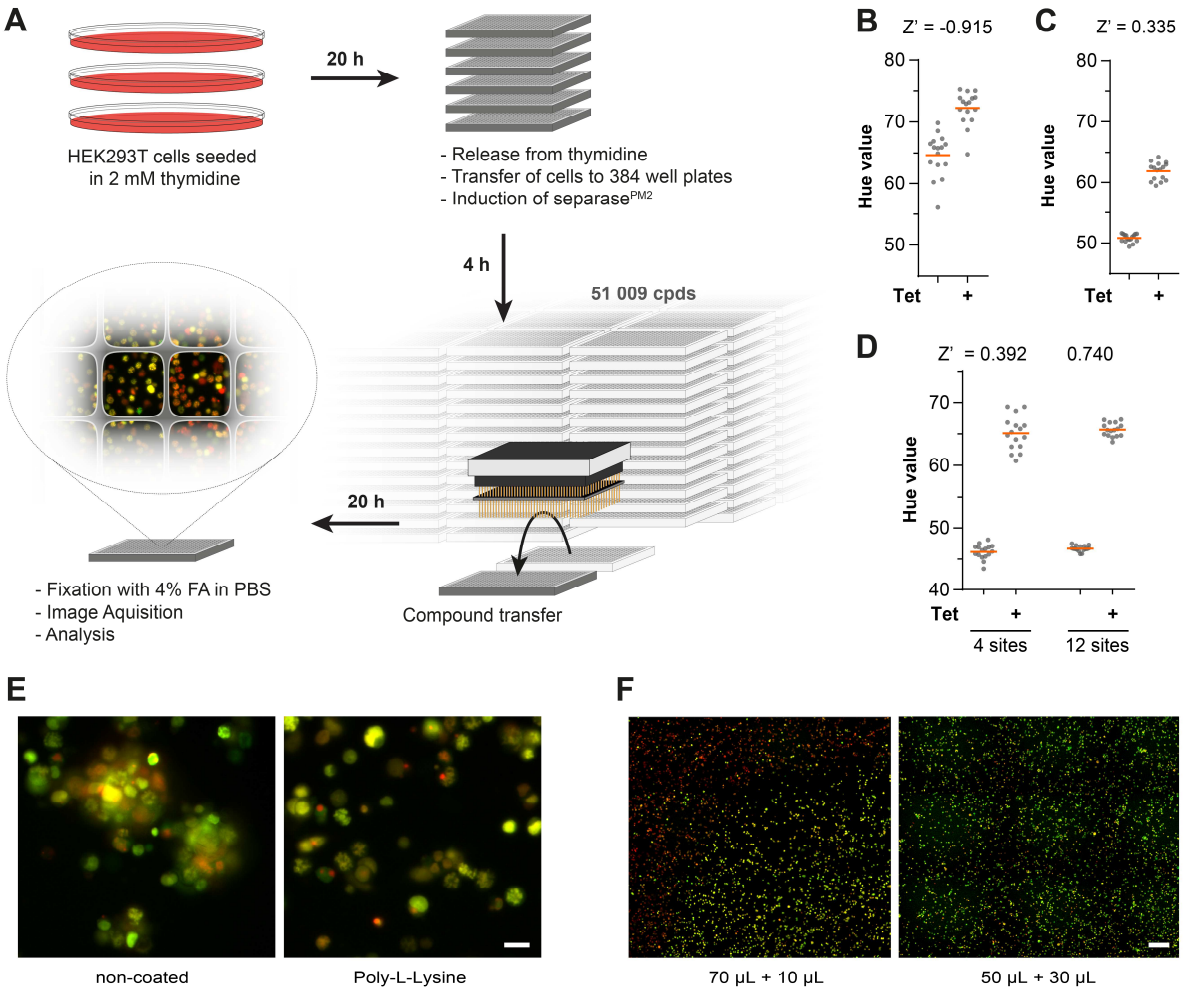


**Figure 6: Optimization of HTS setup. (A)** Schematic workflow of the experimental setup of the cell-based HTS. **(B)** scatter plot displaying the hue values of control wells; Z' value is calculated from the shown controls. **(C)** scatter plot as in (B) but an additional washing step with PBS was added after cells were fixed. **(D)** scatter plot as in (B) but with cells with a lower passage number; influence of the number of sites that are acquired in each well. **(E)** Exemplary images of HEK293T screening cells in 384 well assay plates coated with poly-L-lysine or without additional coating; scale bar 20 µm **(F)** Stitched tiled view of top left well corner. Increased volume of mixing medium after cpd transfer on the assay plate improved the equal distribution of cpds inside the well; scale bar 200 µm

For the high-throughput screening setup the cells were fixed with formaldehyde 24 hrs after release from thymidine and imaged with an automated screening microscope as the timeline in Figure 6A shows. To validate the robustness and reproducibility of the setup, we calculated the Z' value of the assay with the following equation:

$$Z' = 1 - \frac{(3\sigma_n + 3\sigma_p)}{|\mu_n - \mu_p|}$$

This variable is mainly affected by the mean values of the positive ($\mu_p$) and negative ($\mu_n$) controls, their standard deviation ($\sigma_n$, $\sigma_p$) and the interval between them and allows to rate the

quality of each individual plate or batch of the assay. Z' values over 0.5 are considered as robust and recommended for high-throughput screening setups (Zhang et al., 1999). Prometaphase-arrested cells with tetracycline-induced separase$^{PM2}$ had the highest protease activity and therefore were defined as the negative control. The lack of a potent small molecule separase inhibitor, that could have served as a positive control, prompted us to use cells without separase$^{PM2}$ induction, which mimics a full inhibition, as positive control. On each 384-well assay plate, 16 wells for each control were analyzed as constant quality control during the entire HTS and only assay plates with a Z' of 0.5 or higher were used for analysis or were otherwise repeated.

The initial Z' value was below -0.9 (Figure 6B) which was far from optimal. To improve the setup and increase the robustness, that was mainly flawed by a rather high standard deviation of the two controls, the fixed cells were washed two additional times with PBS to remove residual amounts of cell culture medium containing phenol red, which could account for a higher background fluorescence. This greatly increased the Z' value to 0.335 (Figure 6C). Until this point, only four positions per well were acquired. The increase to 12 positions per well, improved the robustness even further and yielded a Z' value of 0.740 (Figure 6D). Due to a strong cell clustering of the HEK293T screening cell line, automated image analysis, which would include cell segmentation and subsequent classification, would be very error prone because single cells cannot be distinguished in large cell clumps. Precoating the assay plates with poly-L-Lysine before the assay, greatly reduced the number of huge cell clusters and allowed an even cell distribution over the surface of the well (Figure 6E). During the first preliminary tests with small molecules, we occasionally noticed a drastic effect in sensor cleavage in the center of the well with a sharp defined border towards the edges of the well (Figure 6F). We reasoned that this effect was caused by insufficient mixing after the compound was added and as a result created a gradient of high concentration of compound and DMSO in the center of each well and a low concentration at the edges. To reach a more equal distribution, we increased the volume of cell culture medium, that was used to disperse the small molecules after the compounds were transferred. The addition of 30 $\mu$L to 50 $\mu$L, instead of 10 $\mu$L to 70 $\mu$L, solved the issue (Figure 6F).

## 4.2 Reduction of False Positives by Mitotic Classification

Due to the nuclear export signal of separase, the protease is not able in interphase cells to reach the sensor, which localizes to chromatin in the nucleus because of its fusion with H2B. Consequently, only in mitotic cells the cleavage status of the sensor can be used as a readout of separase activity. Thus, potential false positive hits in this high-throughput assay setup could be compounds that prevent cells from entering mitosis, by either cytotoxic mode of action or specifically by arresting or delaying cells in S- or G2-phase (Figure 7A). An automatic

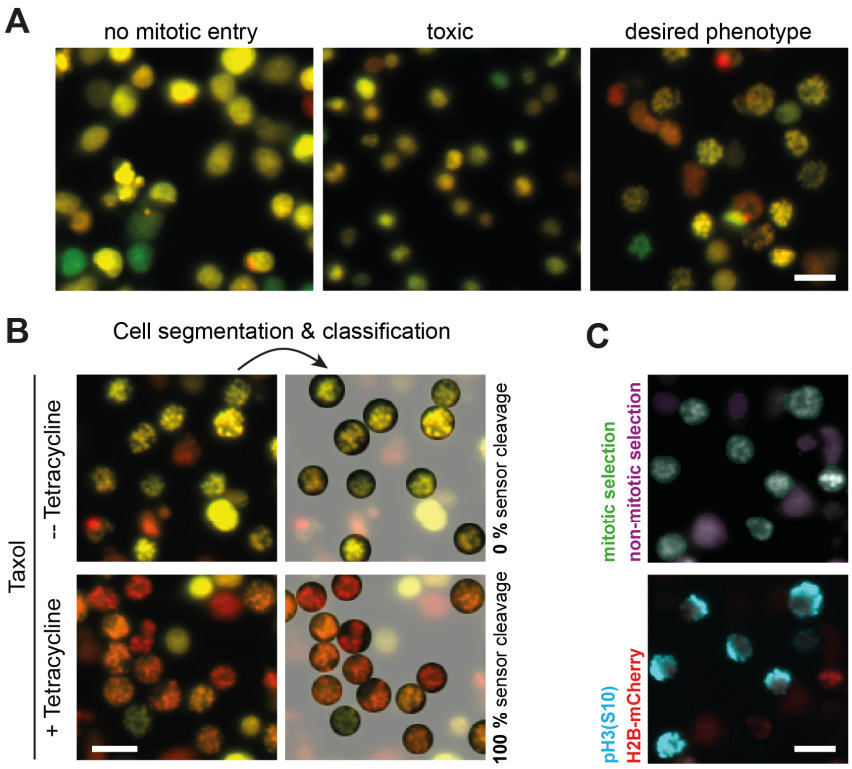


**Figure 7: Cell segmentation and classification. (A)** Exemplary phenotypes of false positives and desired phenotype. **(B)** Schematic mitotic cell selection. **(C)** Comparison of automated classification (top) and immunofluorescent analysis of phospho-histone H3 at serine 10 (bottom), scale bars 20 µm

classification algorithm identified mitotic cells and calculated the percentage of mitotic cells, which will be referred to as mitotic index. This information enabled us to immediately detect compounds that prevent mitotic entry. More importantly, the implementation of this classification enabled us to restrict the analysis of sensor cleavage to exclusively mitotic cells. Comparison of the automated mitotic selection with an immunofluorescent analysis of phospho-histone H3 on serine 10, a mitotic marker, showed that this algorithm correctly classifies cells with an accuracy of more than 80 % (Figure 7B-C) and therefor is suitable for the analysis in our HTS setup.

## 4.3 Separase Knockdown does not Reduce Mitotic Index

The defined thresholds for a hit were firstly the reduction of sensor cleavage to less than 30% relative to DMSO treated separase$^{PM2}$ expressing cells and secondly a relative mitotic index of more than 80 % compared to DMSO treated separase$^{PM2}$ expressing cells. As it was shown before (Gimenez-Abian et al., 2005), knockdown of separase in HeLa cells can lead to a delay in G2/M transition and therefore could potentially reduce the mitotic index in our screening setup. To assess if, or to what extent, this delay would reduce the mitotic index in the screening setup, we performed the HTS assay with HEK293T cells after a separase knockdown. Incubation with

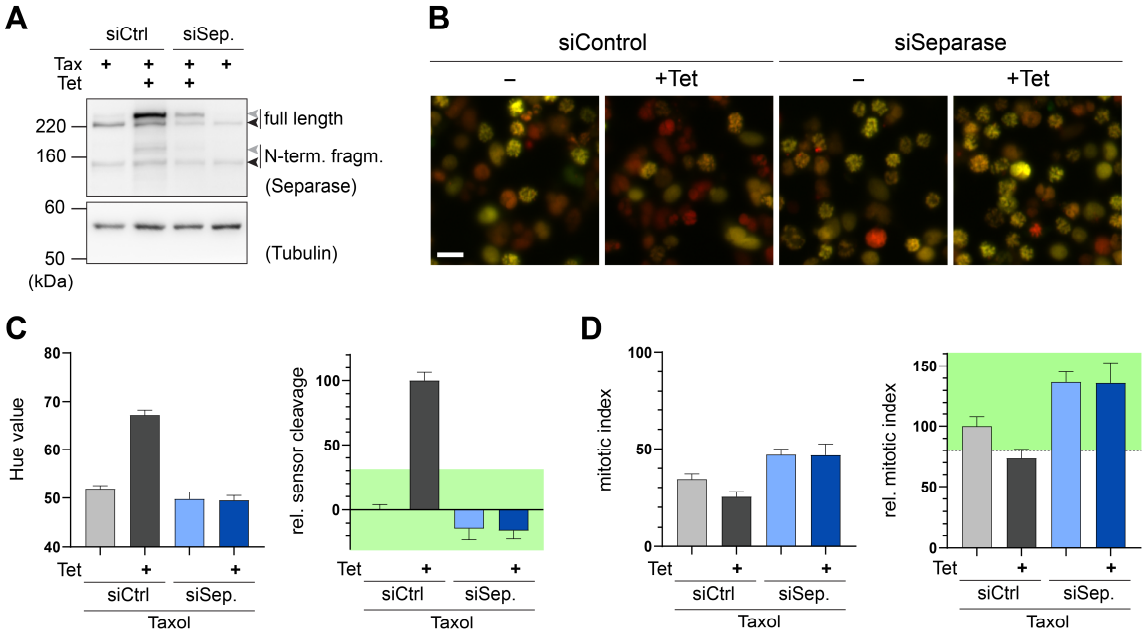


**Figure 8: Separase knock down in HTS setup. (A)** Western blot of taxol-arrested HEK293T cells treated with siRNA targeting separase (siSep) or control siRNA (siCtrl); $Myc_6$-separase$^{PM2}$ expression was induced with tetracycline (+Tet) or not. Grey arrow heads indicate $Myc_6$-separase$^{PM2}$ and black arrow heads indicate endogenous separase. Tubulin serves as loading control. **(B)** Exemplary microscopy images of fixed HEK293T cells treated as in (A); scale bar 20 µm **(C)** (left) Quantification of the hue value in HEK293T cells treated as in (A), shown are mean and SD of 16 individual wells; (right) normalized sensor cleavage; Hue value of cells treated with non-targeting siRNA and without separase$^{PM2}$ overexpression was defined as 0% rel. sensor cleavage; Hue value of cells with separase$^{PM2}$ overexpression equals 100 % sensor cleavage. **(D)** (left) mitotic index of HEK293T cells treated as in (A); (right) relative mitotic index; cells treated with non-targeting siRNA and without separase$^{PM2}$ overexpression equals 100 % rel. mitotic index; green-highlighted areas in (C) and (D) mark the hit criteria for inhibitor selection.

siRNA targeting separase efficiently reduced endogenous and exogenous protease levels (Figure 8A) and surprisingly increased the mitotic index by more than 30 % compared to control-depleted cells (Figure 8B and D). These findings proof that in our HTS setup a reduced separase activity does not result in a lower mitotic population and therefore the mitotic index can be used as suitable criteria for hit selection. Additionally, the sensor cleavage in control-depleted cells was slightly higher than in separase-depleted cells, which shows that residual separase activity, that originates from background expression of separase$^{PM2}$ in uninduced cells,

lead to a minimal level of separase sensor cleavage. This consequently leads to negative values of relative sensor cleavage in separase-depleted cells (Figure 8C). These findings show that greatly reduced separase activity in HEK293T cells leads to hue values and mitotic indices that are inside our defined thresholds for a small molecule inhibitor.

Of the 51 009 tested small molecules of the pharmacophore compound library, 495 potential inhibitors satisfied the selected criteria and were picked for follow up validation experiments.

## 4.4 Reconstitution of Active Separase Variants for *in vitro* Assays

To validate if the identified active compounds are able to inhibit separase directly, reconstituted active separase was purified from HEK293T cells to be used in an *in vitro* Rad21 cleavage assay.

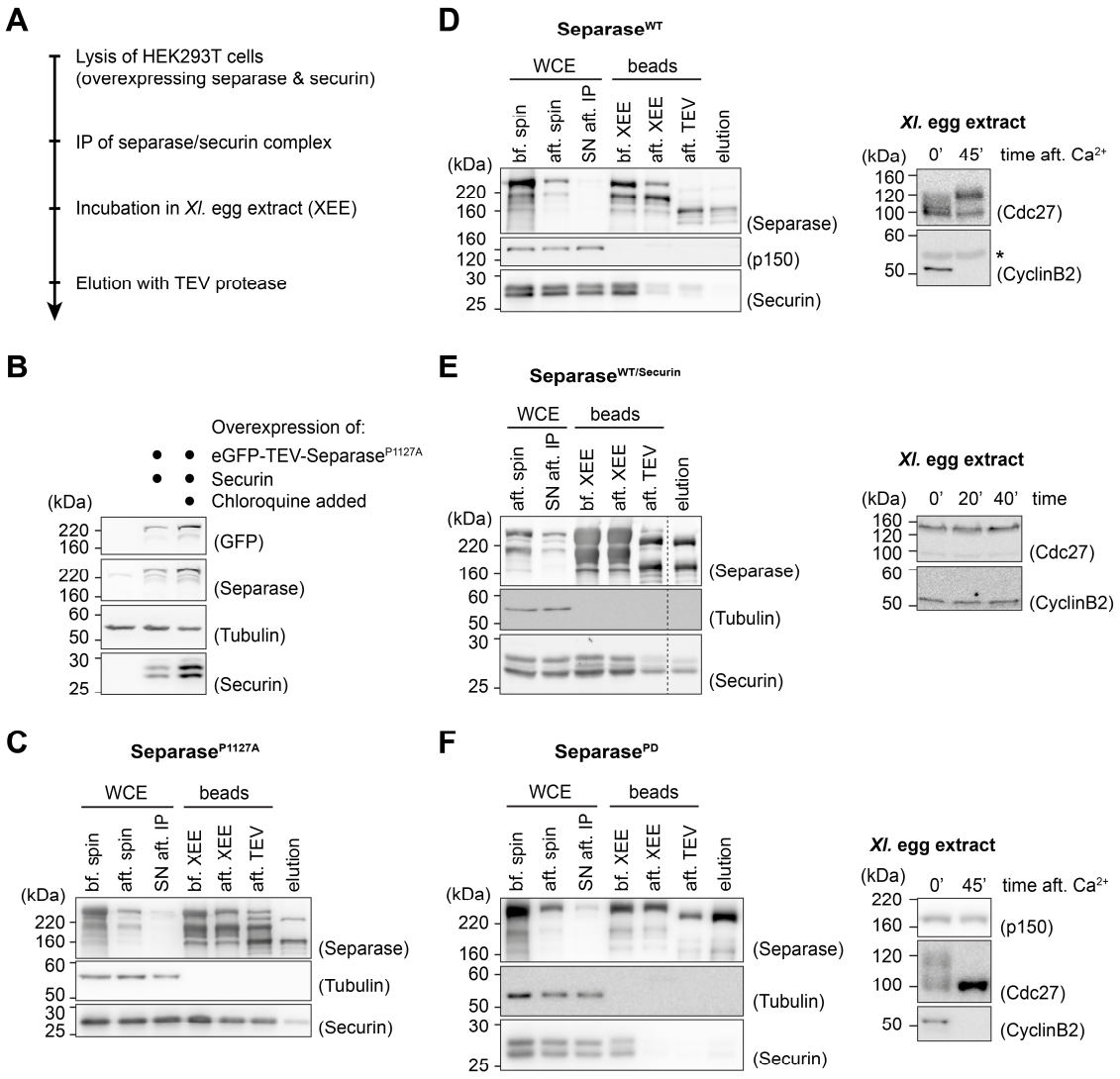


**Figure 9: Reconstitution of different separase variants.** Used separase variants were wildtype (WT), a less aggregation-prone mutant (P1127A) and a protease dead mutant (C2029A, PD). **(A)** Experimental setup, **(B)** Western blot of HEK293T cells after 48 hrs of transfection with securin and GFP-tagged separase$^{P1127A}$, **(C-F)** Western blot analysis of individual steps during the separase preparations of the different separase variants.

In short, different GFP-tagged separase variants, wild type (WT), P1127A, PD) together with securin were transiently overexpressed in HEK293T cells and immunoprecipitated with a GFP-nanobody. Co-immunoprecipitated securin was degraded by incubation in *Xenopus laevis* anaphase extract and subsequent TEV-protease digestion cleaved the affinity tag consequently eluting active separase (Figure 9A). Transient transfection was performed in the presence of 50 $\mu$M chloroquine due to reported higher transfection/expression efficiency (Hasan et al., 1991; Luthman and Magnusson, 1983) (Figure 9B). With all separase variants the immunoprecipitation showed an efficient reduction of ectopically expressed separase in the cell lysate and a strong signal for bound protease on the beads. The incubation in *Xenopus* egg extract that progresses through anaphase or stayed in an anaphase-like state significantly reduced the co-precipitated securin levels on the beads (Figure 9C, D and F). The anaphase-like state of the egg extract was checked by hyperphosphorylation of Cdc27 and degradation of cyclinB2 (Figure 9D-F). With separase$^{WT}$ and separase$^{P1127A}$ but not with separase$^{PD}$, the securin degradation coincided with efficient auto-cleavage of separase on the beads which suggests a successful activation of the protease. Separase$^{WT}$ incubated in non-released metaphase-arrested egg extract did not show any securin degradation nor auto-cleavage of the protease on the beads validating that securin degradation via the ubiquitin-proteasome system of the anaphase *Xenopus* egg extract is necessary to activate the reconstituted separase variants (Figure 9E-F).

## 4.5 Five Compounds Reduce Rad21 Cleavage *in vitro* in a Non-Covalent Manner

An *in vitro* assay with reconstituted separase$^{P1127A}$ and $^{35}$S-labeled *in vitro* translated (IVT) Rad21 as substrate was used to validate the identified potential hits. To reduce the fast aggregation of securin-free separase, a more stable variant (P1127A) was used, which cannot be isomerized to the more aggregation prone *cis*-conformation. Rad21 IVT cleavage could be observed after incubation with separase$^{P1127A}$, tolerated DMSO concentrations up to 10 % and was inhibited by Sepin-1, a previously identified separase inhibitor (Zhang et al., 2014), in a dosage dependent manner (Figure 10A). Testing all 495 identified compounds and quantifying the faster migrating cleavage product of the Rad21 IVT just below 30 kDa, revealed that 81 potential inhibitors reduced separase activity to less than 50 % compared to the DMSO control (Figure 10B and Supplemental Figure S1). Small molecules that act in a covalent or oxidative manner, tend to be less specific and to have higher toxicity, due to unspecific reactions with other biomolecules(Dahlin and Walters, 2014). To exclude this unspecific group of inhibitors, we retested the remaining 81 compounds in the presence of 1 mM DTT. As a reducing agent, DTT prevents the oxidation of the crucial thiol group on the active site cysteine of separase.

Additionally the excess of the thiol groups of DTT will prevent most covalent modifiers to rather react with DTT than with the active site cysteine of separase. In the presence of 1 mM DTT the cleavage of the Rad21 IVT with separase$^{P1127A}$ increased by more than two fold (Figure 10C), which suggests that during the preparation of separase$^{P1127A}$ a significant fraction was oxidized. Of the remaining 81 compounds, the majority lost their inhibitory effect in the presence of DTT (Figure 10D) and only five small molecules reduced activity of separase$^{P1127A}$ below 50 %. Incubation of Rad21 IVT with enzymatically inactive separase$^{PD}$ (C2029A) did not result in Rad21 cleavage, which shows that the identified compounds inhibit separase and not another proteolytic enzyme that might have co-purified with separase (Figure 10E). We titled the identified compounds Separase Inhibitory Compounds 1-5 (SIC1 - SIC5). They show no obvious similarities in their chemical structures (Figure 10F). Interestingly, Sepin-1 almost completely lost its inhibitory effect in the presence of 1 mM DTT (Figure 10D). Until this point, only the less aggregation-prone separase$^{P1127A}$ was used for validation of potential hits. To eliminate the possibility that all SICs only inhibit this specific variant, the assay was repeated with separase$^{WT}$. All SICs reduced separase$^{WT}$ activity in a dose dependent manner with SIC4 being the most potent compound (Figure 10G and H). Sepin-1 only showed very minor inhibition on separase$^{WT}$ activity.

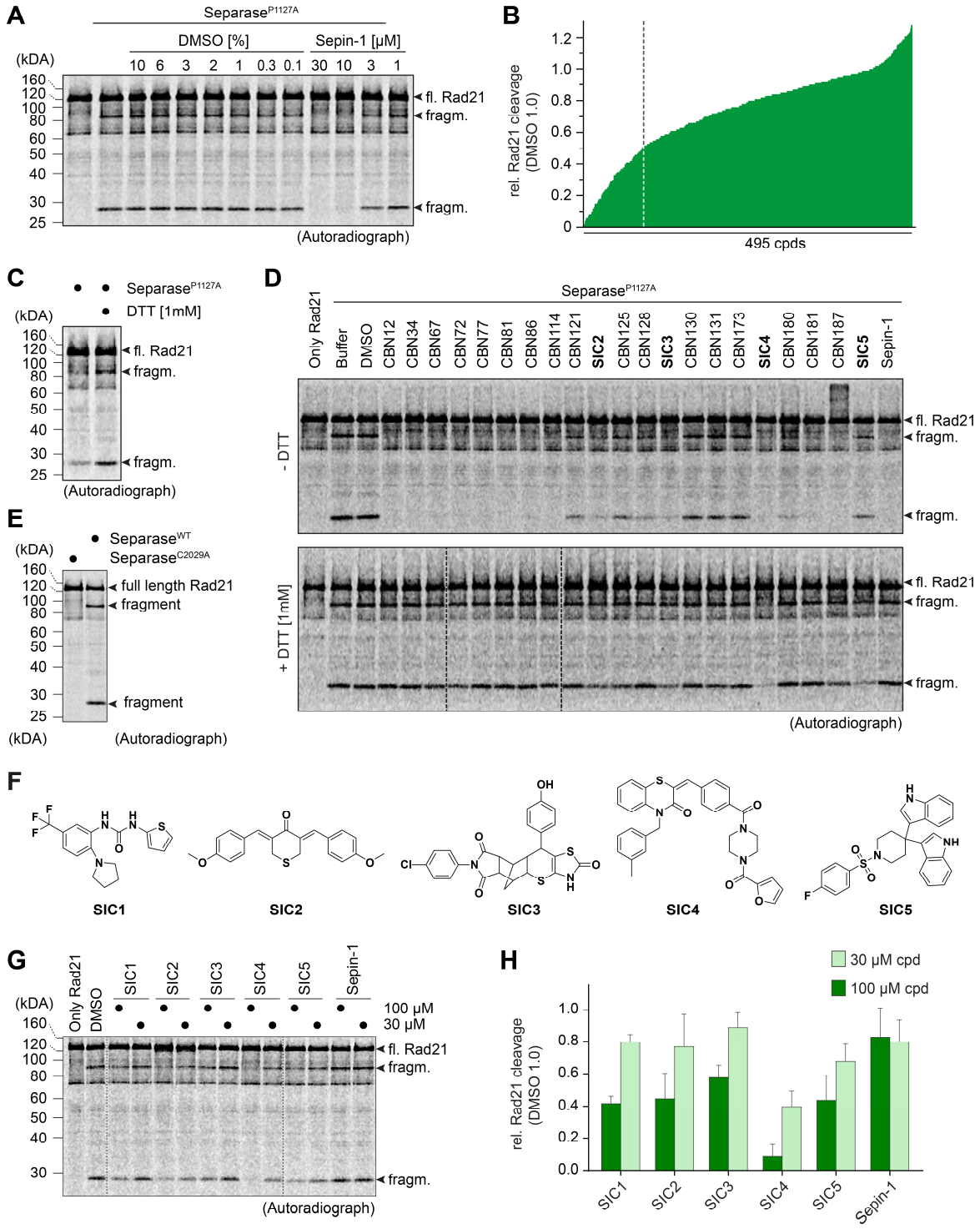


**Figure 10: Hit validation with Rad21 cleavage assay. (A)** Autoradiograph of Rad21 cleavage assay; separase$^{P1127A}$ mediated cleavage of Rad21 IVT; DMSO and Sepin-1 were used at indicated percentages or concentrations. **(B)** Quantification of Rad21 cleavage assay with all 495 hits from HTS; fast migrating cleavage fragment was quantified with ImageJ. **(C)** Autoradiograph of Rad21 IVT cleavage with and without 1 mM DTT. **(D)** Exemplary autoradiograph of Rad21 cleavage assay with 21 potential separase inhibitors and Sepin-1 with and without 1 mM DTT; all compounds were used at 20 µM **(E)** Rad21 cleavage assay with separase$^{WT}$ and catalytic dead separase$^{C2029A}$. **(F)** Chemical structures of SIC1 to SIC5. **(G)** Exemplary autoradiograph of Rad21 cleavage assay using separase$^{WT}$ in the presence of 1 mM DTT. **(H)** Quantification of autoradiographs in (G); mean and SD of three independent experiments.

## 4.6 Reconstituted Separase not Suitable for DREIMR Peptide Assay

To further characterize the identified SICs in a kinetic fashion, we utilized a peptide based assay with a fluorescent substrate that was previously used by D. Pati and colleagues to identify Sepin-1 (Basu et al., 2009; Zhang et al., 2014). This substrate consists of Rhodamine110 (Rh110) that is conjugated to two hexapeptides which resemble the main

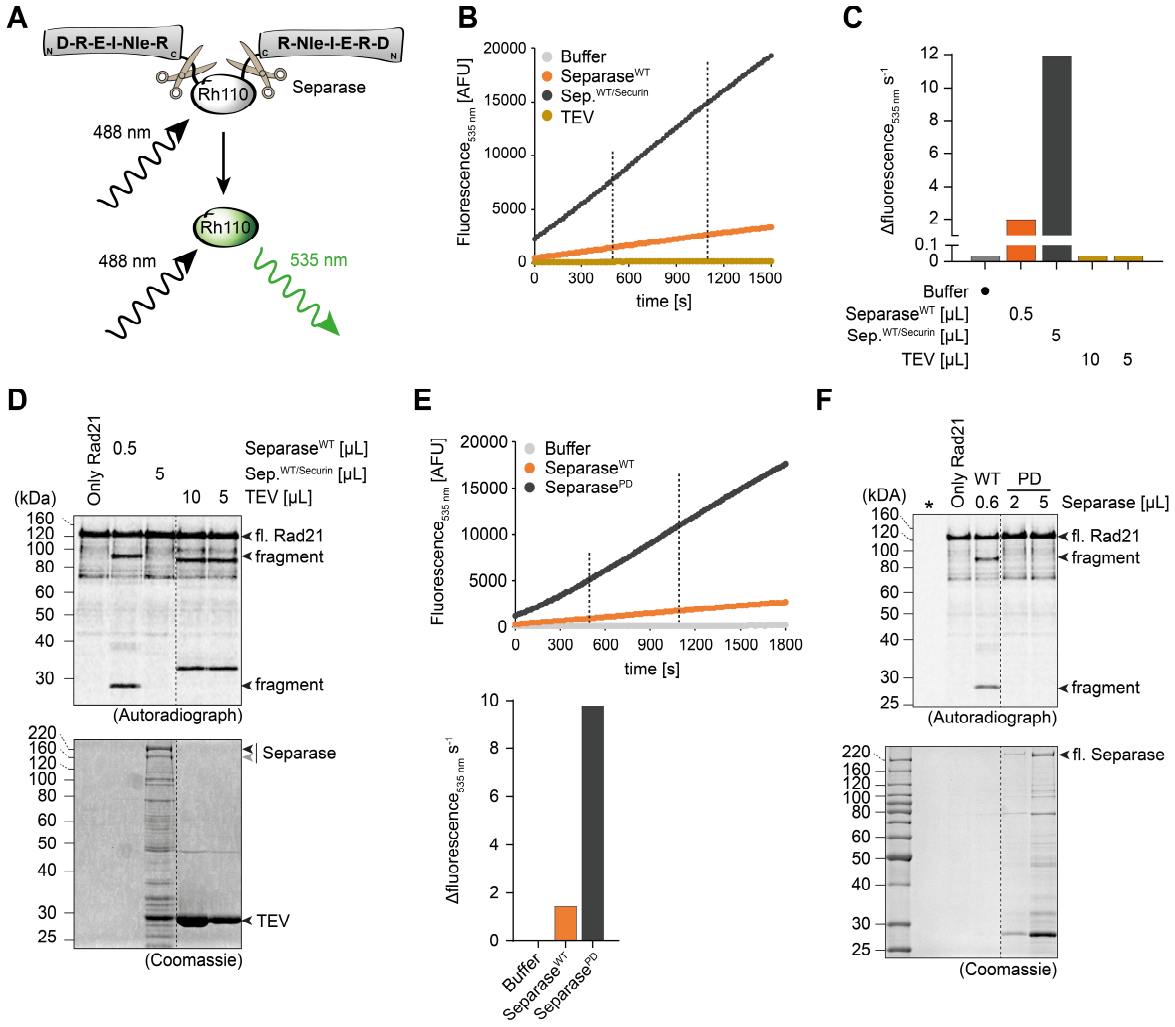


**Figure 11: Peptide assay (A)** Scheme of the basic principle of the peptide-based activity assay. **(B)** Kinetic of substrate cleavage over time. Increase of fluorescence (Ex485/Em535nm) over time is used to determine the reaction rate; separase$^{WT}$, separase$^{WT/securin}$ or TEV protease are tested. **(C)** Quantification of the reaction velocity by linear regression in the interval indicated in (B). **(D)** Rad21 cleavage assay; performed as in **Figure 10**. **(E)** Fluorescent peptide assay as in (B) with quantification of the reaction velocity. **(F)** Rad21 cleavage assay with separase$^{WT}$ and separase$^{PD}$

cleavage site of human Rad21 ($^{167}$DR**E**IM**R**$^{172}$). To prevent the oxidation of the methionine on the peptide, Norleucine (Nle) was used instead. Upon cleavage of the peptides, the fluorescence of free Rh110 increases more than 100 fold (Basu et al., 2009; Zhang et al., 2014) and can be used as a readout for protease activity (Figure 11A). Unfortunately, not only reconstituted securin-free separase$^{WT}$ was able to cleave the substrate but also the not activated securin-

separase$^{WT}$ complex showed efficient substrate conversion in this assay (Figure 11B-C). Reconstituted securin-separase$^{WT}$ complex from the same batch, as used in the peptide assay, was not able to cleave $^{35}$S-labelled Rad21 IVT whereas separase$^{WT}$, in very low quantities as judged by Coomassie staining, efficiently cleaved Rad21 (Figure 11D). Due to the fact that all immunoprecipitated separase variants are eluted from beads with a TEV protease that is therefore present in all activity assays, we tested if this protease is able to cleave the applied substrates. Surprisingly, the TEV protease, was able to cleave $^{35}$S-labelled Rad21 IVT but the emerging cleavage fragments have a different size than separase-dependent cleavage fragments, suggesting that the TEV protease does not recognize the main separase cleavage site ($^{167}$DR**E**IM**R**$^{172}$) on Rad21 (Figure 11D). Based on this result, it is not surprising that the fluorescent peptide substrate is not processed by the TEV protease even in higher quantities as judged by Coomassie staining (Figure 11B and C). To exclude that the observed peptide cleavage with the securin-separase$^{WT}$ complex is a result of the small size of the substrate, compared to the full-length Rad21 protein, which might account for binding to separase even in a securin-associated state, we additionally tested the catalytic inactive separase$^{PD}$. Unfortunately, also the incubation with separase$^{PD}$ resulted in efficient cleavage of the fluorescent substrate without showing any Rad21 cleavage (Figure 11E and F). These results strongly suggest that there is an additional protease present in our preparations of the different separase variants, that is able to cleave the peptide-based substrate but not full length Rad21 IVT. Hence, the peptide-based setup is not specific enough to test separase-dependent substrate conversion for the further kinetic characterization of the remaining SICs.

## 4.6 SICs Specifically Inhibit Separase over Caspase-1

To assess the specificity of the identified SICs, we tested their ability to inhibit a similar protease, caspase-1. Separase belongs with caspase-1 to the cysteine proteases of the CD clan superfamily and shares significant structure similarities to caspase-1 (Boland et al., 2017; Uhlmann et al., 2000). To assess the specificity of the identified SICs, we used a commercially available caspase-1 *in vitro* assay. As substrate, Ac-YVAD-AMC was used, which is a tetrapeptide conjugated to the fluorophore 7-Amino-4-Methylcoumarin (AMC). Upon cleavage by caspase-1 after the aspartate, the rate of emerging free AMC was measured by fluorescence. Recombinant caspase-1 efficiently cleaved the substrate, as judged by the increase in fluorescent signal over time. The caspase-1 inhibitor Ac-YVAD-CHO completely abolished any increase in fluorescence, which validated the experimental setup (Figure 12A). Of the remaining five compounds, SIC2 and SIC4 show moderate inhibition of caspase-1 at a concentration of 100 $\mu$M whereas SIC1, SIC3

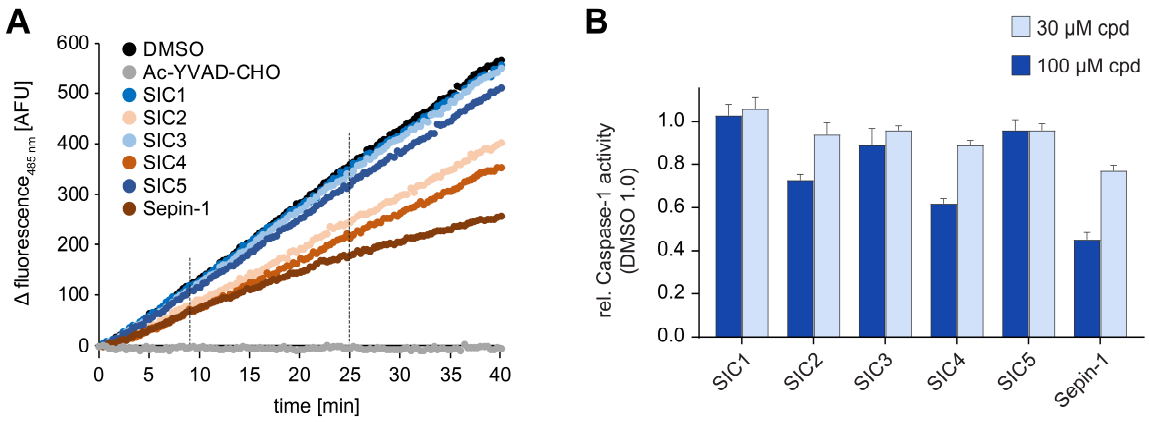


**Figure 12: Caspase-1 activity assay. (A)** Exemplary caspase-1 assay results; increase in fluorescent signal from cleaved AMC at 485 nm over time; all compounds were used at 100 µM; dashed lines indicate interval that was used for the rate calculation. **(B)** Relative to DMSO set to 100% Caspase-1 activity of three independent experiments, mean and SD

and SIC5 barely reduced caspase-1 activity at all. Surprisingly, Sepin-1 showed the strongest inhibitory effect on caspase-1 activity showing that the identified SICs have a higher specificity towards separase compared to Sepin-1 (Figure 12B).

## 4.7 The Majority of SICs Delay Anaphase Events

Up to this point, we only assessed separase inhibition based on either mutated separase variants in cells or wildtype separase in reconstituted assay setups. Motivated by the promising results of SIC1 to SIC5, we next wanted to test their inhibitory potential on endogenous separase activity in anaphase of living cells. For this, HeLa cells were arrested in prometaphase by the MT drug taxol and subsequently pushed into anaphase by small molecule inhibition of Aurora B with ZM447439. The resulting inactivation of the SAC leads to the activation of the APC/C and degradation of its substrates cyclin B1 and securin as well as to the dephosphorylation of the APC/C subunit Cdc27. Active separase then cleaves itself and the cohesin subunit Rad21. Analysis of these processes were tracked by western blot. In DMSO-treated cells, cyclin B1 and securin signals were almost undetectable 40 mins after ZM447439 addition and Rad21 cleavage and separase self-cleavage started 30 minutes after ZM447439 addition (Figure 13A-L). Cells that were incubated with 20 $\mu$M SIC1 completely abolished the degradation of cyclin B1 and securin as well as separase dependent cleavage processes (Figure 13A and B). 10 $\mu$M SIC2, 30 $\mu$M SIC3, 10 $\mu$M SIC4 or 30 $\mu$M SIC5 all showed a delay in separase-mediated cleavage processes but in all cases with an accompanied delay in cyclin B1 and securin degradation as well as a delay of Cdc27 dephosphorylation. SIC3 delayed anaphase events by 10 min, which was the second strongest delay of the tested compounds after SIC1 (Figure 13C-L).

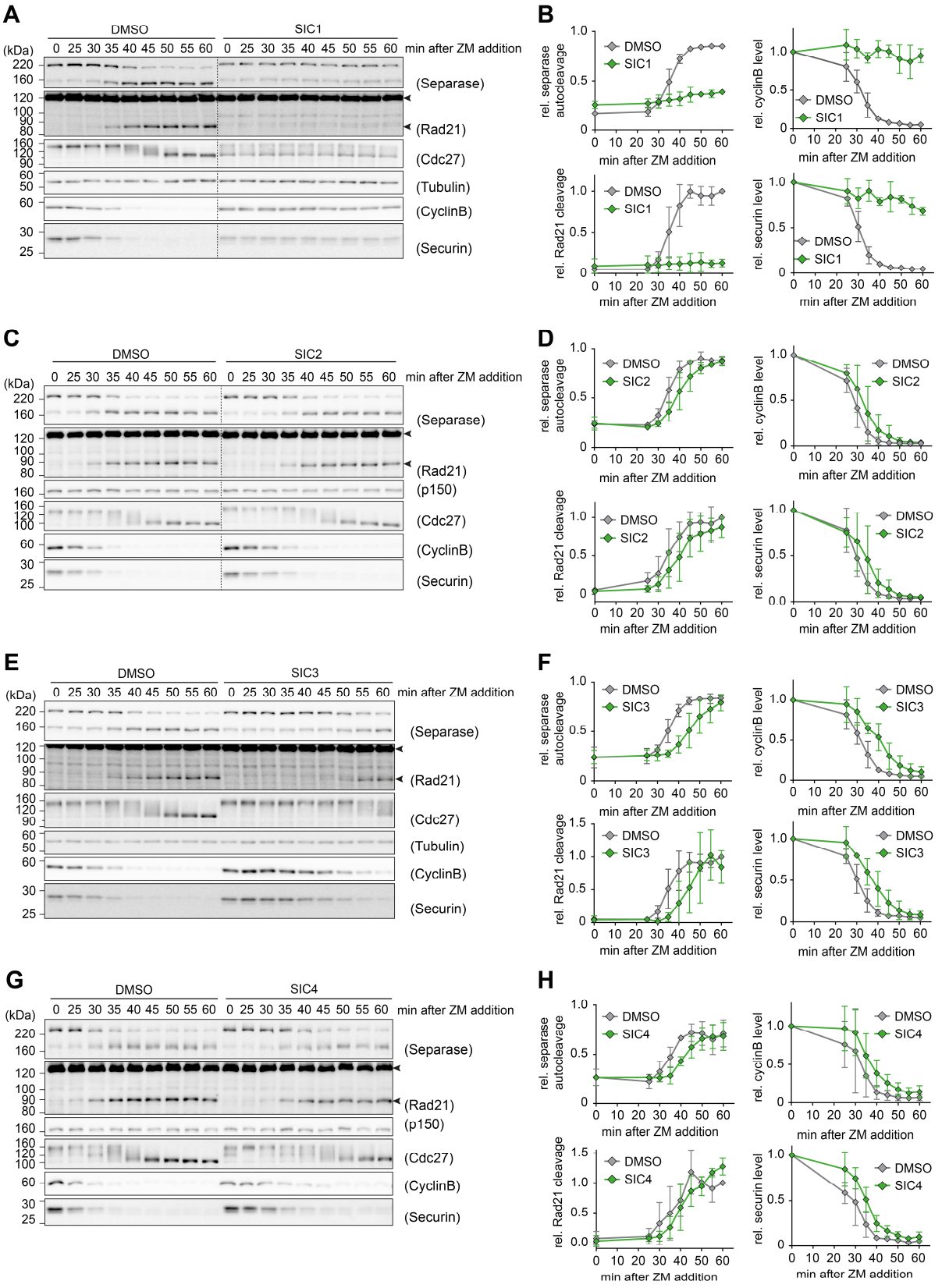
A
DMSO
SIC1
(kDa)
0 25 30 35 40 45 50 55 60
0 25 30 35 40 45 50 55 60
min after ZM addition
220
160
120
100
90
80
160
120
90
60
50
60
30
25
(Separase)
(Rad21)
(Cdc27)
(Tubulin)
(CyclinB)
(Securin)
B
rel. separase autocleavage
rel. cyclinB level
rel. Rad21 cleavage
rel. securin level
DMSO
SIC1
min after ZM addition
C
DMSO
SIC2
(p150)
D
DMSO
SIC2
E
DMSO
SIC3
F
DMSO
SIC3
G
DMSO
SIC4
H
DMSO
SIC4

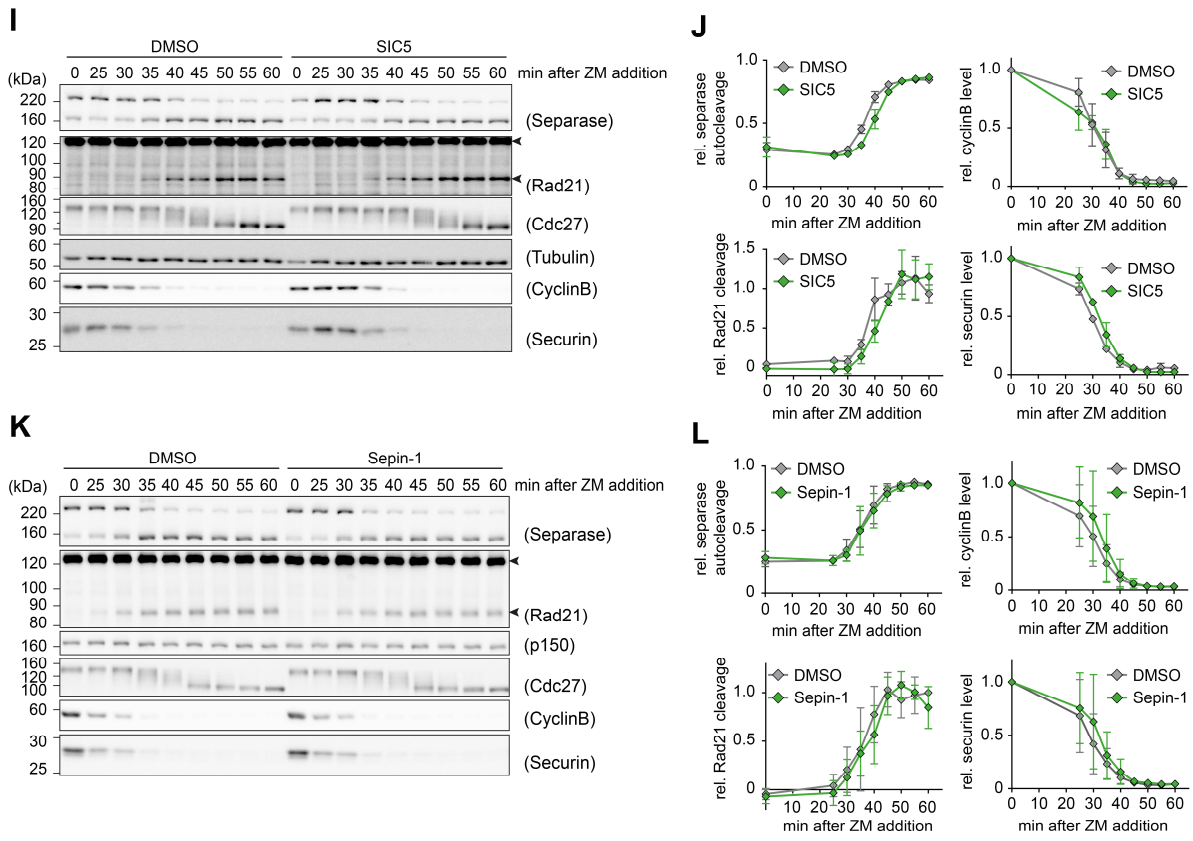


**Figure 13: SAC override experiments. (A-L)** Western blot analysis of ZM447439-triggered override of taxol-arrested HeLa cells in the presence of SIC1 to SIC5, Sepin-1 or DMSO as control; Quantification of indicated proteins from three independent experiments (mean + SD); dotted lines indicate that samples were on the same membrane but not adjacent to each other; rel. separase auto-cleavage was quantified as ratio of N-terminal fragment / (N-term.+ full length separase)

## 4.8 SIC1 Triggers Apoptosis in Prometaphase-Arrested Cells

The drastic effect of SIC1 on prometaphase cells, lead us to test if this compound induces apoptosis and as a result blocks any normal cell progression. Indeed, incubation of taxol-treated prometaphase cells with 20 $\mu$M of SIC1 for 2 hrs triggered apoptotic events as judged by efficient PARP-1 cleavage already before addition of ZM447439. DMSO treated cells did not show significant cleavage of PARP-1 (Figure 14A). To exclude that PARP-1 cleavage is in any way caused by taxol or ZM447439, the SAC override was repeated with Nocodazole to arrest cells in prometaphase and the Mps1 inhibitor Reversine to inactivate the SAC. Also with this setup, 20 $\mu$M SIC1 caused PARP-1 cleavage already before the addition of Reversine, confirming that SIC1 induced apoptosis in prometaphase-arrested cells independent of the small molecule setup that was used to drive the experiment in and out of mitosis (Figure 14B).

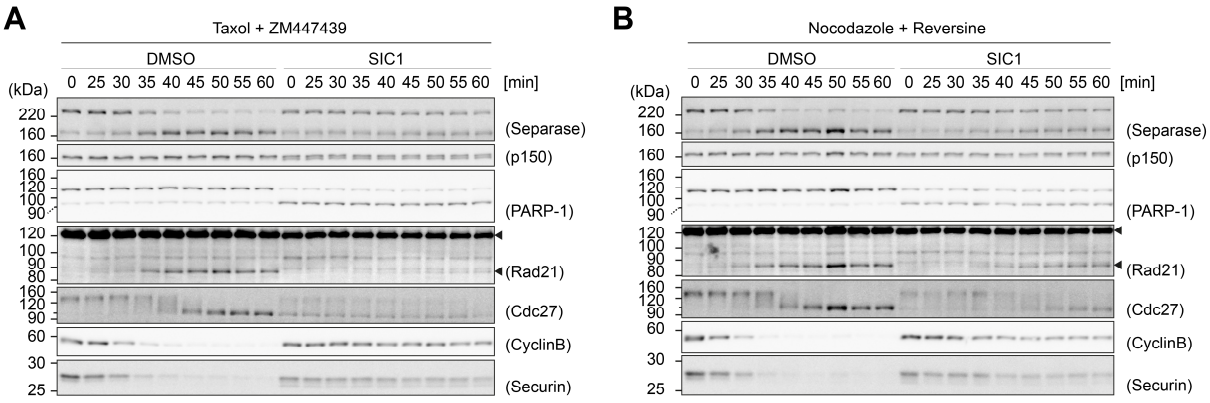


**Figure 14: SIC1 triggers apoptosis. (A)** Western blot time course of taxol-arrested HeLa cells that were pushed into anaphase by ZM447439 in the presence of 20 µM SIC1 or DMSO. **(B)** Western blot time course of nocodazole arrested HeLa cells that were pushed into anaphase by Reversine in the presence of 20 µM SIC1 or DMSO.

## 4.9 Separase$^{\Delta SLR}$ is Not Able to Cleave Rad21 *in vitro*

Based on the results of the SAC override experiments (Figure 13), that showed that all SICs did delay anaphase processes already upstream of separase activation, we reasoned that it would be highly unlikely that the identified SICs have a dual mode of action and inhibit separase and the APC/C. Since it was shown that separase does interact with the APC/C (Bakos et al., 2018), we reasoned that a small molecule that binds to separase at an APC/C binding site, might also

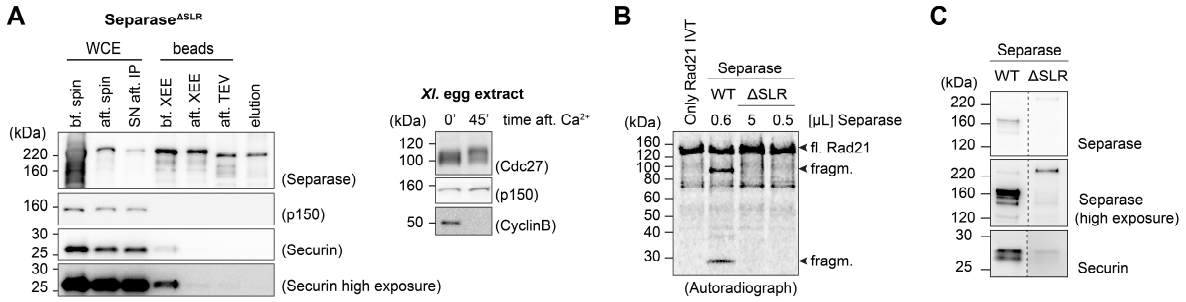


**Figure 15: Preparation of separase$^{\Delta SLR}$. (A)** Western blot analysis of individual steps during the separase$^{\Delta SLR}$ preparation; **(B)** Rad21 cleavage assay with separase$^{WT}$ and separase$^{\Delta SLR}$. **(C)** Western blot of separaseWT and separase$^{\Delta SLR}$ elutions

bind to APC/C coactivators and as a result would affect APC/C activity as well. A potential APC/C binding motif on separase is the c-terminal LR-tail. Cdc20 and Cdh1 also interact with the APC/C via this motif (Vodermaier et al., 2003). To investigate if our SICs inhibit separase by binding to the LR tail of separase, we generated a c-terminal truncated variant (separase$^{\Delta SLR}$), that lacks the three last amino acids. After the expression and immunoprecipitation of the GFP-tagged separase$^{\Delta SLR}$ from HEK293T cells and subsequent degradation of associated securin in *Xl.* egg extract (Figure 15A), the reconstituted separase variant was used in the Rad21 cleavage

assay. Surprisingly, separase$^{\Delta SLR}$ was not able to cleave Rad21 IVT at all (Figure 15B). Additionally, although co-immunoprecipitated securin was almost quantitatively degraded in *Xenopus* egg extract (Figure 15A), separase$^{\Delta SLR}$ did not cleave itself (Figure 15C), which corroborates the absence of catalytic activity of this mutant and therefore is not further pursued.

## 4.10 SIC1, SIC3 and SIC5 Cause Segregation Errors in Partial Separase Depleted Cells

Because the experimental setup of the SAC override experiments was based on an artificial and forced anaphase onset, which could mask or alter potential inhibitory effects of the tested compounds, we next wanted to test the inhibitors in a normal mitotic progression and check if they are able to trigger segregation defects. Unfortunately, none of the final lead compounds caused abnormalities during mitosis in HeLa cells (data not shown). Recollection of initial knock down experiments of separase in HeLa cells did show that insufficient depletion of separase does not lead to segregation defects (data not shown). We reasoned that minor amounts of active separase suffice for a normal mitotic progression. As a consequence, inhibition by small molecules can only lead to a phenotype, if most, if not the entire pool of separase is bound with inhibitory ligands and intermediate inhibition will not result in a noticeable phenotype. To create a condition with reduced separase levels that still allows normal chromosome segregation, separase was only partly depleted with a low concentration of siRNA (0.05 nM). Cells with residual separase protein levels of less than 25 %, as judged by western blot analyses, were able to exit mitosis with a comparable frequency of segregation errors as cells treated with non-targeting siRNA (Figure 16A-D). Cells with no detectable protein levels of separase show in more than 95 % of the cases severe segregation errors (Figure 16A-D). Observed phenotypes are anaphase bridges, lagging chromosomes, furrow ingression before chromosome segregation and multilobed daughter nuclei (Figure 16B). Partial separase-depleted HeLa cells were additionally incubated with 10 $\mu$M SIC1, 30 $\mu$M SIC3, 30 $\mu$M SIC5 or 10 $\mu$M Sepin-1, which triggered a higher occurrence of segregation errors compared to DMSO treated cells with SIC5 being the most potent compound (Figure 16E-F). The observed phenotypes were similar to the segregation defects in cells fully depleted of separase (Figure 16E and B). These results show that SIC1, SIC3 and SIC5 can inhibit endogenous separase in living cells.

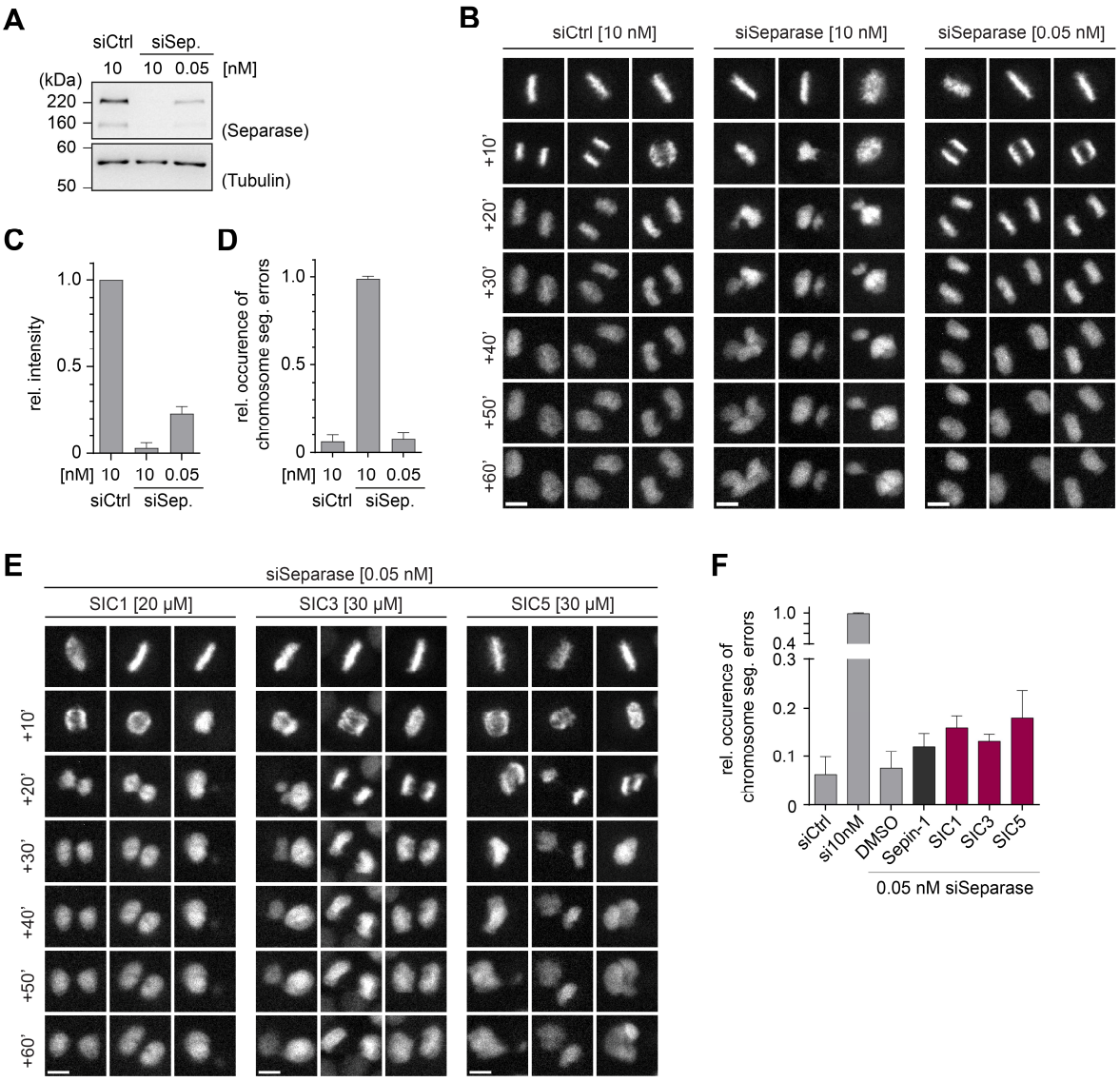


**Figure 16: Segregation errors in partial separase-depleted HeLa cells. (A)** Western Blot of HeLa cells treated with separase targeting siRNA or non-targeting siRNA at indicated concentrations. **(B)** Fluorescence microscopy of HeLa cells expressing H2B-mCherry. Three exemplary cells from each condition of the time lapse experiment are shown. Observed segregation errors are furrow ingression before chromosome segregation, anaphase bridges and multilobed nuclei; scale bar 10 µm. **(C)** Quantification of separase levels from (A), data from three independent experiments (mean and SD). **(D)** Quantification of segregation error frequencies from cells treated as in (B); quantified were more than 50 cells for each condition of one replicate, shown are mean and SD from three independent experiments. **(E)** Fluorescence microscopy of HeLa cells as in (B), partly depleted of separase, treated with SIC1, SIC3, SIC5, Sepin-1 and DMSO (0.5 %) as control; scale bar 10 µm. **(F)** Quantification of segregation errors from (E), quantified were more than 50 cells for each condition of one replicate; mean and SD from three independent experiments.

## 4.11 SAR Analysis Reveals Importance of Di-Indole and Halogen Moieties of SIC5

Next, we took a closer look on the chemical structure of SIC5 and tested the relevance of three main characteristic moieties of the lead compound: (i) the two indoles on the piperidine ring, by comparing the activity of two mono indole derivates; (ii) the sulfonyl group in the center, by substitution with a carbonyl group and (iii) the heteroatom in para-position on the phenyl

ring, which was substituted with different halogen atoms (Figure 17A-B). The Rad21 cleavage assay revealed that substituting the fluorine of SIC5 with a chlorine (SIC5-4), a bromine (SIC5-5) or an iodine (SIC5-6) was tolerated and even had an increased inhibitory effect. The carbonyl derivate (SIC5-3) did show a reduced inhibition but was still able to reduce Rad21 cleavage. The two mono-indole derivates vary in the absence (SIC5-1) or presence (SIC5-2) of a double bond in the piperidine ring that results in different orientation of the indole group. Both mono-indole derivates show greatly reduced inhibitory activity on Rad21 cleavage, which

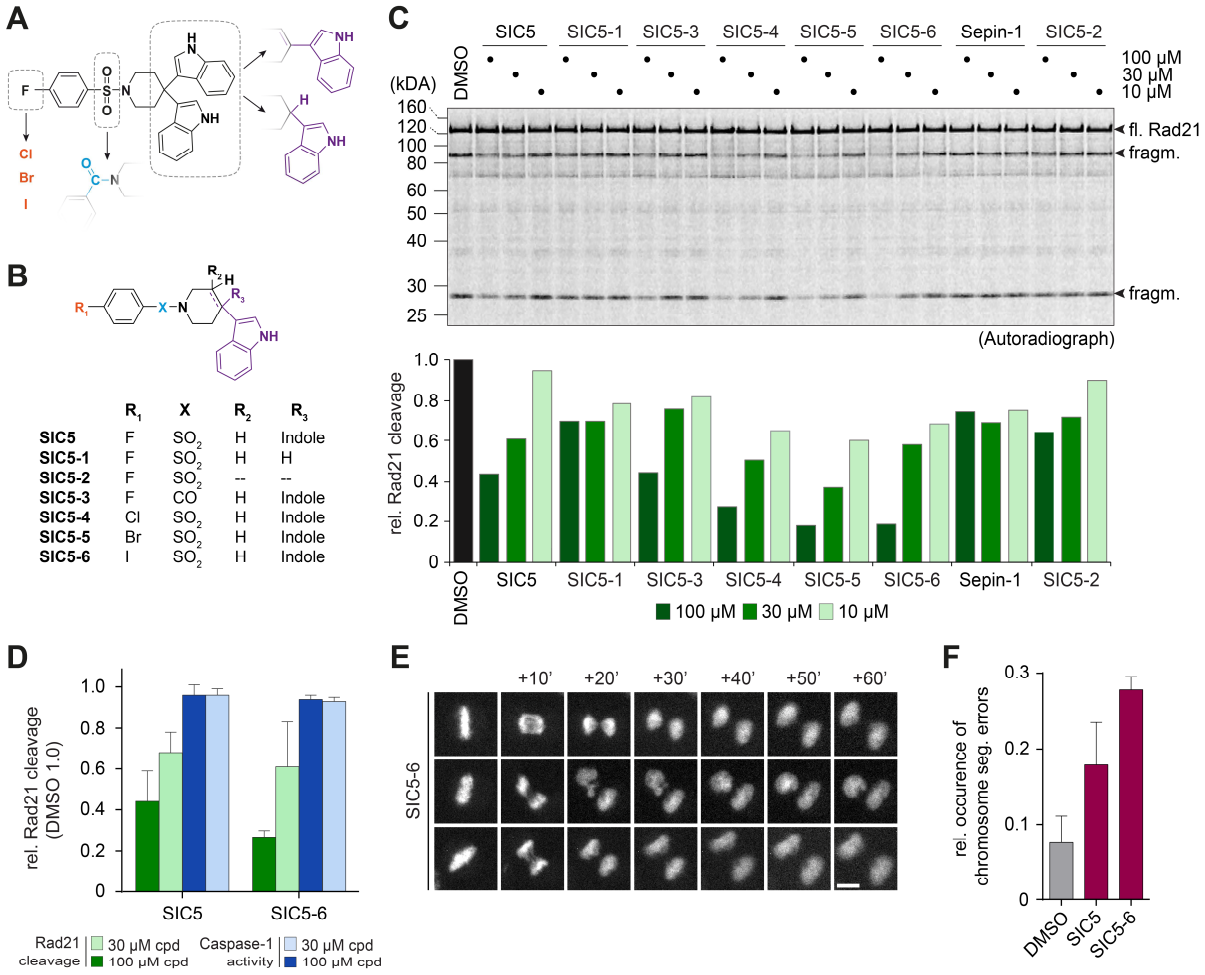


**Figure 17: Structure activity relation of SIC5. (A)** Chemical structure of SIC5 with different moieties highlighted that were changed to create derivates. **(B)** Summary of all SIC5 analogues with names. **(C)** (upper panel) Exemplary autoradiograph of Rad21 cleavage assay with SIC5 derivates and Sepin-1 at indicated concentrations; (lower panel) quantification of faster migrating Rad21 IVT fragment from upper panel. **(D)** Rad21 cleavage assay and Caspase-1 assay with SIC5 and SIC5-6; mean and SD from three independent experiments. **(E)** Fluorescence microscopy of HeLa cells expressing H2B-mCherry. Three exemplary cells from partly separase-depleted HeLa cells (as in Figure 13E) that were incubated with 30 µM SIC5-6 and show segregation errors; scale bar 10 µm. **(F)** Quantification of segregation error frequency of (E).

suggests an importance of the two indoles for inhibition of separase (Figure 17C). Based on the results of the separase *in vitro* assays and low solubility of SIC5-4 and SIC5-5 (data not shown), SIC5-6 was chosen for resynthesis. Just as SIC5, its iodine derivate (SIC5-6) did barely reduce

caspase-1 activity *in vitro* (Figure 17D). Motivated by the results of the reconstitution assays, we set out to test this improved inhibitor *in cellulo* with our partial separase-depleted cell setup. SIC5-6 triggered segregation errors in almost 30 % of all observed cells, which is 1.5 fold more than in cells treated with the original lead compound SIC5 (Figure 17E-F).

Overall, these results show the successful identification of new, noncovalent and specific small molecule inhibitors for separase, that are capable to trigger segregation errors in HeLa cells with reduced separase levels at mitotic exit.

# 5. Discussion

The aim of this study was to identify small molecule inhibitors that inhibit the protease activity of separase in cells. The results of this work show that the developed high-throughput screen, which was based on a reverse chemical genetics approach in living cells, and the subsequent validation with an activity assay, using the reconstituted target protease, succeeded in identifying specific small molecule inhibitors for separase that are able to trigger segregation errors in HeLa cells at mitotic exit.

## 5.1 High-throughput Screening Setup

In order to identify compounds that inhibit separase activity directly rather than by any upstream regulatory mechanism, the established cell-based HTS setup in this study was designed in a way that the measured protease activity was dependent on the overexpression of the ectopic hyperactive separase$^{PM2}$ variant in prometaphase arrested cells, where the endogenous protease is inactive. Due to the inability of separase$^{PM2}$ to be regulated by cyclin B1 (Stemmann et al., 2001) and the fact that its overexpression should exceed the available amount of endogenous securin, the sole remaining hindrance of sensor cleavage was supposed to be the different localization of the cytosolic protease and the nuclear substrate at the chromatin (Sun et al., 2006). Hence, one could expect the resulting sensor cleavage to happen at nuclear envelope breakdown as soon as these cells have entered mitosis. Surprisingly, sensor cleavage occurred only after 3.5 hours after mitotic entry (Figure 5E).

One explanation is the modulated expression of securin, which is able to adapt to the corresponding separase levels. It was shown in HEK293 cells, that ectopic expression of separase$^{PM2}$ is accompanied by a significant increase of securin expression (Holland and Taylor, 2006). Additionally, the recently revealed inhibitory regulation by Sgo2-Mad2 (Hellmuth et al., 2020) was not yet discovered and hence was not considered during the establishment of the screening setup and as a consequence may have reduced the amount of free and uninhibited separase. Yet, the earlier sensor cleavage was still dependent on the overexpression of separase$^{PM2}$. Assuming that during a prolonged prometaphase arrest the weakening of the SAC leads to a slow but steady degradation rate of securin, as it happens to cyclin B1 before mitotic slippage (Lok et al., 2020), it will eventually lead to a free pool of active separase and cause an earlier sensor cleavage. Additionally, the inability of separase$^{PM2}$ to be isomerized by Pin1 (Hellmuth et al., 2015b) and as a consequence remains in the less aggregation-prone *trans* conformation, increases the amount of active securin-free separase$^{PM2}$ during the prolonged

prometaphase arrest. Also it is very likely that during the overexpression, almost all available securin is bound by separase and the pool of separase-free securin is rather small. Consequently, already a small amount of securin degradation would be able to result in active separase.

In order to verify the robustness of the primary assay we used the Z' value, which is a statistical parameter to assess the quality of an experimental setup during a high-throughput screening (Zhang et al., 1999). Z' values greater than 0.5 are considered an excellent setup and therefor all assay plates with a Z' value below 0.5 were repeated. In fact, the majority of all assay plates scored a Z' value over 0.7 (Supplemental Table S1) and attests a high quality of the primary assay setup.

## 5.2 Validation of High-Throughput Screening

The primary assay of the HTS yielded 495 potential inhibitors out of the tested 51 009 small molecules, that sufficiently reduced the sensor cleavage in cells, while still allowing enough cells to enter mitosis. The resulting hit rate of 0.97 % is within the range that can be expected for a cell-based primary screening setup (Brito et al., 2020; Faloon et al., 2010; Hughes et al., 2011; Mayer et al., 1999). As secondary validation an *in vitro* activity assay with reconstituted separase was chosen, since orthogonal experimental setups are recommended to identify false positive compounds that act for instance on the assay readout rather than on the protein target (Thorne et al., 2010). During this subsequent *in vitro* validation assay, only 81 compounds inhibited separase activity and were able to reduce substrate cleavage to less than 50 % (Figure 10B). Hence, the majority of compounds that were identified in the primary assay turned out to be false positive hits.

One cause for false positive inhibitors might be a delay in mitotic entry. Because the correct correlation between sensor cleavage and separase activity during the HTS is only observed after a prolonged prometaphase arrest, compounds that delay - but not abolish - the entry into mitosis will score as hits, as long as this delay pushes the 3.5 hour window between mitotic entry and sensor cleavage to the moment of fixation. Aggregation-based inhibition can as well cause false positive hits during an inhibitor screen (Auld et al., 2004; Owen et al., 2012). Here, compounds form aggregates and subsequently form a suspension of large particles, that interact with proteins unspecifically and hinder substrate binding or reduce enzyme activity and might even trigger aggregation or precipitation of proteins themselves. A study that in particular searched for aggregation-based inhibitors in a cell-free assay setup, identified 1.7 % out of 70 563 molecules as detergent-sensitive compounds (Feng et al., 2007), which shows that this unspecific mode of inhibition has to be considered to cause a significant number of false

positives. As our primary HT setup was cell-based, an aggregation-based inhibition is less likely to happen by direct interaction with the intracellular target protein but is possible by indirectly affecting and slowing down cell cycle progression, for instance by interfering with membrane-bound receptors (Sassano et al., 2013) or by manipulation of extracellular components such as growth factors (Nishimura et al., 2016; Owen et al., 2012) and a resulting delay in cell cycle progression would consequently cause a delay in sensor cleavage as described above. The third cause for a false positive refers to the context discussed in chapter 5.1. Because separase$^{PM2}$ was only active after a prolonged arrest in prometaphase and was not fully independent of spindle assembly checkpoint activity, consequently means that any small molecule, which interferes with ubiquitination or proteasomal degradation of securin or enhances spindle assembly checkpoint activity, would score as a potential separase inhibitor in our high-throughput setup.

After the second validation step, of the remaining 81 compounds only five inhibitors remained (SIC1-SIC5) that significantly reduced separase activity in the presence of DTT (Figure 10D). Here, most likely compounds that act in an oxidative or covalent mode of action were eliminated. Although during the last decades covalent small molecule inhibitors have in a number of cases turned out to be specific and were even used for blockbuster drug development (Singh et al., 2011), we decided not to proceed with this class of inhibitors due to a high chance for off-target effects. Furthermore, the decreased inhibitory effect of Sepin-1 in the presence of DTT suggests that it as well acts in a covalent or oxidative mode of action and does not meet our requirements for a separase inhibitor after the secondary assays (Figure 10D+G). Results of the caspase-1 activity assay corroborated the latter finding due to a strong inhibitory effect of Sepin-1 and additionally demonstrated the high specificity of SIC1, SIC3 and SIC5 towards separase over caspase-1 (Figure 12A-B).

## 5.3 Additional Protease in Reconstituted Separase Preparations

During the attempt to use the peptide-based separase activity assay with our reconstituted separase in order to characterize the identified SICs with a kinetic readout, we unfortunately observed that the preparation of the catalytically inactive separase variant (separase$^{PD}$) seemed to efficiently cleave the fluorophore-conjugated substrate. As a consequence this assay setup was dismissed for further compound validation and was not further followed up on. Currently only speculations about the cause of this unspecific protease activity can be made. Although the preparation of the involved reconstituted separase was performed with almost the identical protocol as was used for obtaining active separase for the *in vitro* activity assay during the HTS that identified Sepin-1 (Zhang et al., 2014), the non-activated separase reconstitution in the

study of Basu and colleagues was not able to cleave the small peptide-based substrate (Basu et al., 2009). Although there, instead of Rhodamine-110, 7-Amino-4-Methylcoumarin (AMC) was used as reporter fluorophore, which is only conjugated with a single peptide and might explain the different outcomes.

Where could this protease activity originate from? After excluding the TEV protease, which was an obvious cause for the contaminating protease activity, since it is present in the elutions of all separase variants, but was unable to digest the fluorophore-conjugated substrate (Figure 12B-C), the inadvertent peptidase presumably originates from the HEK293T cell lysate or the *Xenopus* egg extract and was co-immunoprecipitated during the separase preparation. Additional size exclusion chromatography or dialysis might solve this issue but will most likely have to compromise with a lower yield due to the fast aggregation of securin-free separase (Hellmuth et al., 2015a).

## 5.4 Separase Inhibitors Delay Anaphase Events During Forced Mitotic Exit

To assess the impact of the inhibitors on native separase in anaphase on a biochemical level, all SICs were tested during a SAC override experiment. Except SIC1, all tested compounds caused a general delay in anaphase events by 5-10 minutes. Hence, the observed delay in separase activity could not be directly assigned to the inhibition of separase. Although the high-throughput setup would identify APC/C inhibitors as hits, all SICs have shown inhibition of Rad21 cleavage *in vitro*. The idea that all inhibitors, additional to separase, also inhibit the APC/C is highly unlikely, and consequently one might suggest a positive feedback loop in which separase promotes APC/C activation. Except for the interaction of separase with the APC/C (Bakos et al., 2018), there is currently no evidence to corroborate this hypothesis. However, the work from Mansfeld and collogues nicely shows the interaction of separase with the E3 ligase but the responsible binding motif on separase remains to be found. The c-terminal LR-tail of human separase could act as a possible APC/C binding motif and preliminary results hint that c-terminally truncated separase$^{\Delta SLR}$ indeed co-precipitates less APC/C compared to wildtype separase (data not shown). Further potential binding motifs on separase could be the auto-cleavage sites. Once cleaved, all three sites are MR- or LR-tails and are located on an unstructured loop that would facilitate sufficient flexibility to be accessible (Yu et al., 2021). This theory would allow interaction of separase with the APC/C only after separase activation and therefore inhibition of the latter would perturb their interaction and consequently a potential positive feedback would be affected as well. Further studies need to verify these hypotheses.

The most drastic effect during the SAC override experiments displayed SIC1, which efficiently induced apoptosis within two hours. Surprisingly, cells treated with the same concentration of SIC1 in interphase, as was done for the live-cell microscopy experiments with partial separase-depleted cells (Figure 17E-F) or with completely unperturbed cells (data not shown), did not show any apoptotic phenotype or any other cell cycle perturbations. Further studies with SIC1 might shed light onto this conundrum.

## 5.5 C-terminal Tail of Separase Is Essential for its Catalytic Activity

The discovery that truncating separase by three amino acids at the very c-terminal end leads to a complete loss of catalytic activity *in vitro* was unexpected. Data from Andreas Gericke's master thesis showed that in HeLa cells, which were depleted of endogenous separase, the ectopic expression of truncated separase$^{\Delta SLR}$ was not able to reverse the chromosome segregation error phenotype, whereas the ectopic wildtype protease did. Unfortunately, detailed information about the protein structure of human separase was not available at the time of the observation but the recent cryo-EM data from Boland and colleagues (Yu et al., 2021) shows that the c-terminal end of human separase is a structured region and Arginine2120 interacts with Glutamine1941 and Aspartate1944, which might positively contribute to an active conformational form of the enzyme. The lack of this interaction might lead to a severe conformational change or a destabilization of the active protease domain that eventually leads to the observed complete loss of activity but further investigation is needed to fully understand this phenomenon. However, comparing the available structure data of separase's active protease domains from human, yeast, nematode and fungus (Boland et al., 2017; Lin et al., 2016; Luo and Tong, 2017; Yu et al., 2021) reveals that the corresponding c-terminal region contributes to a β-sheet structure in the other three orthologs and supports this hypothesis.

## 5.6 A Fraction of Intracellular Separase Suffices for Mitotic Exit

Due to the lack of a small molecule separase inhibitor that is active in cells, which could serve as a reference to validate the new compounds, we decided to apply a knockdown approach to compare the cellular effects of the remaining SICs. This is a common approach for validation of small molecule inhibitors of new target proteins (Chen and Lampson, 2021). SiRNA-mediated separase knockdown, resulted in the described phenotypes of chromosome mis-segregation (Hauf et al., 2001; Waizenegger et al., 2002) including CUT (cell-untimely-torn, where chromosome masses are pinched-off by the cleavage furrow during cytokinesis, without fully

completing cytokinesis), DNA-bridges and multinucleated daughter cells with irregular shaped nuclei (Figure 17B). Importantly, the reduction of separase to only a quarter of its common protein level, still allowed a normal mitotic exit without a significant increase in segregation errors (Figure 17A-D). The purpose of this excess in separase levels is unknown and it consequently makes it for a small molecule inhibitor challenging to cause a phenotype. Since separase's high overexpression in cancer cells is known (Meyer et al., 2009; Zhang et al., 2008), one might consider untransformed cells with a regular protease level to be more suitable for this biological context and furthermore would expect cells to be more susceptible to small reductions in separase activity, be it caused by depletion or small molecule-inhibition. Surprisingly, preliminary results show that in untransformed RPE-1 cells, separase levels can be reduced to more than 50 % and do not show segregation errors (data not shown). Nevertheless, it is of great interest how the identified SICs behave when treated on RPE-1 cells.

## 5.7 Structure-activity relationship of SIC5 derivates

In order to gain insights into the significance of individual moieties of SIC5 that contribute to its inhibitory activity, six structurally similar derivates were synthesized. Based on the results of their inhibition *in vitro*, first crude conclusions of the structure-activity relationship could be drawn and revealed that in SIC5 (i) the two indole rings are essential for its biological activity, (ii) the sulfonyl group can be substituted by a carbonyl group but leads to a minor reduction of inhibition and (iii) the substitution in the para-position with other halogen atoms improved the inhibitory activity of the compound. Concerning the importance of the two indole groups, a number of small molecule protease inhibitors that contain an indole moiety and specifically target viral proteases are promising lead compounds to treat HIV or SARS-CoV-2 (Hattori et al., 2021; Nie et al., 2021; Sahin, 2021) and there is a noticeable interest in identifying new small molecule inhibitors that are based on an indole scaffold (Chehardoli and Bahmani, 2021). However, with our current results, which lack the mode of action and binding site of SIC5 on separase, it would be pure speculation to venture a guess on the potential interaction partners of the two indoles. Vinyl sulfonyl groups have been shown to efficiently inhibit cysteine proteases when conjugated to peptides (Palmer et al., 1995). Possibly the sulfonyl group of SIC5 might have a similar role for separase inhibition. The nucleophilic thiol of the active site cysteine could attack at the ortho-position of the phenyl ring, which should have an electrophilic character due to the sulfonyl group. Assuming this mode of action, a stronger electron withdrawing substitution in para-position of the phenyl ring would increase the electrophilic character and increase the inhibitory potential. However, fluorine has a stronger electron withdrawing effect than iodine, therefore SIC5 should have been more active than SIC5-6, if

this would be the only feature responsible for the efficacy of the compounds. Assuming that the moiety at the para-position interacts with less polar surfaces on separase, would result in a beneficial cumulative outcome for iodine over fluorine at this position.

Ultimately, a more complex and precise analysis of the structure-activity-relationship of the lead structure is only possibly after further derivatization of SIC5 to gain a more detailed correlation of essential moieties and potential tolerated substitutions that would eventually increase aqueous solubility and improve the biological availability. A revised compound with a four-fold increase of inhibitory activity should already be capable to trigger a phenotype in cells without prior partial depletion of separase.

## 5.8 Conclusion

In summary, we established a cellular system to monitor separase activity in living cells and successfully applied this approach to identify noncovalent inhibitors of separase. SIC1, SIC3, and SIC5 efficiently inhibited separase *in vitro*, but did not affect caspase-1, which, like separase, belongs to the CD clan of cysteine protease, indicating that they act in a specific manner. As shown by our RNAi experiments, minimal amounts of separase are sufficient to ensure the proper segregation of chromosomes implicating that inhibitors of separase have to be extraordinarily potent in order to inhibit the growth of cancer cells, which as shown by clinical studies often highly overexpress separase. In line with these observations, only HeLa cells partially depleted of separase displayed chromosome segregation errors when treated with SIC1, SIC3, or SIC5. On the basis of our *in vitro* and cellular analyses, we identified SIC5-6 as the most promising compound for the further development of bioactive separase inhibitors. Given the high overexpression of separase in a number of human cancers, the prime focus of future studies will be on the optimization of SIC5-6's potency, while maintaining its specificity for separase.

# 6. Materials and Methods

## 6.1 Materials

### 6.1.1 Information about chemicals, reagents and solutions

If not stated otherwise, all reagents were purchased from Sigma Aldrich at analytical reagent grade (p.a. purity) or cell culture grade and were used without further purification. Stock solutions of reagents were prepared in filtered, deionized ultrapure water of Milli-Q grade (Millipore) or in DMSO. For cellular experiments, the concentration of DMSO in cell culture medium never exceeded 0.5 % and experiments with appropriate solvent controls were performed to exclude DMSO related effects.

### 6.1.2 Antibodies

Listed are antibodies that were used in this study. For western blot analysis, all antibodies were prepared with the indicated dilution in blocking buffer with the exception of the Rad21 antibody, that was prepared in 5 % BSA in TBST. For immunofluorescence experiments, antibodies were diluted with the indicated dilutions in Abdil.

**Table 1: Antibodies used for western blot and immunofluorescence microscopy.** Information of primary and secondary antibodies used in this study, TUM # refers to internal identification system of the lab.

| Type | Recognized Antigen | TUM # | Host Species | Supplier | Dilution |
|---|---|---|---|---|---|
| Primary | Caspase-1 | 571 | mouse | Santa Cruz (sc-56036) | 1:1000 |
| Primary | Cdc27 | 363 | rabbit | self-made | 1:500 |
| Primary | Cyclin B2 (xenopus) | 493 | mouse | Santa Cruz (sc-53239) | 1:1000 |
| Primary | Cyclin B1 (human) | 308 | mouse | Millipore (05-373) | 1:2000 |
| Primary | GFP | 548 | mouse | Invitrogen (MA5-15256) | 1:1500 |
| Primary | H2B | 556 | rabbit | Abcam (ab1790) | 1:1000 |
| Primary | Histone H3 (phosphorylated at Ser10) | 327 | rabbit | Millipore, (06-570) | 1:1000 (IF) |
| Primary | mCherry tag | 401 | mouse | biorbyt (orb66657) | 1:1000 |
| Primary | p150 Glued | 537 | mouse | BD Laboratories (610473) | 1:1000 |
| Primary | PARP-1 | 629 | mouse | gift from AG Bürkle | 1:300 |
| Primary | Rad21 | 557 | rabbit | Abcam (ab992) | 1:2000 |
| Primary | Securin (human) | 541 | mouse | Abcam (DCS-280) | 1:1000 |
| Primary | Securin (xenopus) | 545 | rabbit | gift from O.Stemmann | 1:1000 |
| Primary | Separase | 543 | rabbit | gift from O.Stemmann | 1:1500 |
| Secondary (HRP) | rabbit | s33 | donkey | Dianova | 1:5000 |
| Secondary (HRP) | mouse | s34 | donkey | Dianova | 1:5000 |
| Secondary (HRP) | rabbit | s33 | donkey | Dianova | 1:5000 |

### 6.1.3 Buffers

Listed are all buffers that were used in this study. Buffers used for *in vitro* assays with reconstituted separase were sterile filtered (pore size 0.2 $\mu$m) before use.

**Table 2: Buffers and their composition used in this study.**

| Buffers | Composition |
|---|---|
| Abdil | 10 mM Tris-HCl (pH 7.4), 150 mM NaCl, 0.1 % Triton X-100, 2 % BSA, 0.02 % NaN3 |
| Blocking buffer | 5 % (w/v) milk powder in PBST or 5 % (w/v) BSA in TBST |
| Caspase assay buffer | 50 mM HEPES (pH 7.4), 100 mM NaCl, 0.1% (w/v) CHAPS, 10 mM DTT, 1 mM EDTA, 10% (v/v) glycerol |
| Coupling buffer | 0.2 M $NaHCO_3$, 0.5 M NaCl, pH 8.3 |
| CSF-XB | 10 mM HEPES/KOH (pH 7.7), 100 mM KCl, 0.1 mM $CaCl_2$, 2 mM $MgCl_2$, 50 mM Sucrose, 5 mM EGTA/KOH (pH 8.0) |
| Dejelly solution | 2 % L cysteine, 100 mM KCl, 1 mM $MgCl_2$, 0.1 mM $CaCl_2$ (pH 7.8) |
| ECL | 100 mM Tris/HCl (pH 8.5), 225 µM coumaric acid, 1.25 mM luminol, 0.01 % $H_2O_2$ |
| Laemmli buffer (3x) | 180 mM Tris-HCl (pH 6.8), 10 % (w/v) SDS, 30 % (w/v) glycerol, 15 % (w/v) β-mercaptoethanol, bromophenol blue |
| Lysis Buffer | 20 mM Tris-HCl (pH 7.7), 100 mM NaCl, 10 mM NaF, 20 mM β-glycerophosphate, 5 mM $MgCl_2$, 0.1 % Triton X-100, 5 % Glycerol, 1 mM EDTA, Roche cOmplete protease inhibitor cocktail |
| MMR | 5 mM Na-Hepes/NaOH (pH 7.8), 0.1 mM EDTA, 0.1 M NaCl, 2 mM KCl, 1 mM $MgCl_2$, 2 mM $CaCl_2$ |
| PBS | 137 mM NaCl, 2.7 mM KCl, 10 mM $Na_2HPO_4$, 1.8 mM $KH_2PO_4$ (pH 7.4) |
| PBST | 137 mM NaCl, 2.7 mM KCl, 10 mM $Na_2HPO_4$, 1.8 mM $KH_2PO_4$ (pH 7.4), 0.1 % Tween 20 |
| PERM puffer (4x) | 400 mM Pipes/KOH (pH 6.8), 40 mM EGTA, 4 mM $MgCl_2$, 0.8 % Triton-X-100 |
| Rad21 Assay buffer | 10 mM HEPES/KOH (pH 7.7), 50 mM NaCl, 25 mM NaF, with or without 10 mM DTT, 1 mM EGTA, 20% (v/v) glycerol |
| TBST | 10 mM Tris-HCl (pH 7.4), 150 mM NaCl, 0.1 % Triton X-100 |
| TEV cleavage buffer | 10 mM HEPES/KOH (pH 7.7), 50 mM NaCl, 25 mM NaF, 1 mM EGTA, 20 % (v/v) glycerol |

### 6.1.4 siRNA Oligos

Listed are siRNA oligos and their nucleotide sequence used in this study to for separase knockdown experiments.

**Table 3: List of nucleotide oligos.**

| TUM # | target protein | target sequence | Supplier |
|---|---|---|---|
| 241 | non-targeting siRNA | not revealed by data sheet | Qiagen, Cat. No 1027281 |
| 250 | Separase | CCGAGGAUCACUUGAAAUA | Dharmacon, On-TARGET plus, Cat. NoJ-004104-05 |

### 6.1.5 Primers

Listed are all primers that were used to generate separase mutants, which were used in this study or to check the sequence of the generated separase variants. Nucleotides given in capital letters correspond to original human template sequences as found in the wild type gene or cDNA and nucleotides given in lower case correspond to changes for the introduction of mutations.

**Table 4: Information of used primers in this study.** Nucleotide sequence and type of application of used primers. TUM number refers to internal identification system in the Mayer lab.

| TUM # | Name | Sequence | Type |
|---|---|---|---|
| 3072 | hu_ESPL1_P1 | CCTAGTACTCTTGGAGGATG | sequencing primer |
| 3073 | hu_ESPL1_P2 | TTGTCTGGATGCTGGAGG | sequencing primer |
| 3074 | hu_ESPL1_P3 | CAGGAAGGTATCGAGCGG | sequencing primer |
| 3075 | hu_ESPL1_P4 | TGCTGATGGGCAGTGAC | sequencing primer |
| 3076 | hu_ESPL1_P5 | CCCCCTCCTTGGTTCCA | sequencing primer |
| 3077 | hu_ESPL1_P6 | CCAGAGGGCCAGTGAC | sequencing primer |
| 3078 | hu_ESPL1_P7 | CTGGAAAAGGACAGTCCC | sequencing primer |
| 3414 | hu_Separase ΔSLR fwd | TGGCTTGCCTGTCTaaCTGCGGTAAGG | forward primer to mutate Ser2118 to STOP |
| 3415 | hu_Separase ΔSLR rev | CCTTACCGCAGttAGACAGGCAAGCCA | reverse primer to mutate Ser2118 to STOP |
| 3470 | hu_Separase C2029A fwd | CTGCTGTTTGGCgctAGCAGTGCGGCC | forward primer to mutate Cys2029 to Ala (Protease Dead) |
| 3471 | hu_Separase C2029A rev | GGCCGCACTGCTagcGCCAAACAGCAG | forward primer to mutate Cys2029 Ala (Protease Dead) |

### 6.1.6 Plasmids

Listed are plasmids that were used in this study.

**Table 5: Plasmid list.** Information of insert and backbone of used vectors in this study. TUM number refers to the internal identification system in the Mayer lab.

| TUM # | Gene insert | Insert Specification | Vector | Tag |
|---|---|---|---|---|
| 1865 | GFP-binding protein | | pET28a | C-term: His |
| 3026 | Rad21 | WT | pCS2 | |
| 3010 | Securin | WT | pCS2 | |
| 3243 | Separase(WT) | WT | pCS2 | N-term: eGFP-TEV |
| 3009 | Separase(P1127A) | P1127A mutant | pCS2 | N-term: eGFP-TEV |
| 3401 | Separase(C2029A, PD) | C2029A mutant (PD) | pCS2 | N-term: eGFP-TEV |
| 3337 | Separase(ΔSLR) | lacks C-term. aa2118-2120 | pCS2 | N-term: eGFP-TEV |
| 2842 | phiC31 integrase | | pCMV-Int | |
| 2926 | Separase sensor | H2B-mCherry-Rad21(aa128-268)-eGFP | pcDNA3.1 | |

## 6.1.7 Compounds from Cherry Picking

**Table 6: Small molecule IDs.** Compounds that were cherry picked for hit validation experiments. Listed are consecutive IDs from Cherry Picking (PickID) and screening facility internal unique IDs (uiid) from hit compounds that scored in the HTS as inhibitors.

| PickID | uiid |
|---|---|
| CDI01 | CD101C02 |
| CDI02 | CD101G13 |
| CDI03 | CD101H11 |
| CDI04 | CD101J15 |
| CDI05 | CD102B14 |
| CDI06 | CD102F16 |
| CDI07 | CD102F18 |
| CDI08 | CD102G11 |
| CDI09 | CD102L17 |
| CDI10 | CD102N07 |
| CDI11 | CD103C08 |
| CDI12 | CD103F20 |
| CDI13 | CD103G19 |
| CDI14 | CD103H20 |
| CDI15 | CD103J05 |
| CDI16 | CD103L20 |
| CDI17 | CD103N08 |
| CDI18 | CD104F02 |
| CDI19 | CD104K06 |
| CDI20 | CD106L01 |
| CDI21 | CD107I12 |
| CDI22 | CD108A03 |
| CDI23 | CD108P11 |
| CDI24 | CD109L02 |
| CDI25 | CD109O09 |
| CDI26 | CD111C14 |
| CDI27 | CD113B04 |
| CDI28 | CD113F19 |
| CDI29 | CD114D06 |
| CDI30 | CD114L08 |
| CDI31 | CD115F17 |
| CDI32 | CD116E06 |
| CDI33 | CD119L12 |
| CDI34 | CD120O02 |
| CDI35 | CD122I20 |
| CDI36 | CD122N05 |
| CDI37 | CD122N20 |
| CDI38 | CD125K02 |
| CDI39 | CD125M17 |
| CDI40 | CD126A11 |
| CDI41 | CD126C03 |
| CDI42 | CD126L03 |
| MB01 | MB003G09 |
| MB02 | MB004B06 |
| MB03 | MB004G01 |
| MB04 | MB004J16 |
| MB05 | MB005B06 |
| MB06 | MB006F11 |
| MB07 | MB006K07 |
| MB08 | MB006M03 |
| MB09 | MB007H01 |
| MB10 | MB008J19 |
| MB11 | MB010D08 |
| MB12 | MB010F18 |
| MB13 | MB010J13 |
| MB14 | MB013L20 |
| MB15 | MB019N12 |
| MB16 | NATx10F11 |
| MB17 | NATx10M08 |
| MB18 | NATx9L08 |
| MB19 | MB004E07 |
| MB20 | MB004G07 |

| PickID | uiid |
|---|---|
| MB21 | MB004M15 |
| MB22 | MB006H10 |
| MB23 | MB006O12 |
| MB24 | MB007A13 |
| MB25 | MB008D05 |
| MB26 | MB013O07 |
| MB27 | MB019F02 |
| MB28 | NATx10C09 |
| MB29 | NATx10E15 |
| MB30 | NATx10I13 |
| MB31 | MB001B15 |
| MB32 | MB001C14 |
| MB33 | MB001L20 |
| MB34 | MB001N20 |
| MB35 | MB002O13 |
| MB36 | MB003F18 |
| MB37 | MB003I19 |
| MB38 | MB003J09 |
| MB39 | MB003J14 |
| MB40 | MB003L09 |
| MB41 | MB004C17 |
| MB42 | MB004C20 |
| MB43 | MB004F15 |
| MB44 | MB004H01 |
| MB45 | MB004K08 |
| MB46 | MB005J14 |
| MB47 | MB005L14 |
| MB48 | MB005N04 |
| MB49 | MB006A07 |
| MB50 | MB007C06 |
| MB51 | MB007L10 |
| MB52 | MB008F05 |
| MB53 | MB008G14 |
| MB54 | MB008G16 |
| MB55 | MB008H18 |
| MB56 | MB008I18 |
| MB57 | MB009F02 |
| MB58 | MB010B02 |
| MB59 | MB010B10 |
| MB60 | MB010B16 |
| MB61 | MB010D16 |
| MB62 | MB010D18 |
| MB63 | MB010F08 |
| MB64 | MB010F20 |
| MB65 | MB010J16 |
| MB66 | MB010L20 |
| MB67 | MB010P20 |
| MB68 | MB011E14 |
| MB69 | MB011L14 |
| MB70 | MB011O07 |
| MB71 | MB012B02 |
| MB72 | MB012C04 |
| MB73 | MB012N20 |
| MB74 | MB013J15 |
| MB75 | MB013K13 |
| MB76 | MB013O17 |
| MB77 | MB013P02 |
| MB78 | MB015B17 |
| MB79 | MB015D07 |
| MB80 | MB015E10 |
| MB81 | MB015F03 |
| MB82 | MB015G13 |

| PickID | uiid |
|---|---|
| MB83 | MB015H09 |
| MB84 | MB015N20 |
| MB85 | MB016B01 |
| MB86 | MB017E17 |
| MB87 | MB017K13 |
| MB88 | MB017L16 |
| MB89 | MB017M08 |
| MB90 | MB018C08 |
| MB91 | MB018I06 |
| MB92 | MB018I07 |
| MB93 | MB018J18 |
| MB94 | MB018M07 |
| MB95 | MB018O05 |
| MB96 | MB018P03 |
| MB97 | MB019D06 |
| MB98 | MB019N09 |
| MB99 | MB020A02 |
| MB100 | MB020B17 |
| MB101 | MB020C06 |
| MB102 | MB020D04 |
| MB103 | MB020H13 |
| MB104 | MB020O11 |
| MB105 | MB020O17 |
| MB106 | MB022B08 |
| MB107 | MB022F17 |
| MB108 | MB022J02 |
| MB109 | MB022P15 |
| MB110 | MB023D19 |
| MB111 | MB023E06 |
| MB112 | MB023F05 |
| MB113 | MB023J16 |
| MB114 | MB023M04 |
| MB115 | MB023N17 |
| MB116 | MB024J19 |
| MB117 | MB024K11 |
| MB118 | MB024L19 |
| MB119 | MB024M14 |
| MB120 | MB025I19 |
| MB121 | MB026I17 |
| MB122 | MB027E17 |
| MB123 | MB027G19 |
| MB124 | MB027J19 |
| NATx01 | NATx2G20 |
| NATx02 | NATx2O18 |
| NATx03 | NATx4I12 |
| NATx04 | NATx4P21 |
| NATx05 | NATx5L17 |
| NATx06 | NATx6A10 |
| NATx07 | NATx6E06 |
| NATx08 | NATx6E07 |
| NATx09 | NATx6F14 |
| NATx10 | NATx6I10 |
| NATx11 | NATx6K08 |
| NATx12 | NATx6M04 |
| NATx13 | NATx6N05 |
| NATx14 | NATx6O21 |
| NATx15 | NATx7C08 |
| NATx16 | NATx7E12 |
| NATx17 | NATx7G10 |
| NATx18 | NATx7G21 |
| NATx19 | NATx7O07 |
| NATx20 | NATx8A16 |

| PickID | uiid |
|---|---|
| NATx21 | NATx8F04 |
| NATx22 | NATx8L05 |
| NATx23 | NATx8M16 |
| NATx24 | NATx8O22 |
| NATx25 | NATx9D08 |
| NATx26 | NATx9F08 |
| NATx27 | NATx9H05 |
| NATx28 | NATx9I07 |
| NATx29 | NATx9J06 |
| NATx30 | NATx9J13 |
| NATx31 | NATx9L08 |
| NATx32 | NATx9N09 |
| NATx33 | NATx9P08 |
| NATx34 | NATx10A10 |
| NATx35 | NATx10F11 |
| NATx36 | NATx10M08 |
| NATx37 | NATx11F07 |
| NATx38 | NATx11K16 |
| NATx39 | NATx12F08 |
| NATx40 | NATx12J07 |
| NATx41 | NATx12N15 |
| NATx42 | NATx13C21 |
| NATx43 | NATx13D14 |
| NATx44 | NATx13D20 |
| NATx45 | NATx13E06 |
| NATx46 | NATx13F13 |
| NATx47 | NATx13I17 |
| NATx48 | NATx13J18 |
| NATx49 | NATx13J20 |
| NATx50 | NATx13L18 |
| NATx51 | NATx13N14 |
| NATx52 | NATx14G06 |
| NATx53 | NATx16A05 |
| NATx54 | NATx16D05 |
| NATx55 | NATx16O22 |
| CBN01 | CBP1001K11 |
| CBN02 | CBP1001C18 |
| CBN03 | CBP1003C11 |
| CBN04 | CBP1003G11 |
| CBN05 | CBP1003M22 |
| CBN06 | CBP1004N10 |
| CBN07 | CBP1004F14 |
| CBN08 | CBP1005I08 |
| CBN09 | CBP1005F19 |
| CBN10 | CBP1006G11 |
| CBN11 | CBP1006O11 |
| CBN12 | CBP1006O08 |
| CBN13 | CBP1006C14 |
| CBN14 | CBP1006L04 |
| CBN15 | CBP1007K17 |
| CBN16 | CBP1007G02 |
| CBN17 | CBP1007H01 |
| CBN18 | CBP1007B17 |
| CBN19 | CBP1008C08 |
| CBN20 | CBP1008N02 |
| CBN21 | CBP1009E15 |
| CBN22 | CBP1010J21 |
| CBN23 | CBP1010P02 |
| CBN24 | CBP1011N09 |
| CBN25 | CBP1011L11 |
| CBN26 | CBP1011J04 |
| CBN27 | CBP1011F18 |

| PickID | uiid |
|---|---|
| CBN28 | CBP1012C01 |
| CBN29 | CBP1012I10 |
| CBN30 | CBP1012F09 |
| CBN31 | CBP1012P19 |
| CBN32 | CBP1012B16 |
| CBN33 | CBP1013M05 |
| CBN34 | CBP1013J05 |
| CBN35 | CBP1013H06 |
| CBN36 | CBP1015E22 |
| CBN37 | CBP1015F20 |
| CBN38 | CBP1016C05 |
| CBN39 | CBP1016K04 |
| CBN40 | CBP1016G20 |
| CBN41 | CBP1016J09 |
| CBN42 | CBP1016J19 |
| CBN43 | CBP1017C01 |
| CBN44 | CBP1017K02 |
| CBN45 | CBP1017A04 |
| CBN46 | CBP1017B13 |
| CBN47 | CBP1018C14 |
| CBN48 | CBP1018G20 |
| CBN49 | CBP1018I20 |
| CBN50 | CBP1018H13 |
| CBN51 | CBP1020I16 |
| CBN52 | CBP1020B17 |
| CBN53 | CBP1021G20 |
| CBN54 | CBP1022B08 |
| CBN55 | CBP2I19 |
| CBN56 | CBP2A06 |
| CBN57 | CBP2C08 |
| CBN58 | CBP2A20 |
| CBN59 | CBP2B01 |
| CBN60 | CBP2F09 |
| CBN61 | CBP2J17 |
| CBN62 | CBP4M19 |
| CBN63 | CBP4J19 |
| CBN64 | CBP4N21 |
| CBN65 | CBP5K01 |
| CBN66 | CBP5F18 |
| CBN67 | CBP6I11 |
| CBN68 | CBP6K13 |
| CBN69 | CBP6F07 |
| CBN70 | CBP8D20 |
| CBN71 | CBP8F20 |
| CBN72 | CBP8L20 |
| CBN73 | CBP9J13 |
| CBN74 | CBP9F15 |
| CBN75 | CBP9B19 |
| CBN76 | CBP10G15 |
| CBN77 | CBP10F20 |
| CBN78 | CBP10H20 |
| CBN79 | CBP10N20 |
| CBN80 | CBP10F22 |
| CBN81 | CBP10H22 |
| CBN82 | CBP10N22 |
| CBN83 | CBP10P22 |
| CBN84 | CBP11B12 |
| CBN85 | CBP11L12 |
| CBN86 | CBP12E09 |
| CBN87 | CBP12G20 |
| CBN88 | CBP12O22 |
| CBN89 | CBP12N17 |
| CBN90 | CBP12F02 |
| CBN91 | CBP13O01 |
| CBN92 | CBP13E03 |
| CBN93 | CBP13O03 |
| CBN94 | CBP13A05 |
| CBN95 | CBP13I13 |
| CBN96 | CBP13L12 |
| CBN97 | CBP14M19 |
| CBN98 | CBP14A21 |
| CBN99 | CBP15I08 |
| CBN100 | CBP15M08 |
| CBN101 | CBP15O08 |
| CBN102 | CBP16B11 |
| CBN103 | CBP16D19 |
| CBN104 | CBP16P04 |
| CBN105 | CBP16L06 |
| CBN106 | CBP16H08 |
| CBN107 | CBP16J08 |
| CBN108 | CBP16L08 |
| CBN109 | CBP17C04 |
| CBN110 | CBP17N21 |
| CBN111 | CBP18E08 |
| CBN112 | CBP18O22 |
| CBN113 | CBP19K02 |
| CBN114 | CBP20M03 |
| CBN115 | CBP20E09 |
| CBN116 | CBP20A13 |
| CBN117 | CBP20E19 |
| CBN118 | CBP20C20 |
| CBN119 | CBP20F12 |
| CBN120 | CBP21A19 |
| CBN121 | CBP21B05 |
| CBN122 | CBP22K22 |
| CBN123 | CBP22H11 |
| CBN124 | CBP23C08 |
| CBN125 | CBP24C01 |
| CBN126 | CBP24C07 |
| CBN127 | CBP24C12 |
| CBN128 | CBP24K12 |
| CBN129 | CBP24B07 |
| CBN130 | CBP24J15 |
| CBN131 | CBP24D17 |
| CBN132 | CBP24L17 |
| CBN133 | CBP24J12 |
| CBN134 | CBP25K21 |
| CBN135 | CBP27I11 |
| CBN136 | CBP27O22 |
| CBN137 | CBP28G02 |
| CBN138 | CBP28N17 |
| CBN139 | CBP29O18 |
| CBN140 | CBP30C22 |
| CBN141 | CBP31I11 |
| CBN142 | CBP31A17 |
| CBN143 | CBP31A10 |
| CBN144 | CBP34E08 |
| CBN145 | CBP34A10 |
| CBN146 | CBP34G12 |
| CBN147 | CBP35C13 |
| CBN148 | CBP35K13 |
| CBN149 | CBP35C15 |
| CBN150 | CBP35E15 |
| CBN151 | CBP35O15 |
| CBN152 | CBP35A17 |
| CBN153 | CBP35E17 |
| CBN154 | CBP35A19 |
| CBN155 | CBP35E19 |
| CBN156 | CBP35M21 |
| CBN157 | CBP35K04 |
| CBN158 | CBP35I06 |
| CBN159 | CBP35C16 |
| CBN160 | CBP35E16 |
| CBN161 | CBP35A18 |
| CBN162 | CBP35M18 |
| CBN163 | CBP35O20 |
| CBN164 | CBP35D07 |
| CBN165 | CBP35H13 |
| CBN166 | CBP35J13 |
| CBN167 | CBP35P04 |
| CBN168 | CBP35L08 |
| CBN169 | CBP35N10 |
| CBN170 | CBP35L18 |
| CBN171 | CBP36E02 |
| CBN172 | CBP36C04 |
| CBN173 | CBP36G04 |
| CBN174 | CBP36C16 |
| CBN175 | CBP36L14 |
| CBN176 | CBP36L16 |
| CBN177 | CBP37I19 |
| CBN178 | CBP37M21 |
| CBN179 | CBP37F17 |
| CBN180 | CBP38G17 |
| CBN181 | CBP38E06 |
| CBN182 | CBP38L12 |
| CBN183 | CBP39M05 |
| CBN184 | CBP39I13 |
| CBN185 | CBP39K15 |
| CBN186 | CBP39C17 |
| CBN187 | CBP39E17 |
| CBN188 | CBP39C16 |
| CBN189 | CBP39B19 |
| CBN190 | CBP39J10 |
| CBN191 | CBP40K13 |
| CBN192 | CBP40L03 |
| CBN193 | CBP40H15 |
| CBN194 | CBP40N19 |
| CBN195 | CBP40B02 |
| CBN196 | CBP40N06 |
| CBN197 | CBP40D10 |
| CBN198 | CBP41I15 |
| CBN199 | CBP41C17 |
| CBN200 | CBP41E17 |
| CBN201 | CBP41C02 |
| CBN202 | CBP41J17 |
| CBN203 | CBP41H18 |
| CBN204 | CBP42K05 |
| CBN205 | CBP42O05 |
| CBN206 | CBP42O07 |
| CBN207 | CBP43M18 |
| CBN208 | CBP43O18 |
| CBN209 | CBP43C20 |
| CBN210 | CBP44L21 |
| CBN211 | CBP44L04 |
| CBN212 | CBP45J12 |
| CBN213 | CBP46G06 |
| CBN214 | CBP46E20 |
| CBN215 | CBP46H07 |
| CBN216 | CBP47F14 |
| CBN217 | CBP3012E09 |
| CBN218 | CBP3012G15 |
| CBN219 | CBP3012J01 |
| CBN220 | CBP3012D03 |
| CBN221 | CBP3012L05 |
| CBN222 | CBP3012P13 |
| CBN223 | CBP3012F12 |
| CBN224 | CBP4008C12 |
| CBN225 | CBP4008A22 |
| CBN226 | CBP4008N01 |
| CBN227 | CBP4008H05 |
| CBN228 | CBP4009K01 |
| CBN229 | CBP4009J05 |
| CBN230 | CBP4009D13 |
| CBN231 | CBP4009L10 |
| CBN232 | CBP4009B16 |
| CBN233 | CBP4010E17 |
| CBN234 | CBP4010G17 |
| CBN235 | CBP4010I17 |
| CBN236 | CBP4010O17 |
| CBN237 | CBP4010A19 |
| CBN238 | CBP4010C21 |
| CBN239 | CBP4010E02 |
| CBN240 | CBP4010E06 |
| CBN241 | CBP4010E10 |
| CBN242 | CBP4010H05 |
| CBN243 | CBP4010L05 |
| CBN244 | CBP4010J06 |
| CBN245 | CBP4010N10 |
| CBN246 | CBP4010P22 |
| CBN247 | CBP4011O15 |
| CBN248 | CBP4011E17 |
| CBN249 | CBP4011C19 |
| CBN250 | CBP4011O19 |
| CBN251 | CBP4011C21 |
| CBN252 | CBP4011K04 |
| CBN253 | CBP4011M04 |
| CBN254 | CBP4011K22 |
| CBN255 | CBP4011F05 |
| CBN256 | CBP4011N12 |
| CBN257 | CBP4012A01 |
| CBN258 | CBP4012I13 |
| CBN259 | CBP4012E10 |
| CBN260 | CBP4012G10 |
| CBN261 | CBP4012G16 |
| CBN262 | CBP4012B07 |
| CBN263 | CBP4012D19 |
| CBN264 | CBP4012J21 |
| CBN265 | CBP4012D04 |
| CBN266 | CBP4012F16 |
| CBN267 | CBP4012L22 |
| AD01 | AD151B20 |
| AD03 | AD152B02 |
| AD05 | AD152F07 |
| AD06 | AD152F10 |
| AD07 | AD152F15 |
| AD08 | AD152L19 |
| AD09 | AD152M20 |
| AD11 | ICCB204D07 |
| AD12 | ICCB204N19 |
| AD13 | ICCB205A10 |
| AD14 | ICCB204F05 |
| AD15 | CBP4010E10 |
| AD16 | ICCB205A16 |
| AD18 | ICCB205C03 |
| AD19 | CBP1001C18 |
| AD20 | CBP1021G20 |

### 6.1.8 Small Molecules for Cell Experiments

**Table 7: List of used mall molecules.** Information about used compounds that were used for cell-based experiments. PickIDs are consecutive numbers from Cherry Picking and Uiids are screening facility-specific IDs.

| Name | Supplier/Source | PickID | uiid |
|---|---|---|---|
| Reversine | Sigma Aldrich | | |
| Sepin-1 | Vita-M Lab., Ltd (Cat. No. STK834355) | | |
| SIC1 | Maybridge, Ltd (Cat. No. HTS09338) | MB76 | MB013O17 |
| SIC2 | Vita-M Lab., Ltd (Cat. No. STL333156) | CBN124 | CBP23C08 |
| SIC3 | ChemDiv, Inc. (Cat. No. D008-0106) | CBN129 | CBP24B07 |
| SIC4 | ChemDiv, Inc. (Cat. No. K788-9124) | CBN179 | CBP37F17 |
| SIC5 | Synthesized by Matthias Frese (AG Marx) | CBN191 | CBP40K13 |
| SIC5-1 | Synthesized by Matthias Frese (AG Marx) | | |
| SIC5-2 | Synthesized by Matthias Frese (AG Marx) | | |
| SIC5-3 | Synthesized by Matthias Frese (AG Marx) | | |
| SIC5-4 | Synthesized by Matthias Frese (AG Marx) | | |
| SIC5-5 | Synthesized by Matthias Frese (AG Marx) | | |
| SIC5-6 | Synthesized by Matthias Frese (AG Marx) | | |
| ZM447439 | TOCRIS (Cat. No. 2458) | | |

## 6.2 Methods

### 6.2.1 Basic Molecular Biology Methods

#### 6.2.1.1 Cloning

All enzymes used in this study were purchased from New England BioLabs (NEB), if not otherwise stated. 1 µg DNA was digested using FseI (4 units/reaction) and AscI (8 units/reaction) restriction enzymes in 50 $\mu$L CutSmart buffer (NEB) for 1 h at 37°C. The 5'-phosphate of the digested plasmid backbone was removed by incubating with Calf intestinal phosphatase (CIP, 10 units/reaction) for 10 min at 37°C. Products of the restriction digest were supplemented with DNA loading buffer (2.5 % Ficoll 400, 0.04 % Orange G) and separated on a 0.8 % agarose gel in TBE buffer by gel electrophoresis at 100 V. DNA was recovered from agarose gel slices using the ZymocleanTM Gel DNA Recovery Kit (Zymo Research) according to the enclosed protocol of the kit. Ligation of an insert into a new vector backbone was carried out with T4 DNA ligase overnight at 16°C.

For transformation, an aliquot of competent *E. coli* TG1 bacteria (100 $\mu$L) was thawed on ice and half of the ligation reaction was added. After incubation on ice for 20 min, a heat shock for 45 s at 42°C was done and subsequently bacteria were spread on LB agar plates supplemented with 100 µg/mL ampicillin and incubated overnight at 37°C. For plasmid amplification, 4 mL of liquid LB or TB medium supplemented with 100 µg/mL ampicillin were inoculated with a single bacterial colony and grown for 6 h at 37°C and 180 rpm. Cells were harvested and the plasmid DNA purified using the NucleoSpin Plasmid EasyPure kit (Macherey-Nagel) according to the enclosed protocol of the kit with the exception that the elution was done with Milli-Q water. For larger plasmid amplification, 100 mL of TB medium were inoculated, grown overnight at 30°C and plasmid DNA was purified using the NucleoBond Xtra Midi kit (Macherey-Nagel) according to the enclosed protocol of the kit. Validation of the correct nucleotide sequences was performed by GATC/Eurofins.

#### 6.2.1.2 Site-directed Mutagenesis

To generate the different separase variants, site-directed mutagenesis according to the manufacturer's protocol (QuikChange site-directed mutagensis, Stratagene) was performed in a Veriti™ 96-Well Thermal Cycler. The newly synthesized DNA was transformed into competent *E. coli* Turbo bacteria as described in section 6.2.1.1.

#### 6.2.1.3 SDS Polyacrylamide Gel Electrophoresis (SDS-PAGE)

Laemmli sample buffer (1.5 x final concentration) was added to protein samples, lysate or collected cell pellets. After boiling the samples for 5 min at 95°C, samples were loaded on denaturing SDS-polyacrylamide gels based on a discontinuous buffer system (separating gel: 375 mM Tris (pH 8.8), 0.1 % SDS, 8-12 % acrylamide/bisacrylamide; stacking gel: 62.5 mM Tris (pH 6.8), 0.025 % SDS, 5 % acrylamide/bisacrylamide). Proteins were separated according to their molecular weight and electrophoretic mobility by applying a current of 25-35 mA for a small gel (15 samples) and 50-75 mA for a large gel (30 samples). PageRuler™ Unstained Protein Ladder (ThermoFisher Scientific) and Pre-stained BenchMark™ (Invitrogen) were used as a size ladder for protein electrophoresis. Separated protein samples were either directly visualized by Coomassie Brilliant Blue staining or further processed for western blot analysis (see following section).

#### 6.2.1.4 Western Blotting

For immunological detection separated proteins were electrophoretically transferred via a wet blot method on a nitrocellulose blotting membrane (Amersham™ Protran™, 0.45 µm NC, GE Healthcare) using inhouse made blotting chambers. The transfer was performed for 1 h for small gels (15 samples) or 2 h for large gels (30 samples) at 4°C in ice-cold transfer blot buffer at a constant voltage of 120 V. Subsequently, membranes were incubated 45 min in blocking buffer at room temperature. Membranes were incubated with primary antibodies (table 8) overnight at 4°C. Subsequently, the membrane was washed three times for 5 min with PBST or TBST and incubated for 45 min at room temperature with a horseradish- peroxidase (HRP)-conjugated secondary antibody (table 9). After three 5 min washes with PBST or TBST, bound antibodies were detected via a chemiluminescence reaction using an enhanced chemiluminescence (ECL) solution. Light signals were detected using a LAS-3000 system (Fujifilm).

### 6.2.2 Cell Culture

All cells were cultured in DMEM (Gibco, ThermoFisher Scientific, REF. 61965-026) supplemented with 5 % FCS (Gibco, ThermoFisher Scientific) for high throughput screening or 10 % FCS for all other experiments and incubated at 37 °C and 5 % $CO_2$. HeLa and HEK293-T cell lines stably expressing H2B-mCherry-Rad21$^{128\text{-}268}$-eGFP (separase activity sensor) were generated using PhiC31 integrase for recombination with attB sites. Clones were selected with 0.5 mg/mL Geniticin (Invivogen). For stable and inducible expression of myc-tagged separase$^{PM2}$ the corresponding transgene was stably integrated into HEK293-FlpIn-TRex (Invitrogen) already carrying the separase sensor. Clones were selected with 150 µg/mL Hygromycin B (Roth).

#### 6.2.2.1 Ectopic Separase$^{PM2}$ Expression Time Course

For the seprasePM2 expression time course, an 80 % confluent 15 cm cell culture dish with thymidine synchronized HEK293 screening cells was released from S-phase arrest by washout with PBS and reseeded in a 10 cm cell culture dish. During the following 6 hrs of incubation, samples were taken every 30 minutes, which agitated the cell suspension sufficiently to prevent the adhesion of cells. Samples were centrifuged (350 g, 5 min), washed once with PBS and flash-frozen in liquid nitrogen and subsequently analyzed by SDS-Page and western blot.

### 6.2.2.2 Cell-based High Throughput Screen

HEK293-T cells stably expressing the separase activity sensor were incubated in 2 mM thymidine for 20 hrs to arrest them in G1/S. After washing two times with PBS, cells were trypsinized and seeded in 384-well plates (10,000 cells/well; 50 $\mu$L) in full growth medium supplemented with tetracycline (1 $\mu$g/$\mu$L) and taxol (230 nM) to induce expression of separase$^{PM2}$ and to arrest cells in prometaphase. 4 hrs after release from thymidine, screening compounds (80 nL) in DMSO were transferred to the assay plate with a liquid handling robot (TECAN Freedom Evo workstation) and 30 $\mu$L medium was added to each well with a Multidrop® to equally distribute the added compounds in each well. 24 hrs after thymidine release, cells were fixed with 4 % formaldehyde in PBS for 12 minutes and washed twice with 80 $\mu$L PBS. Image acquisition was done with a Molecular Devices ImageXpress$^{MICRO}$ equipped with a Nikon Plan Apo 20x/0.75 DIC N2. Cell segmentation, mitotic classification and hue value measurements were done with KNIME. Compounds that did not reduce the relative mitotic index (compared to the control cells that do not express separase$^{PM2}$) below 80 % and inhibited the relative sensor cleavage (compared to the control cells that do not express separase$^{PM2}$) in mitotic cells to more than 70 % were selected.

In total, 51009 small molecules from commercially available libraries (Maybridge: Hitkit9000 [9000 compounds with unknown target], ChemBioNet 1-3 [27231 compounds with unknown target], ChemDiv [8298 compounds with unknown target] , Analyticon Discovery 1 [1000 natural compounds], Analyticon Discovery 2 [5000 semi-natural compounds] and Biomol ICCB [480 compounds with known target]) were tested.

### 6.2.2.3 Immunofluorescence Microscopy

HEK293T screening cells were treated as described in section 6.2.2.2 with a different fixation buffer. All following steps were performed in the 384 well plate with a volume of 50 $\mu$L. Cells were fixed with PERM buffer (100 mM Pipes/KOH (pH 6.8), 10 mM EGTA, 1 mM $MgCl_2$, 0.2 % Triton-X-100) supplemented with 4 % formaldehyde for 15 min at RT. After removal of the PERM buffer, fixed cells were washed once with TBST and blocked with Abdil buffer at 4°C overnight. Primary antibodies were diluted (see table 10) in Abdil buffer and incubated on cells for 45 min at RT. After three washes with TBST for 10 min, a Cy5-conjugated secondary antibody (see table 11) was incubated for 45 min at RT. Cells were washed three times with TBST and submitted to image acquisition in a ImageXpress$^{MICRO}$ (Molecular Devices) equipped with a Nikon Plan Apo 20x/0.75 DIC N2.

#### 6.2.2.4 Taxol-ZM Override

HeLa cells from two confluent 15 cm cell culture dishes that were synchronized in S-phase by a single thymidine block, were released in medium containing 250 nM Taxol and distributed on six 10 cm cell culture dishes. After 16 hours, DMSO or the indicated small molecules were added and incubated for additional two hours. Mitotic cells were harvested by mitotic shake-off and pelleted at 350 g for 3 min. Cells were resuspended in $CO_2$-independent medium containing 10% FCS, 1x GlutaMAX and 20 $\mu$M ZM447439. The individual cell suspensions were transferred onto a 6-well plate and further incubated at 37 °C without $CO_2$ atmosphere. To create homogenous cell suspensions before samples were taken for western blot analysis, cells were resuspended with a cut tip prior to every time point. Cells were centrifuged at 1000 g for 1 min, washed once with PBS and flash-frozen in liquid nitrogen. Cells were lysed and analyzed by SDS-PAGE and subsequent western blot (see section 6.2.1.3 and 6.2.1.4).

#### 6.2.2.5 RNA Interference

HeLa cells were transfected with siRNA for 48 h prior to time lapse experiments using Lipofectamine RNAiMAX Transfection Reagent (Invitrogen®, REF13778-075) according to manufacturer's instructions (reverse transfection method) with minor alterations. In brief, 40 000 HeLa cells per well were seeded in a 12-well plate. Dharmacon ON-TARGET*plus* siRNA against separase (5'-GAUCGUUUCCUAUACAGUA-3') was used at 10 nM or 0.05 nM final concentration and non-targeting siRNA was used at 10 nM final concentration. Only 1.5 $\mu$L Lipofectamine reagent per well, instead of 3 $\mu$L, were used for transfection. 48 hrs after siRNA transfection, cells were used for live cell time lapse experiments.

#### 6.2.2.6 Live Cell Microscopy

For live cell microscopy, cells were imaged in 12 well or 24 well plates using a VisiScope Analyzer microscope setup (Visitron), which includes a Zeiss Observer Z1 with an incubation chamber environment, a Zeiss Colibri LED illumination system and a Zeiss Definite Focus system. Cells were synchronized by S-phase arrest with 2 mM thymidine for 18 hrs and released by washing three times with PBS. For partial/full depletion experiments using siRNA, cells were prior subjected to a knockdown procedure (see section 1.2.2.5). Addition of potential hit compounds was done directly after release from thymidine using $CO_2$-independent medium (Gibco, REF 18045-54) supplemented with 10 % FCS and 1x GlutaMax. During the time lapse

acquisition, cells were imaged every 10 minutes until 24 hrs after release from thymidine. Image analysis was done with MetaXpress (Molecular Devices) and ImageJ.

### 6.2.3 Preparation of Reconstituted Separase

#### 6.2.3.1 Recombinant Expression and Purification of GFP-Binding Protein (GBP)

As published by Heinrich Leonhardt and coworkers (Rothbauer et al., 2008), the GBP can be recombinantly expressed and used for immunoprecipitations of GFP-tagged proteins. The coding sequence of the GFP-binding VHH domain was cloned into the pET28(+) vector (received from the Stemmann group, University of Bayreuth), with a C-terminal $His_6$-tag. The GBP was expressed in bacteria and purified using affinity chromatography with Protino Ni-IDA resin (*Macherey-Nagel*) following the manufacturer's instructions with minor modifications. *E.coli* bacteria (strain BL21(DE3)-RIL) were transformed with the before mentioned pET28(+) plasmid and grown in 20 mL LB media supplemented with 100 µg/ml ampicillin and 34 µg/ml chloramphenicol at 37°C overnight. The overnight culture was used to inoculate 1 L LB media supplemented with ampicillin and chloramphenicol and grown until the $OD_{600}$ of 0.8 was reached. Protein expression was then induced by addition of 1 mM isopropyl β-D-1-thiogalactopyranoside (IPTG) and the cell suspension was cooled down to 20°C. After 20 hrs of shaking at 20°C, the cells were harvested by centrifugation (6000 g, 10 min, 4°C), washed with PBS and centrifuged again (4000 g, 10 min, 4°C). The Pellet was resuspended in 80 mL Milli-Q-water supplemented with protease inhibitor cocktail (Roche, cOmplete EDTA-free protease inhibitors) and distributed equally in two falcon tubes. The cell suspension was slowly frozen at -20°C overnight and thawed on ice. For thorough lysis an EmulsiFlex-C5 (Avestin) was used and the resulting lysate was cleared by centrifugation (30000 g, 30 min, 4°C). To the cleared supernatant 50 mM $NaH_2PO_4$ buffer (pH 8.0) and 0.3 M NaCl (final concentrations) were added. For binding, the cleared supernatant was distributed equally in three tubes to 200 mg (500 µL) Protino Ni-IDA resin and incubated for 1 h on a rotating wheel at room temperature. The lysate resin suspensions were transferred to three empty chromatography columns (BioRad). The resin was washed with 50mM $NaH_2PO_4$ buffer containing 0.3M NaCl (pH 8.0). His-tagged GBP was eluted in fractions by adding half the bed volume of elution buffer (50 mM $NaH_2PO_4$ buffer containing 0.3 M NaCl and 0.1 M Imidazole (pH 8.0)) eight times. Fractions with the highest protein concentration from all columns, judged by the absorbance at 280 nm and Coomassie stained gel, were pooled and the final concentration was adjusted to 1 mg/mL with 50 mM $NaH_2PO_4$ buffer. The purified GBP was aliquoted, flash-frozen in liquid nitrogen and stored at -80 °C.

#### 6.2.3.2 Coupling of GFP-Binding Protein (GBP) to NHS-Activated Beads

NHS-activated Sepharose beads (GE Healthcare, 17-0906-01) were conjugated with GBP according to the manufacturer's instructions with minor modifications. In short, 800 $\mu$L bead slurry (400 $\mu$L beads) were coupled with 2 mg GBP in coupling buffer (0.2 M $NaHCO_3$, 0.5 M NaCl, pH 8.3) over night at 4°C on a rotating wheel. To block unreacted NHS groups, the beads were blocked with 5% BSA in lysis buffer (20 mM Tris-HCl (pH 7.7), 100 mM NaCl, 10 mM NaF, 20 mM β-glycerophosphate, 5 mM $MgCl_2$, 0.1 % Triton X-100, 5 % Glycerol, 1 mM EDTA, Roche cOmplete protease inhibitor cocktail) over night at 4 °C. Beads were washed with lysis buffer stored in a 50 % slurry in lysis buffer containing 0.025% $NaN_3$ at 4°C.

#### 6.2.3.3 Preparation of *Xenopus laevis* CSF Extract

For each separase preparation, *Xenopus laevis* eggs arrested in MII of meiosis were collected from 6 to 8 frogs. Collected eggs were washed with MMR buffer (5 mM Na-Hepes/NaOH (pH 7.8), 0.1 mM EDTA, 0.1 M NaCl, 2 mM KCl, 1 mM $MgCl_2$, 2 mM $CaCl_2$) until all dirt and other non-egg particles were removed. Eggs were incubated for 6 min in dejellying solution (2 % L-cysteine, 100 mM KCl, 1 mM $MgCl_2$, 0.1 mM $CaCl_2$, pH 7.8) and washed with CSF-XB (10 mM HEPES/KOH (pH 7.7), 100 mM KCl, 0.1 mM $CaCl_2$, 2 mM $MgCl_2$, 50 mM sucrose, 5 mM EGTA/KOH (pH 8.0)) four to six times. Dejellied eggs were transferred with a widened glass pipette into BECKMAN centrifuge tubes prefilled with 800 $\mu$L CSF-XB supplemented with 0.1 mg/mL cytochalasin B and centrifuged shortly (165 g, 1 min followed by 330 g, 1 min, 4°C) to stack eggs and to collect excess of buffer, which was carefully removed with a pipette. After the crushing spin (16500 g, 10 min, 4°C), the cytoplasmic fraction, which is located between the cell debris at the bottom and the lipid layer at the top of the resulting egg extract, was collected with a syringe that was punched through the centrifuge tube. The collected CSF extract was supplemented with 10 $\mu$g/mL cytochalasin B and stored on ice and used within the next 3 hrs.

#### 6.2.3.4 Preparation of Activated Separase

Isolation and activation of the different separase variants was performed as described previously (Hellmuth et al., 2015b; Stemmann et al., 2001) with minor modifications. As expression system for the different separase variants, HEK293-T cells were used. For each separase preparation five 15 cm cell culture dishes were transfected with 40 $\mu$g plasmid coding for the separase construct (see table 12) and 20 $\mu$g plasmid coding for securin (see table 13). All

constructs were transfected with calcium phosphate precipitation and supplemented with 50 $\mu$M Chloroquine to enhance the transfection efficiency. 30 hrs after transfection, taxol (250 nM) was used to arrest the cells in prometaphase. After a total of 48 hrs after the transfection, all cells were collected, washed once in PBS and flash-frozen in liquid nitrogen. After the cell pellet was thawed on ice, cell clumps were removed by a rotating dounce tissue homogenizer before cell lysis in 10 mL lysis buffer. GFP-tagged separase/securin complexes were immunoprecipitated using 200 - 300 $\mu$L GBP-coupled sepharose beads (see section 6.2.3.2) for 4 hrs at 4°C. After the immunoprecipitation, the beads were washed twice with 10 mL lysis buffer and three times with CSF-XB. To strip separase from its co-immunoprecipitated inhibitor securin, the beads were incubated in anaphase-like *Xenopus laevis* egg extract (calcium-released CSF extract (see section 6.2.3.3), supplemented with energy mix (3 mM creatine phosphate, 4 mM ATP, 4 mM $MgCl_2$), 10 $\mu$g/mL creatine phosphokinase, 60 $\mu$g/mL ubiquitin (BostonBiochem) and 200 - 500 nM cyclinB1$^{\Delta 90}$) for 45 min at 20°C on a roller. Beads were washed five times with 10 mL CSF-XB and three times with 10 mL TEV-cleavage buffer. Elution of activated separase from beads was achieved using recombinant TEV protease (0.56 mg/mL) in 150 $\mu$L TEV-cleavage buffer (10 mM HEPES/KOH pH 7.7, 50 mM NaCl, 25 mM NaF, 1 mM EGTA, 20% (v/v) glycerol) at 4°C for 4 hrs. The elution step was repeated one or two additional times and yielded in total 3-5 $\mu$g securin-free separase.

### 6.2.4 *In vitro* Biochemical Assays

#### 6.2.4.1 Rad21 Cleavage Assay

[$^{35}$S]-methionine-labeled Rad21 was *in vitro* expressed using (TnT® SP6 High-Yield Wheat Germ Protein Expression System from Promega) in presence of [$^{35}$S]-methionine according to the manufacturers' instructions. 8 ng separase in 12 $\mu$L assay buffer (10 mM HEPES/KOH (pH 7.7), 50 mM NaCl, 25 mM NaF, with or without 10mM DTT, 1 mM EGTA, 20% (v/v) glycerol) was incubated with compounds or DMSO for 5 minutes on ice. [$^{35}$S]-methionine-labeled *in vitro* translated (IVT) Rad21 was used as substrate. 10 nL Rad21 IVT in 3 $\mu$L assay buffer were added to the reaction and mixed. The reaction was incubated at 30°C for 30 minutes in a Veriti™ 96-Well Thermal Cycler. Addition of Lämmli buffer stopped the reaction and samples were cooked at 95°C for 5 min. Cleaved Rad21 was separated by SDS-PAGE and visualized by autoradiography. The smaller cleavage fragment was quantified using ImageJ.

#### 6.2.4.2 Caspase-1 Assay

To measure Caspase-1 activity the Caspase-1 assay kit for drug discovery (Enzo BML-AK701-0001) was used according to the manufacturer's instructions with minor alterations. The assay was scaled down to 50 $\mu$L total reaction volume (instead of 100 $\mu$L) and performed in a clear bottom 384 well plate (Greiner Bio-One). In brief, 25 U of Caspase-1 was mixed with DMSO or the compound to be tested in 25 $\mu$L assay buffer (50 mM HEPES (pH 7.4), 100 mM NaCl, 0.1% (w/v) CHAPS, 10 mM DTT, 1 mM EDTA, 10% (v/v) glycerol), transferred to the assay plate and preincubated 10 minutes at assay temperature (30°C). The reaction was started by adding the substrate Ac-YVAD-AMC in 25 $\mu$L assay buffer and the reaction kinetics was measured by fluorescence (Ex/Em: 340/485 nm) in a Tecan F500 plate reader every 20 seconds for 30 minutes at 30°C. Caspase-1 inhibitor Ac-YVAD-CHO was used as a negative control. Enzyme activity was determined by linear regression analysis using Microsoft Excel.

#### 6.2.4.3 Separase Peptide Cleavage Assay

The peptide-based separase activity assay was performed as published in works from the Pati lab (Basu et al., 2009; Zhang and Pati, 2018) with minor modifications. In brief, different quantities of reconstituted separase (see section 6.2.3.4) or TEV protease in 25 $\mu$L assay buffer (10 mM HEPES/KOH (pH 7.7), 50 mM NaCl, 25 mM NaF, 10mM DTT, 1 mM EGTA, 20% (v/v) glycerol) were incubated for 5 minutes on ice. All reaction mixes were transferred to a 384 well plate and warmed up to 30°C on a plate incubator. The addition of 10 $\mu$L assay buffer with the peptide substrate (D-R-E-I-Nle-R)$_2$-Rh110 (40 $\mu$M final concentration) started the reaction. The substrate turnover was monitored by fluorescence intensity (Ex/Em: 485/535 nm) every 20 s for 30 min at 30°C in a TECAN F500 plate reader. Enzyme activity was determined by linear regression analysis using Microsoft Excel.

# 7. References

Alexandru, G., Uhlmann, F., Mechtler, K., Poupart, M.A., and Nasmyth, K. (2001). Phosphorylation of the cohesin subunit Scc1 by Polo/Cdc5 kinase regulates sister chromatid separation in yeast. Cell *105*, 459-472.

Alexandru, G., Zachariae, W., Schleiffer, A., and Nasmyth, K. (1999). Sister chromatid separation and chromosome re-duplication are regulated by different mechanisms in response to spindle damage. The EMBO journal *18*, 2707-2721.

Auld, D.S., Inglese, J., and Dahlin, J.L. (2004). Assay Interference by Aggregation. In Assay Guidance Manual, S. Markossian, A. Grossman, K. Brimacombe, M. Arkin, D. Auld, C.P. Austin, J. Baell, T.D.Y. Chung, N.P. Coussens, J.L. Dahlin*, et al.*, eds. (Bethesda (MD)).

Bai, X., and Bembenek, J.N. (2017). Protease dead separase inhibits chromosome segregation and RAB-11 vesicle trafficking. Cell cycle (Georgetown, Tex) *16*, 1902-1917.

Bakos, G., Yu, L., Gak, I.A., Roumeliotis, T.I., Liakopoulos, D., Choudhary, J.S., and Mansfeld, J. (2018). An E2-ubiquitin thioester-driven approach to identify substrates modified with ubiquitin and ubiquitin-like molecules. Nature communications *9*, 4776.

Bardin, A.J., and Amon, A. (2001). Men and sin: what's the difference? Nat Rev Mol Cell Biol *2*, 815-826.

Barnum, K.J., and O'Connell, M.J. (2014). Cell cycle regulation by checkpoints. Methods Mol Biol *1170*, 29-40.

Basu, D., Zhang, N., Panigrahi, A.K., Horton, T.M., and Pati, D. (2009). Development and validation of a fluorogenic assay to measure separase enzyme activity. Anal Biochem *392*, 133-138.

Bembenek, J.N., Richie, C.T., Squirrell, J.M., Campbell, J.M., Eliceiri, K.W., Poteryaev, D., Spang, A., Golden, A., and White, J.G. (2007). Cortical granule exocytosis in C. elegans is regulated by cell cycle components including separase. Development *134*, 3837-3848.

Bembenek, J.N., White, J.G., and Zheng, Y. (2010). A role for separase in the regulation of RAB-11-positive vesicles at the cleavage furrow and midbody. Curr Biol *20*, 259-264.

Boland, A., Martin, T.G., Zhang, Z., Yang, J., Bai, X.C., Chang, L., Scheres, S.H., and Barford, D. (2017). Cryo-EM structure of a metazoan separase-securin complex at near-atomic resolution. Nature structural & molecular biology *24*, 414-418.

Boos, D., Kuffer, C., Lenobel, R., Korner, R., and Stemmann, O. (2008). Phosphorylation-dependent binding of cyclin B1 to a Cdc6-like domain of human separase. The Journal of biological chemistry *283*, 816-823.

Brito, H., Marques, V., Afonso, M.B., Brown, D.G., Borjesson, U., Selmi, N., Smith, D.M., Roberts, I.O., Fitzek, M., Aniceto, N.*, et al.* (2020). Phenotypic high-throughput screening platform identifies novel chemotypes for necroptosis inhibition. Cell Death Discov *6*, 6.

Bueno, A., and Russell, P. (1992). Dual functions of CDC6: a yeast protein required for DNA replication also inhibits nuclear division. The EMBO journal *11*, 2167-2176.

Buheitel, J., and Stemmann, O. (2013). Prophase pathway-dependent removal of cohesin from human chromosomes requires opening of the Smc3-Scc1 gate. The EMBO journal *32*, 666-676.

Chan, K.L., Roig, M.B., Hu, B., Beckouet, F., Metson, J., and Nasmyth, K. (2012). Cohesin's DNA exit gate is distinct from its entrance gate and is regulated by acetylation. Cell *150*, 961-974.

Chehardoli, G., and Bahmani, A. (2021). Synthetic strategies, SAR studies, and computer modeling of indole 2 and 3-carboxamides as the strong enzyme inhibitors: a review. Mol Divers *25*, 535-550.

Chen, G.Y., and Lampson, M.A. (2021). Chemical tools for dissecting cell division. Nat Chem Biol *17*, 632-640.

Chen, G.Y., Renda, F., Zhang, H., Gokden, A., Wu, D.Z., Chenoweth, D.M., Khodjakov, A., and Lampson, M.A. (2021). Tension promotes kinetochore-microtubule release by Aurora B kinase. J Cell Biol *220*.

Chestukhin, A., Pfeffer, C., Milligan, S., DeCaprio, J.A., and Pellman, D. (2003). Processing, localization, and requirement of human separase for normal anaphase progression. Proceedings of the National Academy of Sciences of the United States of America *100*, 4574-4579.

Ciosk, R., Zachariae, W., Michaelis, C., Shevchenko, A., Mann, M., and Nasmyth, K. (1998). An ESP1/PDS1 complex regulates loss of sister chromatid cohesion at the metaphase to anaphase transition in yeast. Cell *93*, 1067-1076.

Csizmok, V., Felli, I.C., Tompa, P., Banci, L., and Bertini, I. (2008). Structural and dynamic characterization of intrinsically disordered human securin by NMR spectroscopy. J Am Chem Soc *130*, 16873-16879.

Dahlin, J.L., and Walters, M.A. (2014). The essential roles of chemistry in high-throughput screening triage. Future Med Chem *6*, 1265-1290.

Dandapani, S., Rosse, G., Southall, N., Salvino, J.M., and Thomas, C.J. (2012). Selecting, Acquiring, and Using Small Molecule Libraries for High-Throughput Screening. Curr Protoc Chem Biol *4*, 177-191.

Faloon, P.W., Dockendorff, C., Germain, A., Yu, M., Nag, P.P., Youngsaye, W., Bennion, M., Lam, G., Paterson, C., Dandapani, S.*, et al.* (2010). A Small Molecule Inhibitor of Scavenger Receptor BI-mediated Lipid Uptake-Probe 2. In Probe Reports from the NIH Molecular Libraries Program (Bethesda (MD)).

Feng, B.Y., Simeonov, A., Jadhav, A., Babaoglu, K., Inglese, J., Shoichet, B.K., and Austin, C.P. (2007). A high-throughput screen for aggregation-based inhibition in a large compound library. J Med Chem *50*, 2385-2390.

Finan, C., Gaulton, A., Kruger, F.A., Lumbers, R.T., Shah, T., Engmann, J., Galver, L., Kelley, R., Karlsson, A., Santos, R.*, et al.* (2017). The druggable genome and support for target identification and validation in drug development. Sci Transl Med *9*.

Gimenez-Abian, J.F., Diaz-Martinez, L.A., Waizenegger, I.C., Gimenez-Martin, G., and Clarke, D.J. (2005). Separase is required at multiple pre-anaphase cell cycle stages in human cells. Cell cycle (Georgetown, Tex) *4*, 1576-1584.

Gorr, I.H., Boos, D., and Stemmann, O. (2005). Mutual inhibition of separase and Cdk1 by two-step complex formation. Molecular cell *19*, 135-141.

Gruber, S., Arumugam, P., Katou, Y., Kuglitsch, D., Helmhart, W., Shirahige, K., and Nasmyth, K. (2006). Evidence that loading of cohesin onto chromosomes involves opening of its SMC hinge. Cell *127*, 523-537.

Gutierrez-Escribano, P., Newton, M.D., Llauro, A., Huber, J., Tanasie, L., Davy, J., Aly, I., Aramayo, R., Montoya, A., Kramer, H.*, et al.* (2019). A conserved ATP- and Scc2/4-dependent activity for cohesin in tethering DNA molecules. Sci Adv *5*, eaay6804.

Haarhuis, J.H., Elbatsh, A.M., and Rowland, B.D. (2014). Cohesin and its regulation: on the logic of X-shaped chromosomes. Developmental cell *31*, 7-18.

Haering, C.H., Farcas, A.M., Arumugam, P., Metson, J., and Nasmyth, K. (2008). The cohesin ring concatenates sister DNA molecules. Nature *454*, 297-301.

Hartwell, L.H., and Weinert, T.A. (1989). Checkpoints: controls that ensure the order of cell cycle events. Science (New York, NY) *246*, 629-634.

Hasan, M.T., Subbaroyan, R., and Chang, T.Y. (1991). High-efficiency stable gene transfection using chloroquine-treated Chinese hamster ovary cells. Somat Cell Mol Genet *17*, 513-517.

Hattori, S.I., Higashi-Kuwata, N., Hayashi, H., Allu, S.R., Raghavaiah, J., Bulut, H., Das, D., Anson, B.J., Lendy, E.K., Takamatsu, Y.*, et al.* (2021). A small molecule compound with an indole moiety inhibits the main protease of SARS-CoV-2 and blocks virus replication. Nature communications *12*, 668.

Hauf, S., Roitinger, E., Koch, B., Dittrich, C.M., Mechtler, K., and Peters, J.M. (2005). Dissociation of cohesin from chromosome arms and loss of arm cohesion during early mitosis depends on phosphorylation of SA2. PLoS biology *3*, e69.

Hauf, S., Waizenegger, I.C., and Peters, J.M. (2001). Cohesin cleavage by separase required for anaphase and cytokinesis in human cells. Science (New York, NY) *293*, 1320-1323.

Hellmuth, S., Bottger, F., Pan, C., Mann, M., and Stemmann, O. (2014). PP2A delays APC/C-dependent degradation of separase-associated but not free securin. The EMBO journal *33*, 1134-1147.

Hellmuth, S., Gomez, H.L., Pendas, A.M., and Stemmann, O. (2020). Securin-independent regulation of separase by checkpoint-induced shugoshin-MAD2. Nature *580*, 536-541.

Hellmuth, S., Gutierrez-Caballero, C., Llano, E., Pendas, A.M., and Stemmann, O. (2018). Local activation of mammalian separase in interphase promotes double-strand break repair and prevents oncogenic transformation. The EMBO journal *37*.

Hellmuth, S., Pohlmann, C., Brown, A., Bottger, F., Sprinzl, M., and Stemmann, O. (2015a). Positive and negative regulation of vertebrate separase by Cdk1-cyclin B1 may explain why securin is dispensable. The Journal of biological chemistry *290*, 8002-8010.

Hellmuth, S., Rata, S., Brown, A., Heidmann, S., Novak, B., and Stemmann, O. (2015b). Human chromosome segregation involves multi-layered regulation of separase by the peptidyl-prolyl-isomerase Pin1. Molecular cell *58*, 495-506.

Hellmuth, S., and Stemmann, O. (2020). Separase-triggered apoptosis enforces minimal length of mitosis. Nature *580*, 542-547.

Hertz, E.P.T., Kruse, T., Davey, N.E., Lopez-Mendez, B., Sigurethsson, J.O., Montoya, G., Olsen, J.V., and Nilsson, J. (2016). A Conserved Motif Provides Binding Specificity to the PP2A-B56 Phosphatase. Molecular cell *63*, 686-695.

Hirano, T., Funahashi, S., Uemura, T., and Yanagida, M. (1986). Isolation and characterization of Schizosaccharomyces pombe cutmutants that block nuclear division but not cytokinesis. The EMBO journal *5*, 2973-2979.

Holland, A.J., Böttger, F., Stemmann, O., and Taylor, S.S. (2007). Protein phosphatase 2A and separase form a complex regulated by separase autocleavage. The Journal of biological chemistry *282*, 24623-24632.

Holland, A.J., and Taylor, S.S. (2006). Cyclin-B1-mediated inhibition of excess separase is required for timely chromosome disjunction. Journal of cell science *119*, 3325-3336.

Hopkins, A.L., and Groom, C.R. (2002). The druggable genome. Nat Rev Drug Discov *1*, 727-730.

Huang, X., Hatcher, R., York, J.P., and Zhang, P. (2005). Securin and separase phosphorylation act redundantly to maintain sister chromatid cohesion in mammalian cells. Mol Biol Cell *16*, 4725-4732.

Hughes, J.P., Rees, S., Kalindjian, S.B., and Philpott, K.L. (2011). Principles of early drug discovery. Br J Pharmacol *162*, 1239-1249.

Huis in 't Veld, P.J., Herzog, F., Ladurner, R., Davidson, I.F., Piric, S., Kreidl, E., Bhaskara, V., Aebersold, R., and Peters, J.M. (2014). Characterization of a DNA exit gate in the human cohesin ring. Science (New York, NY) *346*, 968-972.

Jallepalli, P.V., Waizenegger, I.C., Bunz, F., Langer, S., Speicher, M.R., Peters, J.M., Kinzler, K.W., Vogelstein, B., and Lengauer, C. (2001). Securin is required for chromosomal stability in human cells. Cell *105*, 445-457.

Kanke, M., Tahara, E., Huis In't Veld, P.J., and Nishiyama, T. (2016). Cohesin acetylation and Wapl-Pds5 oppositely regulate translocation of cohesin along DNA. The EMBO journal *35*, 2686-2698.

Kaufmann, S.H. (2008). Paul Ehrlich: founder of chemotherapy. Nat Rev Drug Discov *7*, 373.

Kawasumi, M., and Nghiem, P. (2007). Chemical genetics: elucidating biological systems with small-molecule compounds. J Invest Dermatol *127*, 1577-1584.

Kumada, K., Nakamura, T., Nagao, K., Funabiki, H., Nakagawa, T., and Yanagida, M. (1998). Cut1 is loaded onto the spindle by binding to Cut2 and promotes anaphase spindle movement upon Cut2 proteolysis. Curr Biol *8*, 633-641.

Lara-Gonzalez, P., Westhorpe, F.G., and Taylor, S.S. (2012). The spindle assembly checkpoint. Curr Biol *22*, R966-980.

Lee, K., and Rhee, K. (2012). Separase-dependent cleavage of pericentrin B is necessary and sufficient for centriole disengagement during mitosis. Cell cycle (Georgetown, Tex) *11*, 2476-2485.

Lin, Z., Luo, X., and Yu, H. (2016). Structural basis of cohesin cleavage by separase. Nature *532*, 131-134.

Lipinski, C.A., Lombardo, F., Dominy, B.W., and Feeney, P.J. (2001). Experimental and computational approaches to estimate solubility and permeability in drug discovery and development settings. Adv Drug Deliv Rev *46*, 3-26.

Lok, T.M., Wang, Y., Xu, W.K., Xie, S., Ma, H.T., and Poon, R.Y.C. (2020). Mitotic slippage is determined by p31(comet) and the weakening of the spindle-assembly checkpoint. Oncogene *39*, 2819-2834.

Luo, S., and Tong, L. (2017). Molecular mechanism for the regulation of yeast separase by securin. Nature *542*, 255-259.

Luthman, H., and Magnusson, G. (1983). High efficiency polyoma DNA transfection of chloroquine treated cells. Nucleic Acids Res *11*, 1295-1308.

Maeshima, K., and Eltsov, M. (2008). Packaging the genome: the structure of mitotic chromosomes. J Biochem *143*, 145-153.

Maier, N.K., Ma, J., Lampson, M.A., and Cheeseman, I.M. (2021). Separase cleaves the kinetochore protein Meikin at the meiosis I/II transition. Developmental cell *56*, 2192-2206 e2198.

Matsuo, K., Ohsumi, K., Iwabuchi, M., Kawamata, T., Ono, Y., and Takahashi, M. (2012). Kendrin is a novel substrate for separase involved in the licensing of centriole duplication. Curr Biol *22*, 915-921.

Mayer, T.U., Kapoor, T.M., Haggarty, S.J., King, R.W., Schreiber, S.L., and Mitchison, T.J. (1999). Small molecule inhibitor of mitotic spindle bipolarity identified in a phenotype-based screen. Science (New York, NY) *286*, 971-974.

McAleenan, A., Clemente-Blanco, A., Cordon-Preciado, V., Sen, N., Esteras, M., Jarmuz, A., and Aragon, L. (2013). Post-replicative repair involves separase-dependent removal of the kleisin subunit of cohesin. Nature *493*, 250-254.

Mei, J., Huang, X., and Zhang, P. (2001). Securin is not required for cellular viability, but is required for normal growth of mouse embryonic fibroblasts. Curr Biol *11*, 1197-1201.

Meyer, R., Fofanov, V., Panigrahi, A., Merchant, F., Zhang, N., and Pati, D. (2009). Overexpression and mislocalization of the chromosomal segregation protein separase in multiple human cancers. Clin Cancer Res *15*, 2703-2710.

Morgan, D.O. (2007). The cell cycle - Principles of Control; Chapter 01 - Events of the Eukaryotic Cell Cycle

Morgan, D.O. (1997). Cyclin-dependent kinases: engines, clocks, and microprocessors. Annu Rev Cell Dev Biol *13*, 261-291.

Molecular Bilogy of the Cell (2015); Chapter 17: The Cell Cycle; Alberts B., Johnson A., Lewis J., Morgan D., Raff M., Roberts K. and Walter P.

Musacchio, A. (2015). The Molecular Biology of Spindle Assembly Checkpoint Signaling Dynamics. Curr Biol *25*, R1002-1018.

Nagao, K., Adachi, Y., and Yanagida, M. (2004). Separase-mediated cleavage of cohesin at interphase is required for DNA repair. Nature *430*, 1044-1048.

Nagao, K., and Yanagida, M. (2006). Securin can have a separase cleavage site by substitution mutations in the domain required for stabilization and inhibition of separase. Genes Cells *11*, 247-260.

Nakamura, A., Arai, H., and Fujita, N. (2009). Centrosomal Aki1 and cohesin function in separase-regulated centriole disengagement. J Cell Biol *187*, 607-614.

Nasmyth, K., and Haering, C.H. (2009). Cohesin: its roles and mechanisms. Annu Rev Genet *43*, 525-558.

Nie, S., Zhao, J., Wu, X., Yao, Y., Wu, F., Lin, Y.L., Li, X., Kneubehl, A.R., Vogt, M.B., Rico-Hesse, R.*, et al.* (2021). Synthesis, structure-activity relationship and antiviral activity of indole-containing inhibitors of Flavivirus NS2B-NS3 protease. Eur J Med Chem *225*, 113767.

Nishimura, K., Watanabe, S., Hayashida, R., Sugishima, S., Iwasaka, T., and Kaku, T. (2016). Binucleated HeLa cells are formed by cytokinesis failure in starvation and keep the potential of proliferation. Cytotechnology *68*, 1123-1130.

Novak, B., Tyson, J.J., Gyorffy, B., and Csikasz-Nagy, A. (2007). Irreversible cell-cycle transitions are due to systems-level feedback. Nature cell biology *9*, 724-728.

O'Connor, C.J., Laraia, L., and Spring, D.R. (2011). Chemical genetics. Chem Soc Rev *40*, 4332-4345.

Owen, S.C., Doak, A.K., Wassam, P., Shoichet, M.S., and Shoichet, B.K. (2012). Colloidal aggregation affects the efficacy of anticancer drugs in cell culture. ACS chemical biology *7*, 1429-1435.

Palmer, J.T., Rasnick, D., Klaus, J.L., and Bromme, D. (1995). Vinyl sulfones as mechanism-based cysteine protease inhibitors. J Med Chem *38*, 3193-3196.

Papi, M., Berdougo, E., Randall, C.L., Ganguly, S., and Jallepalli, P.V. (2005). Multiple roles for separase auto-cleavage during the G2/M transition. Nature cell biology *7*, 1029-1035.

Pati, D. (2008). Oncogenic activity of separase. Cell cycle (Georgetown, Tex) *7*, 3481-3482.

Pati, D., Haddad, B.R., Haegele, A., Thompson, H., Kittrell, F.S., Shepard, A., Montagna, C., Zhang, N., Ge, G., Otta, S.K.*, et al.* (2004). Hormone-induced chromosomal instability in p53-null mammary epithelium. Cancer Res *64*, 5608-5616.

Piovesan, A., Pelleri, M.C., Antonaros, F., Strippoli, P., Caracausi, M., and Vitale, L. (2019). On the length, weight and GC content of the human genome. BMC Res Notes *12*, 106.

Queralt, E., Lehane, C., Novak, B., and Uhlmann, F. (2006). Downregulation of PP2A(Cdc55) phosphatase by separase initiates mitotic exit in budding yeast. Cell *125*, 719-732.

Rix, U., and Superti-Furga, G. (2009). Target profiling of small molecules by chemical proteomics. Nat Chem Biol *5*, 616-624.

Rosen, L.E., Klebba, J.E., Asfaha, J.B., Ghent, C.M., Campbell, M.G., Cheng, Y., and Morgan, D.O. (2019). Cohesin cleavage by separase is enhanced by a substrate motif distinct from the cleavage site. Nature communications *10*, 5189.

Rothbauer, U., Zolghadr, K., Muyldermans, S., Schepers, A., Cardoso, M.C., and Leonhardt, H. (2008). A versatile nanotrap for biochemical and functional studies with fluorescent fusion proteins. Mol Cell Proteomics *7*, 282-289.

Sahin, K. (2021). Investigation of novel indole-based HIV-1 protease inhibitors using virtual screening and text mining. J Biomol Struct Dyn *39*, 3638-3648.

Sanchez-Puig, N., Veprintsev, D.B., and Fersht, A.R. (2005). Human full-length Securin is a natively unfolded protein. Protein science : a publication of the Protein Society *14*, 1410-1418.

Sassano, M.F., Doak, A.K., Roth, B.L., and Shoichet, B.K. (2013). Colloidal aggregation causes inhibition of G protein-coupled receptors. J Med Chem *56*, 2406-2414.

Schneider-Poetsch, T., and Yoshida, M. (2018). Along the Central Dogma-Controlling Gene Expression with Small Molecules. Annu Rev Biochem *87*, 391-420.

Schockel, L., Mockel, M., Mayer, B., Boos, D., and Stemmann, O. (2011). Cleavage of cohesin rings coordinates the separation of centrioles and chromatids. Nature cell biology *13*, 966-972.

Schreiber, S.L. (2005). Small molecules: the missing link in the central dogma. Nat Chem Biol *1*, 64-66.

Schreiber, S.L. (2019). A Chemical Biology View of Bioactive Small Molecules and a Binder-Based Approach to Connect Biology to Precision Medicines. Isr J Chem *59*, 52-59.

Shindo, N., Kumada, K., and Hirota, T. (2012). Separase sensor reveals dual roles for separase coordinating cohesin cleavage and cdk1 inhibition. Developmental cell *23*, 112-123.

Singh, J., Petter, R.C., Baillie, T.A., and Whitty, A. (2011). The resurgence of covalent drugs. Nat Rev Drug Discov *10*, 307-317.

Stemmann, O., Zou, H., Gerber, S.A., Gygi, S.P., and Kirschner, M.W. (2001). Dual inhibition of sister chromatid separation at metaphase. Cell *107*, 715-726.

Stockwell, B.R. (2000). Chemical genetics: ligand-based discovery of gene function. Nat Rev Genet *1*, 116-125.

Stockwell, B.R., Haggarty, S.J., and Schreiber, S.L. (1999). High-throughput screening of small molecules in miniaturized mammalian cell-based assays involving post-translational modifications. Chem Biol *6*, 71-83.

Strebhardt, K., and Ullrich, A. (2008). Paul Ehrlich's magic bullet concept: 100 years of progress. Nat Rev Cancer *8*, 473-480.

Sullivan, M., Lehane, C., and Uhlmann, F. (2001). Orchestrating anaphase and mitotic exit: separase cleavage and localization of Slk19. Nature cell biology *3*, 771-777.

Sun, Y., Kucej, M., Fan, H.Y., Yu, H., Sun, Q.Y., and Zou, H. (2009). Separase is recruited to mitotic chromosomes to dissolve sister chromatid cohesion in a DNA-dependent manner. Cell *137*, 123-132.

Sun, Y., Yu, H., and Zou, H. (2006). Nuclear exclusion of separase prevents cohesin cleavage in interphase cells. Cell cycle (Georgetown, Tex) *5*, 2537-2542.

Tan, S.Y., and Grimes, S. (2010). Paul Ehrlich (1854-1915): man with the magic bullet. Singapore Med J *51*, 842-843.

Teusel, F., Henschke, L., and Mayer, T.U. (2018). Small molecule tools in mitosis research. Methods in cell biology *144*, 137-155.

Theobald, D.L. (2010). A formal test of the theory of universal common ancestry. Nature *465*, 219-222.

Thorne, N., Auld, D.S., and Inglese, J. (2010). Apparent activity in high-throughput screening: origins of compound-dependent assay interference. Curr Opin Chem Biol *14*, 315-324.

Tsou, M.F., Wang, W.J., George, K.A., Uryu, K., Stearns, T., and Jallepalli, P.V. (2009). Polo kinase and separase regulate the mitotic licensing of centriole duplication in human cells. Developmental cell *17*, 344-354.

Uhlmann, F., Lottspeich, F., and Nasmyth, K. (1999). Sister-chromatid separation at anaphase onset is promoted by cleavage of the cohesin subunit Scc1. Nature *400*, 37-42.

Uhlmann, F., Wernic, D., Poupart, M.A., Koonin, E.V., and Nasmyth, K. (2000). Cleavage of cohesin by the CD clan protease separin triggers anaphase in yeast. Cell *103*, 375-386.

Viadiu, H., Stemmann, O., Kirschner, M.W., and Walz, T. (2005). Domain structure of separase and its binding to securin as determined by EM. Nature structural & molecular biology *12*, 552-553.

Vodermaier, H.C., Gieffers, C., Maurer-Stroh, S., Eisenhaber, F., and Peters, J.M. (2003). TPR subunits of the anaphase-promoting complex mediate binding to the activator protein CDH1. Curr Biol *13*, 1459-1468.

Waizenegger, I., Gimenez-Abian, J.F., Wernic, D., and Peters, J.M. (2002). Regulation of human separase by securin binding and autocleavage. Curr Biol *12*, 1368-1378.

Waizenegger, I.C., Hauf, S., Meinke, A., and Peters, J.M. (2000). Two distinct pathways remove mammalian cohesin from chromosome arms in prophase and from centromeres in anaphase. Cell *103*, 399-410.

Wang, Z., Yu, R., and Melmed, S. (2001). Mice lacking pituitary tumor transforming gene show testicular and splenic hypoplasia, thymic hyperplasia, thrombocytopenia, aberrant cell cycle progression, and premature centromere division. Mol Endocrinol *15*, 1870-1879.

Williams, K.J. (2009). The introduction of 'chemotherapy' using arsphenamine - the first magic bullet. J R Soc Med *102*, 343-348.

Winter, A., Schmid, R., and Bayliss, R. (2015). Structural Insights into Separase Architecture and Substrate Recognition through Computational Modelling of Caspase-Like and Death Domains. PLoS Comput Biol *11*, e1004548.

Wirth, K.G., Wutz, G., Kudo, N.R., Desdouets, C., Zetterberg, A., Taghybeeglu, S., Seznec, J., Ducos, G.M., Ricci, R., Firnberg, N.*, et al.* (2006). Separase: a universal trigger for sister chromatid disjunction but not chromosome cycle progression. J Cell Biol *172*, 847-860.

Xu, J., Wang, M., Gao, X., Hu, B., Du, Y., Zhou, J., Tian, X., and Huang, X. (2011). Separase phosphosite mutation leads to genome instability and primordial germ cell depletion during oogenesis. PLoS One *6*, e18763.

Yu, J., Raia, P., Ghent, C.M., Raisch, T., Sadian, Y., Cavadini, S., Sabale, P.M., Barford, D., Raunser, S., Morgan, D.O.*, et al.* (2021). Structural basis of human separase regulation by securin and CDK1-cyclin B1. Nature *596*, 138-142.

Zhang, J.H., Chung, T.D., and Oldenburg, K.R. (1999). A Simple Statistical Parameter for Use in Evaluation and Validation of High Throughput Screening Assays. Journal of biomolecular screening *4*, 67-73.

Zhang, N., Ge, G., Meyer, R., Sethi, S., Basu, D., Pradhan, S., Zhao, Y.J., Li, X.N., Cai, W.W., El-Naggar, A.K.*, et al.* (2008). Overexpression of Separase induces aneuploidy and mammary tumorigenesis. Proceedings of the National Academy of Sciences of the United States of America *105*, 13033-13038.

Zhang, N., and Pati, D. (2018). Separase Inhibitor Sepin-1 Inhibits Foxm1 Expression and Breast Cancer Cell Growth. J Cancer Sci Ther *10*, 52-59.

Zhang, N., Scorsone, K., Ge, G., Kaffes, C.C., Dobrolecki, L.E., Mukherjee, M., Lewis, M.T., Berg, S., Stephan, C.C., and Pati, D. (2014). Identification and Characterization of Separase Inhibitors (Sepins) for Cancer Therapy. Journal of biomolecular screening *19*, 878-889.

Zou, H., McGarry, T.J., Bernal, T., and Kirschner, M.W. (1999). Identification of a vertebrate sister-chromatid separation inhibitor involved in transformation and tumorigenesis. Science (New York, NY) *285*, 418-422.

Zou, H., Stemman, O., Anderson, J.S., Mann, M., and Kirschner, M.W. (2002). Anaphase specific auto-cleavage of separase. FEBS letters *528*, 246-250.

Zur, A., and Brandeis, M. (2001). Securin degradation is mediated by fzy and fzr, and is required for complete chromatid separation but not for cytokinesis. The EMBO journal *20*, 792-801.

# 8. Appendix

## 8.1 List of Abbreviations

| | |
|---|---|
| aa | amino acid(s) |
| aft | after |
| bf | before |
| AIL | auto-inhibitory loop |
| APC/C | anaphase promoting complex/cyclosome |
| AMC | 7-Amino-4-Methylcoumarine |
| ATP | adenosine 5'-triphosphate |
| BSA | bovine serum albumin |
| CBB | Coomassie brilliant blue |
| CCC | Cdk1-Cyclin B1-Cks1 |
| Cdk | cyclin-dependent kinase |
| *C. elegans* | *Caenorhabditis elegans* |
| CPC | chromosomal passenger complex |
| cpd | compound |
| CSF | cytostatic factor |
| Ctrl | control |
| cut | cell untimely torn |
| Cyc | cyclin |
| D-box | destruction box |
| DMEM | Dulbecco's Modified Eagle Medium |
| DMSO | dimethyl sulfoxide |
| DNA | deoxyribonucleic acid |
| dNTP | deoxynucleoside triphosphate |
| DTT | dithiothreitol |
| *E. coli* | *Escherichia coli* |
| ECL | enhanced chemiluminescence |
| EDTA | ethylendiamine tetraacetic acid |
| EGTA | ethylen glycol tetraacetic acid |
| EM | electron microscopy |
| em | emission |
| ex | excitation |

| | |
|---|---|
| FA | formaldehyde |
| FCS | fetal calf serum |
| fl | full-length |
| fragm | fragment |
| FRET | fluorescence resonance energy transfer |
| GBP | GFP binding protein |
| GFP | green fluorescent protein |
| H2B | histone 2B |
| HRP | horseradish peroxidase |
| HTS | high-throughput screening |
| IF | immunofluorescence |
| IP | immunoprecipitation |
| IPTG | isopropyl-β-D-thiogalactopyranoside |
| IVT | *in vitro* transcription-translation |
| KMN | Knl1-Mis12-Ndc80 |
| LB | lysogeny broth |
| MCC | mitotic checkpoint complex |
| MOM | mitochondrial outer membrane |
| mRNA | messenger ribonucleic acid |
| MT | microtubules |
| NEBD | nuclear envelope breakdown |
| NES | nuclear export signal |
| NHS | N-Hydroxysuccinimide |
| PAGE | polyacrylamide gel electrophoresis |
| PBS | phosphate-buffered saline |
| PCR | polymerase chain reaction |
| PD | protease dead |
| POI | protein of interest |
| PP1 | protein phosphatase 1 |
| PP2A | protein phosphatase 2A |
| RNA | ribonucleic acid |
| RNAi | RNA interference |
| rpm | rounds per minute |
| RT | room temperature |

| | |
|---|---|
| SAC | spindle assembly checkpoint |
| SAR | structure-activity-relationship |
| *S. cerevisiae* | *Saccharomyces cerevisiae* |
| SD | standard deviation |
| Sep | separase |
| SDS | sodium dodecyl sulfate |
| Sgo | Shugoshin |
| SIC | separase inhibiting compound |
| siRNA | small interfering RNA |
| SN | supernatant |
| *S. pombe* | *Schizosaccharomyces pombe* |
| TB | terrific broth |
| Tet | tetracycline |
| TEV protease | Tobacco Etch Virus nuclear-inclusion-a endopeptidase |
| WB | western blot |
| WT | wild type |
| XEE | *Xenopus* egg extract |
| *X. laevis* | *Xenopus laevis* |
| ZM | ZM447439 |

## 8.2 Supplemental Figures

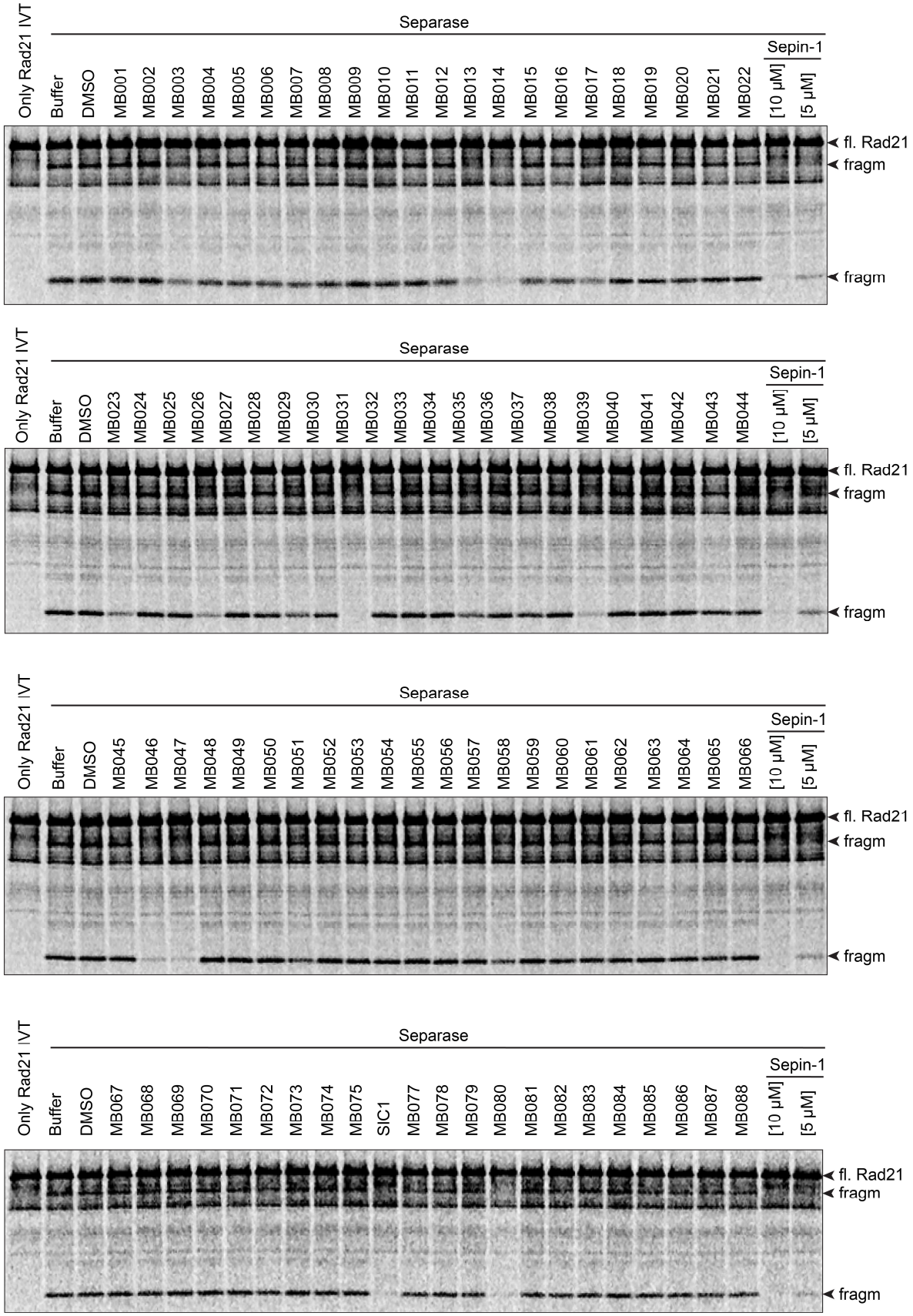

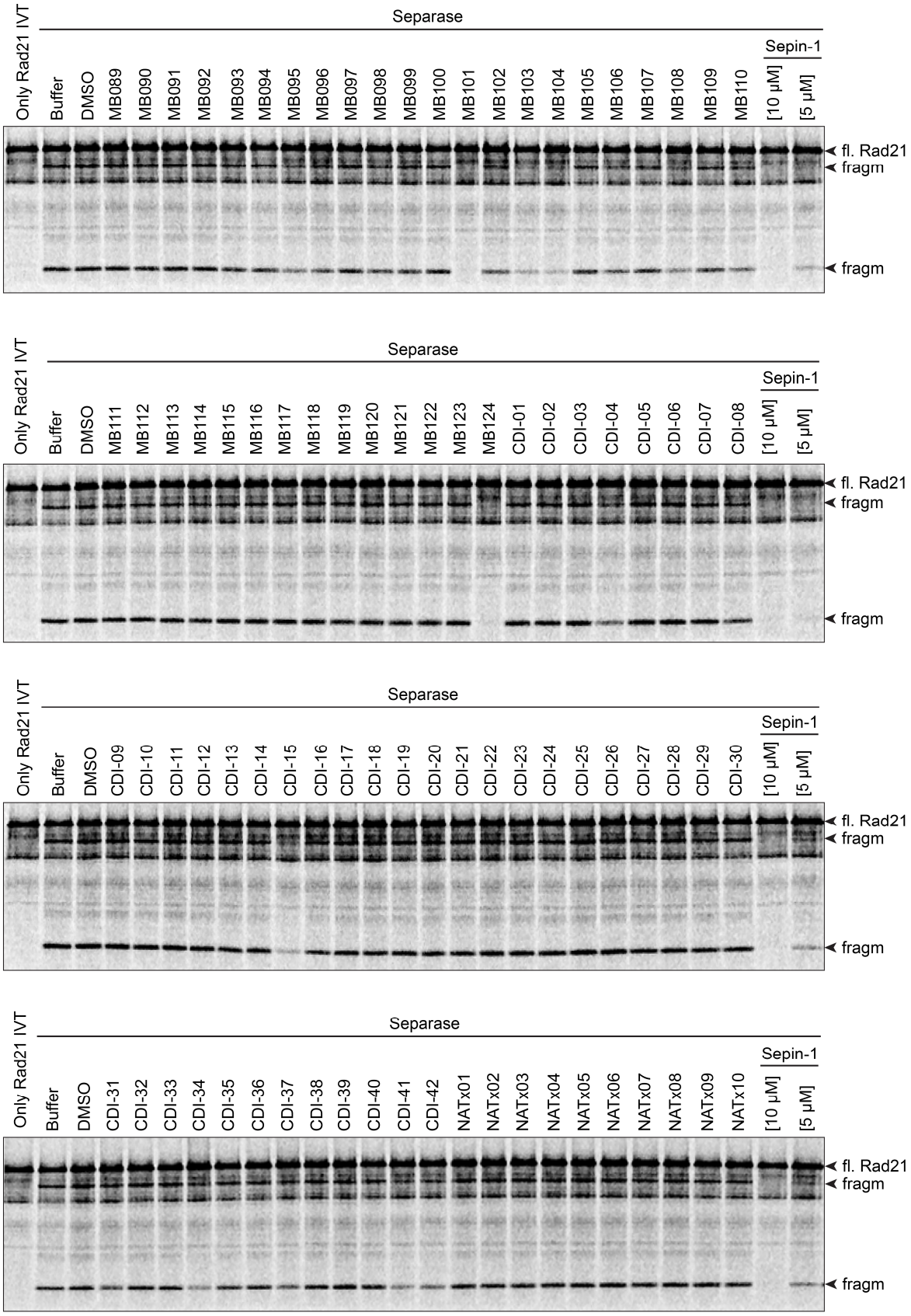
Only Rad21 IVT
Separase
Buffer
DMSO
MB089
MB090
MB091
MB092
MB093
MB094
MB095
MB096
MB097
MB098
MB099
MB100
MB101
MB102
MB103
MB104
MB105
MB106
MB107
MB108
MB109
MB110
Sepin-1
[10 µM]
[5 µM]
fl. Rad21
fragm
fragm
Only Rad21 IVT
Separase
Buffer
DMSO
MB111
MB112
MB113
MB114
MB115
MB116
MB117
MB118
MB119
MB120
MB121
MB122
MB123
MB124
CDI-01
CDI-02
CDI-03
CDI-04
CDI-05
CDI-06
CDI-07
CDI-08
Sepin-1
[10 µM]
[5 µM]
fl. Rad21
fragm
fragm
Only Rad21 IVT
Separase
Buffer
DMSO
CDI-09
CDI-10
CDI-11
CDI-12
CDI-13
CDI-14
CDI-15
CDI-16
CDI-17
CDI-18
CDI-19
CDI-20
CDI-21
CDI-22
CDI-23
CDI-24
CDI-25
CDI-26
CDI-27
CDI-28
CDI-29
CDI-30
Sepin-1
[10 µM]
[5 µM]
fl. Rad21
fragm
fragm
Only Rad21 IVT
Separase
Buffer
DMSO
CDI-31
CDI-32
CDI-33
CDI-34
CDI-35
CDI-36
CDI-37
CDI-38
CDI-39
CDI-40
CDI-41
CDI-42
NATx01
NATx02
NATx03
NATx04
NATx05
NATx06
NATx07
NATx08
NATx09
NATx10
Sepin-1
[10 µM]
[5 µM]
fl. Rad21
fragm
fragm

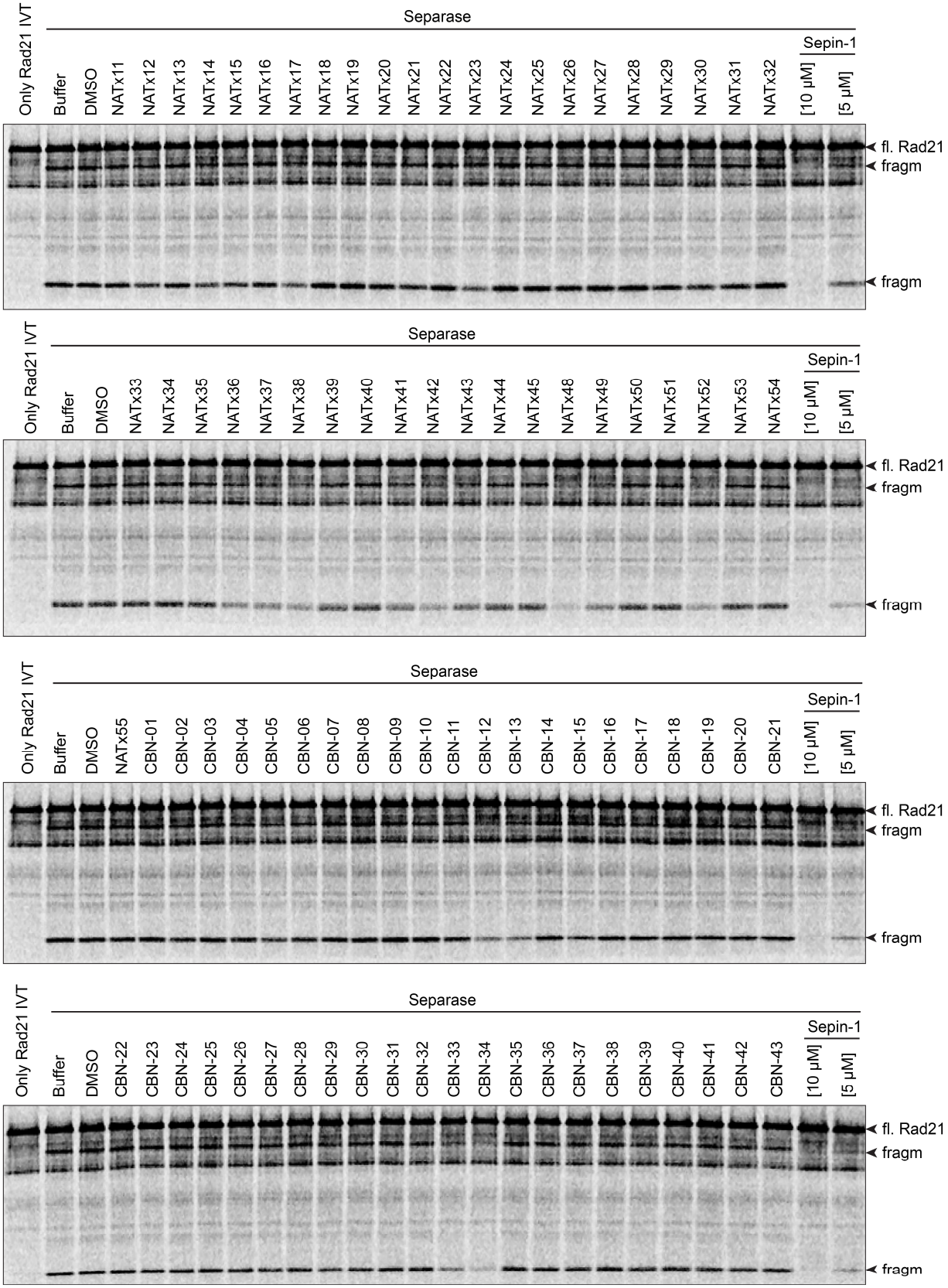
Only Rad21 IVT
Separase
Buffer
DMSO
NATx11
NATx12
NATx13
NATx14
NATx15
NATx16
NATx17
NATx18
NATx19
NATx20
NATx21
NATx22
NATx23
NATx24
NATx25
NATx26
NATx27
NATx28
NATx29
NATx30
NATx31
NATx32
Sepin-1
[10 µM]
[5 µM]
fl. Rad21
fragm
fragm
Only Rad21 IVT
Separase
Buffer
DMSO
NATx33
NATx34
NATx35
NATx36
NATx37
NATx38
NATx39
NATx40
NATx41
NATx42
NATx43
NATx44
NATx45
NATx48
NATx49
NATx50
NATx51
NATx52
NATx53
NATx54
Sepin-1
[10 µM]
[5 µM]
fl. Rad21
fragm
fragm
Only Rad21 IVT
Separase
Buffer
DMSO
NATx55
CBN-01
CBN-02
CBN-03
CBN-04
CBN-05
CBN-06
CBN-07
CBN-08
CBN-09
CBN-10
CBN-11
CBN-12
CBN-13
CBN-14
CBN-15
CBN-16
CBN-17
CBN-18
CBN-19
CBN-20
CBN-21
Sepin-1
[10 µM]
[5 µM]
fl. Rad21
fragm
fragm
Only Rad21 IVT
Separase
Buffer
DMSO
CBN-22
CBN-23
CBN-24
CBN-25
CBN-26
CBN-27
CBN-28
CBN-29
CBN-30
CBN-31
CBN-32
CBN-33
CBN-34
CBN-35
CBN-36
CBN-37
CBN-38
CBN-39
CBN-40
CBN-41
CBN-42
CBN-43
Sepin-1
[10 µM]
[5 µM]
fl. Rad21
fragm
fragm

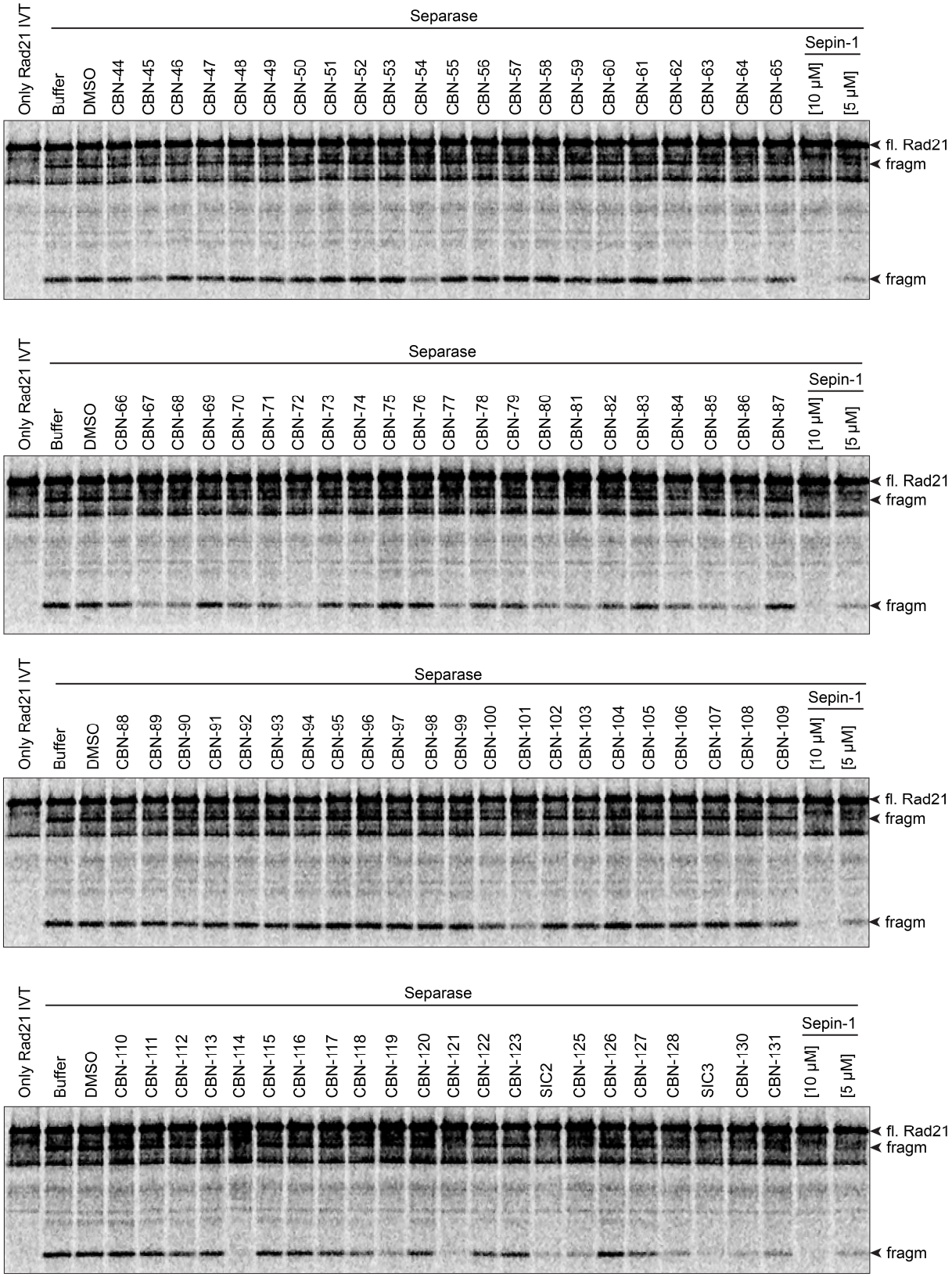
Only Rad21 IVT
Separase
Buffer
DMSO
CBN-44
CBN-45
CBN-46
CBN-47
CBN-48
CBN-49
CBN-50
CBN-51
CBN-52
CBN-53
CBN-54
CBN-55
CBN-56
CBN-57
CBN-58
CBN-59
CBN-60
CBN-61
CBN-62
CBN-63
CBN-64
CBN-65
Sepin-1
[10 µM]
[5 µM]
fl. Rad21
fragm
fragm
Only Rad21 IVT
Separase
Buffer
DMSO
CBN-66
CBN-67
CBN-68
CBN-69
CBN-70
CBN-71
CBN-72
CBN-73
CBN-74
CBN-75
CBN-76
CBN-77
CBN-78
CBN-79
CBN-80
CBN-81
CBN-82
CBN-83
CBN-84
CBN-85
CBN-86
CBN-87
Sepin-1
[10 µM]
[5 µM]
fl. Rad21
fragm
fragm
Only Rad21 IVT
Separase
Buffer
DMSO
CBN-88
CBN-89
CBN-90
CBN-91
CBN-92
CBN-93
CBN-94
CBN-95
CBN-96
CBN-97
CBN-98
CBN-99
CBN-100
CBN-101
CBN-102
CBN-103
CBN-104
CBN-105
CBN-106
CBN-107
CBN-108
CBN-109
Sepin-1
[10 µM]
[5 µM]
fl. Rad21
fragm
fragm
Only Rad21 IVT
Separase
Buffer
DMSO
CBN-110
CBN-111
CBN-112
CBN-113
CBN-114
CBN-115
CBN-116
CBN-117
CBN-118
CBN-119
CBN-120
CBN-121
CBN-122
CBN-123
SIC2
CBN-125
CBN-126
CBN-127
CBN-128
SIC3
CBN-130
CBN-131
Sepin-1
[10 µM]
[5 µM]
fl. Rad21
fragm
fragm

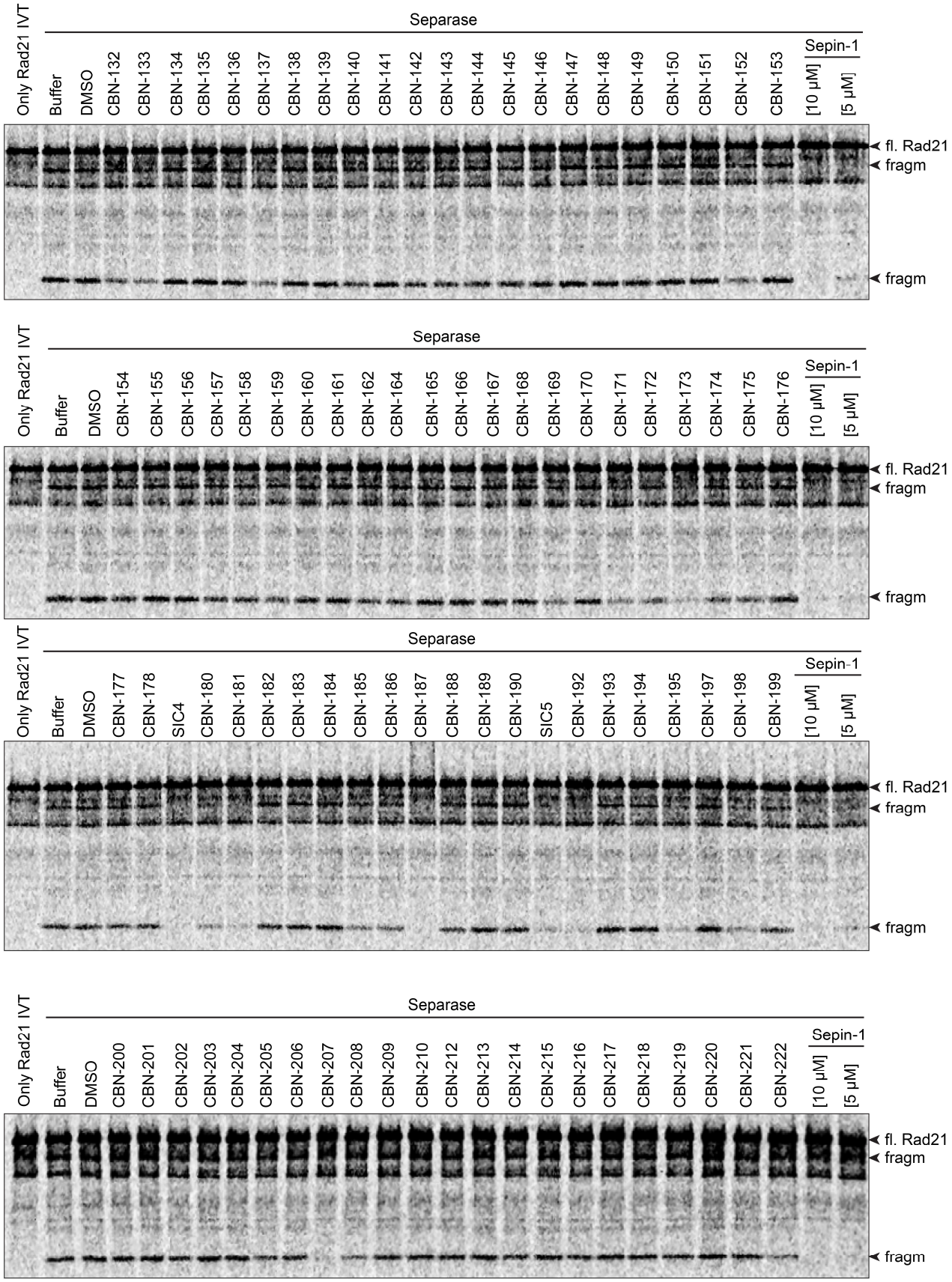
Only Rad21 IVT
Separase
Buffer
DMSO
CBN-132
CBN-133
CBN-134
CBN-135
CBN-136
CBN-137
CBN-138
CBN-139
CBN-140
CBN-141
CBN-142
CBN-143
CBN-144
CBN-145
CBN-146
CBN-147
CBN-148
CBN-149
CBN-150
CBN-151
CBN-152
CBN-153
Sepin-1
[10 µM]
[5 µM]
fl. Rad21
fragm
fragm
Only Rad21 IVT
Separase
Buffer
DMSO
CBN-154
CBN-155
CBN-156
CBN-157
CBN-158
CBN-159
CBN-160
CBN-161
CBN-162
CBN-164
CBN-165
CBN-166
CBN-167
CBN-168
CBN-169
CBN-170
CBN-171
CBN-172
CBN-173
CBN-174
CBN-175
CBN-176
Sepin-1
[10 µM]
[5 µM]
fl. Rad21
fragm
fragm
Only Rad21 IVT
Separase
Buffer
DMSO
CBN-177
CBN-178
SIC4
CBN-180
CBN-181
CBN-182
CBN-183
CBN-184
CBN-185
CBN-186
CBN-187
CBN-188
CBN-189
CBN-190
SIC5
CBN-192
CBN-193
CBN-194
CBN-195
CBN-197
CBN-198
CBN-199
Sepin-1
[10 µM]
[5 µM]
fl. Rad21
fragm
fragm
Only Rad21 IVT
Separase
Buffer
DMSO
CBN-200
CBN-201
CBN-202
CBN-203
CBN-204
CBN-205
CBN-206
CBN-207
CBN-208
CBN-209
CBN-210
CBN-212
CBN-213
CBN-214
CBN-215
CBN-216
CBN-217
CBN-218
CBN-219
CBN-220
CBN-221
CBN-222
Sepin-1
[10 µM]
[5 µM]
fl. Rad21
fragm
fragm

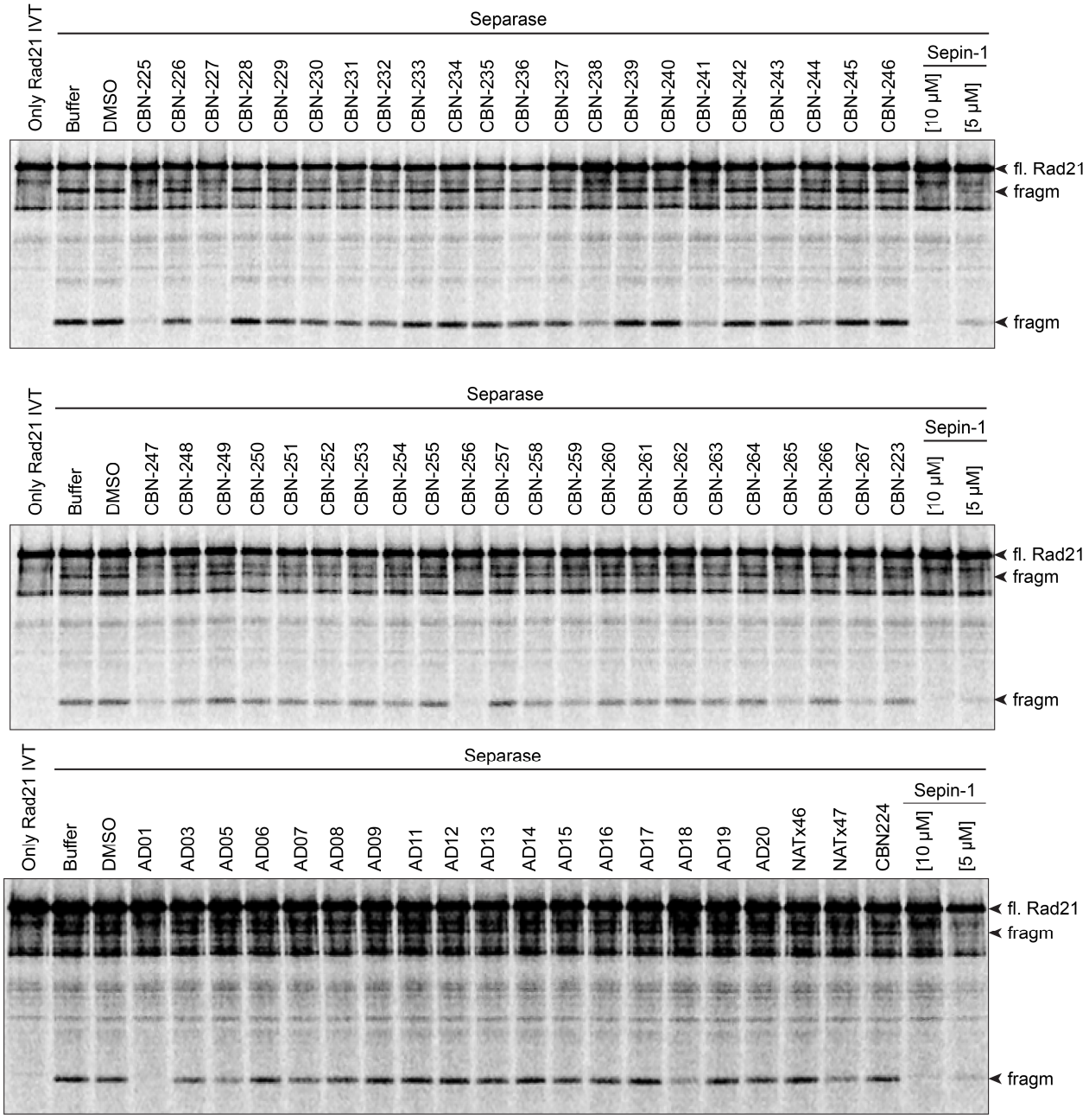


**Supplemental Figure S1: Rad21 cleavage assay of all 495 primary hits.** Autoradiographs of Rad21 cleavage assay; separase$^{P1127A}$ mediated cleavage of $^{35}$S-labelled Rad21 IVT; all compounds were used at 20 µM and Sepin-1 both at 10 µM and 5 µM.

## 8.3 Supplemental Tables

**Table S1**: Overview of all screened plates with corresponding Z' values

| Screening Plate | Z´ value | Screening Plate | Z´ value | Screening Plate | Z´ value |
|---|---|---|---|---|---|
| 151119-001-CDI-101 | 0.659 | 160220-003-CBN-P25 | 0.663 | 160325-003-MBC-021 | 0.650 |
| 151119-002-CDI-102 | 0.739 | 160220-004-CBN-P26 | 0.741 | 160325-004-MBC-022 | 0.739 |
| 151119-003-CDI-103 | 0.664 | 160220-005-CBN-P27 | 0.749 | 160325-005-MBC-023 | 0.672 |
| 151119-004-CDI-104 | 0.669 | 160223-001-CBN-P24 | 0.707 | 160325-006-MBC-024 | 0.797 |
| 151203-001-CDI-105 | 0.767 | 160223-002-CBN-P28 | 0.747 | 160401-001-MBC-025 | 0.751 |
| 151203-002-CDI-106 | 0.695 | 160223-003-CBN-P29 | 0.788 | 160401-002-MBC-026 | 0.637 |
| 151203-003-CDI-107 | 0.692 | 160223-004-CBN-P30 | 0.709 | 160401-003-MBC-027 | 0.728 |
| 151203-004-CDI-108 | 0.614 | 160223-005-CBN-P31 | 0.681 | 160401-004-MBC-028 | 0.618 |
| 151203-005-CDI-109 | 0.748 | 160223-006-CBN-P32 | 0.712 | 160428-001-NATx-10 | 0.803 |
| 151203-006-CDI-110 | 0.666 | 160225-001-CBN-P33 | 0.771 | 160428-002-NATx-11 | 0.769 |
| 151218-001-CDI-111 | 0.733 | 160225-002-CBN-P34 | 0.672 | 160428-003-NATx-12 | 0.798 |
| 151218-002-CDI-112 | 0.757 | 160225-003-CBN-P35 | 0.610 | 160428-004-NATx-13 | 0.646 |
| 151218-003-CDI-113 | 0.713 | 160225-004-CBN-P36 | 0.742 | 160428-005-NATx-14 | 0.759 |
| 151218-004-CDI-114 | 0.738 | 160225-005-CBN-P37 | 0.772 | 160428-006-NATx-15 | 0.723 |
| 151218-005-CDI-115 | 0.735 | 160225-006-CBN-P38 | 0.654 | 160429-001-NATx-8 | 0.722 |
| 160122-001-CDI-116 | 0.555 | 160227-001-CBN-P39 | 0.808 | 160429-002-NATx-9 | 0.695 |
| 160122-002-CDI-117 | 0.689 | 160227-002-CBN-P40 | 0.687 | 160429-003-NATx-5 | 0.745 |
| 160122-003-CDI-118 | 0.695 | 160227-003-CBN-P41 | 0.744 | 160429-005-NATx-7 | 0.765 |
| 160122-004-CDI-119 | 0.553 | 160227-004-CBN-P42 | 0.772 | 160429-006-NATx-16 | 0.666 |
| 160122-005-CDI-120 | 0.673 | 160227-005-CBN-P43 | 0.643 | 160519-001-CBN-P1017 | 0.756 |
| 160128-001-MBC-008 | 0.724 | 160227-006-CBN-P44 | 0.670 | 160519-002-CBN-P1018 | 0.706 |
| 160128-002-MBC-009 | 0.533 | 160303-001-CBN-P45 | 0.732 | 160519-003-CBN-P1019 | 0.777 |
| 160128-003-MBC-019 | 0.735 | 160303-002-CBN-P46 | 0.655 | 160519-004-CBN-P1020 | 0.768 |
| 160203-001-CDI-122 | 0.783 | 160303-003-CBN-P47 | 0.698 | 160519-005-CBN-P1021 | 0.714 |
| 160203-002-CDI-123 | 0.730 | 160303-004-CBN-P48 | 0.665 | 160519-006-CBN-P1022 | 0.701 |
| 160203-003-CDI-124 | 0.589 | 160303-005-CBN-P1001 | 0.641 | 160520-001-CBN-P4008 | 0.697 |
| 160203-004-CDI-125 | 0.762 | 160305-001-CBN-P1002 | 0.797 | 160520-002-CBN-P4009 | 0.691 |
| 160203-005-CDI-126 | 0.763 | 160305-002-CBN-P1003 | 0.764 | 160520-003-CBN-P4010 | 0.723 |
| 160203-006-CDI-127 | 0.761 | 160305-003-CBN-P1004 | 0.781 | 160520-004-CBN-P4011 | 0.538 |
| 160205-001-CBN-P1 | 0.784 | 160305-004-CBN-P1005 | 0.759 | 160520-005-CBN-P4012 | 0.538 |
| 160205-002-CBN-P2 | 0.763 | 160305-005-CBN-P1006 | 0.729 | 160520-006-CBN-P3001 | 0.593 |
| 160205-003-CBN-P3 | 0.769 | 160305-006-CBN-P1007 | 0.735 | 160525-001-CBN-P3006 | 0.715 |
| 160205-004-CBN-P4 | 0.613 | 160317-001-CBN-P1008 | 0.754 | 160525-002-CBN-P3012 | 0.763 |
| 160205-005-CBN-P5 | 0.763 | 160317-002-CBN-P1009 | 0.683 | 160525-003-CBN-P1013 | 0.737 |
| 160205-006-CBN-P6 | 0.758 | 160317-003-CBN-P1010 | 0.728 | 160525-004-CBN-P1011 | 0.694 |
| 160211-001-CBN-P7 | 0.731 | 160317-004-MBC-001 | 0.729 | 160525-005-CBN-P1012 | 0.642 |
| 160211-002-CBN-P8 | 0.640 | 160317-005-MBC-002 | 0.695 | 160616-002-NATx-2 | 0.505 |
| 160211-003-CBN-P9 | 0.681 | 160317-006-MBC-003 | 0.740 | 160616-003-NATx-3 | 0.571 |
| 160211-004-CBN-P10 | 0.757 | 160318-001-MBC-004 | 0.746 | 160616-004-NATx-4 | 0.652 |
| 160211-005-CBN-P11 | 0.651 | 160318-002-MBC-005 | 0.774 | 160616-005-NATx-6 | 0.655 |
| 160211-006-CBN-P12 | 0.643 | 160318-003-MBC-006 | 0.710 | 160616-006-MBC-029 | 0.634 |
| 160213-001-CBN-P13 | 0.702 | 160318-004-MBC-007 | 0.674 | 160617-001-CBN-P1014 | 0.551 |
| 160213-002-CBN-P14 | 0.640 | 160318-005-MBC-010 | 0.788 | 160617-002-CBN-P1015 | 0.554 |
| 160213-003-CBN-P15 | 0.655 | 160318-006-MBC-011 | 0.765 | 160617-003-CBN-P1016 | 0.525 |
| 160213-005-CBN-P17 | 0.613 | 160324-001-MBC-012 | 0.810 | 160617-004-CDI-121 | 0.712 |
| 160218-001-CBN-P16 | 0.773 | 160324-002-MBC-013 | 0.605 | 160819-001-ICCB-204 | 0.633 |
| 160218-002-CBN-P18 | 0.747 | 160324-003-MBC-014 | 0.691 | 160819-002-ICCB-205 | 0.659 |
| 160218-003-CBN-P19 | 0.661 | 160324-004-MBC-015 | 0.781 | 160819-003-ACD-151 | 0.579 |
| 160218-004-CBN-P20 | 0.749 | 160324-005-MBC-016 | 0.770 | 160819-004-ACD-153 | 0.678 |
| 160218-005-CBN-P21 | 0.634 | 160324-006-MBC-017 | 0.808 | 160819-005-ACD-154 | 0.711 |
| 160220-001-CBN-P22 | 0.781 | 160325-001-MBC-018 | 0.700 | 161028-001-ACD-152 | 0.739 |
| 160220-002-CBN-P23 | 0.696 | 160325-002-MBC-020 | 0.727 | 161028-002-NATx-1 | 0.718 |

## 8.4 Publications

The main part of this work has been published in Henschke, L., M. Frese, S. Hellmuth, A. Marx, O. Stemmann, and T. U. Mayer. 2019. 'Identification of Bioactive Small Molecule Inhibitors of Separase', ACS Chem Biol, 14: 2155-59.

Other publications:

Teusel, F., L. Henschke, and T. U. Mayer. 2018. 'Small molecule tools in mitosis research', Methods Cell Biol, 144: 137-55.

Olazaran, F. E., C. A. Garcia-Perez, D. Bandyopadhyay, I. Balderas-Renteria, A. D. Reyes-Figueroa, L. Henschke, and G. Rivera. 2017. 'Theoretical and experimental study of polycyclic aromatic compounds as beta-tubulin inhibitors', J Mol Model, 23: 85.

## 8.5 Contributions

All experimental work presented in this thesis was performed by me, Lars Henschke, with contributions from Susanne Hellmuth, Silke Müller, Christian Dietz, Patrick Winter, Matthias Frese, Martina Baack, Melanie Walter and Andreas Gericke.

Susanne Hellmuth (Chair of Molecular Genetics, University of Bayreuth) generated the stable HEK293T screening cell line expressing the separase sensor and the inducible separase$^{PM2}$.

Silke Müller (Screening Center, University of Konstanz) greatly contributed to perform the HTS and subsequent data analysis.

Christian Dietz and Patrick Winter (AG Berthold, University of Konstanz & KNIME) greatly contributed to establish the image analysis algorithm in KNIME.

Matthias Frese (AG Marx, University of Konstanz) synthesized the lead compound SIC5 and all tested derivates (SIC5-1 to SIC5-6).

Martina Baack generated the stable HeLa 8.01.2926 cell line expressing the separase sensor.

Melanie Walter purified cyclin-B1$^{\Delta 90}$ for activation of reconstituted separase.

Andreas Gericke tested the catalytic activity of separase$^{\Delta SLR}$ in HeLa cells during his master thesis in the lab of Thomas Mayer.

## 8.6 Acknowledgements

First and foremost, I would like to express my deepest gratitude to my supervisor Thomas Mayer for offering me a PhD position in his lab, where I had the great pleasure to work on this interdisciplinary and exciting small molecule project. I am truly grateful for your interest in this work, your constant support, your scientific guidance and the freedom to develop my own ideas. Thank you for being the most caring mentor I had the pleasure of working with so far. It is incredible how you always make time for your PhD students to fix any given problem there might be. You always seem to find the right way to motivate people to do great science! Please, stay the way you are!

I am very grateful to Martin Scheffner and Andreas Marx for being part of my thesis committee. Further I like to thank Christof Hauck and again Andreas Marx for being members of my KoRS-CB graduate school thesis committee and their scientific input.

I am thankful to the graduate school KoRS-CB for funding and for providing a creative, scientific and engaging environment across various research groups of different fields at the university of Konstanz, which made it easy to start collaborations within the campus.

I would like to thank Olaf Stemmann and Susanne Hellmuth for generating the screening cell line, for sharing plasmids and antibodies and for hosting me in their lab to learn the separase preparation.

I would like to thank Silke Müller at the High-Throughput Screening Core Facility for realizing and establishing the automation of the screening assay, solving all technical problems with the liquid handling robots and for help and support during the analysis of the primary data. Furthermore I thank Annegret Schramm, Christian Dietz and Patrick Winter for the competent help with establishing the automated image analysis in ImageJ and for translating and integrating this algorithm to KNIME.

A huge thanks to Matthias Frese, who synthesized SIC5 and all derivates. It's nice to have such a talented chemist just next door.

I am truly grateful to all current and former members of the TUM lab for the helpful scientific discussions, positive work atmosphere, fun canoeing lab outings, thousands of coffee breaks, after work beers, our monthly Stammtisch and your moral support when experiments failed or science did not cooperate the way I wanted.

A thousand thanks to Anna, Andi and Julia for introducing a chemist into molecular biology methods and for sharing your experience with me. Surely, I dodged a lot of beginners mistakes due to your help.
I especially want to thank Beata for tons of competent advice in the lab, for many stunning hikes in the swiss alps, for building ice igloos or snowmen, for great cocktail evenings, for your delicious dinners and for always having a sympathetic ear for me. I could go on and on with this list but it would not cover everything. One thing is certain: It would have not been the same without you in the lab. THANK YOU SO MUCH!
I wish to thank Conny, Konsti, Lena and Marc for reviving my passion for indoor-climbing, for cycling during day or night, for making irresistible cocktails and for keeping me sane during the writing period.
A big thank you goes to Martina and Melanie, who make sure everything runs smoothly in the lab and no one has to worry about general buffer preparation or fight with suppliers or the purchase office when ordering things. Many thanks to Tina, your organizational skills helped me to sort the bureaucratic madness.
I would also like to thank all other members of the lab, Anja, Camilla, Chris, Colin, Elijah, Franzi, Inken, Hiba, Ilinca, Janina, Johanna, Katharina, Lucia, Martin, Norris, Patrick, Rebecca, Rolf, Sascha, Saurav, Stefan and Trusha for helpful comments, suggestions, advice and a lot of fun in the lab and beyond.
I would like to mention all students I had the opportunity to supervise during their VTKs, bachelor or master thesis. Thanks to Alex, Andreas, Conner, Ecem, Fabian, Nadine, Niko, Lea, Lena, Lukas, Özge, Patrick B, Patrick W, Selina, Tatjana and Vera, it was a great experience and hopefully I could spark or increase the scientific interest for your future.

A huge thank you to the “Old Fashioned Group”, Lena, Griseldis, Tanja and Timo, for hosting exceptional dinners either at home or in the common center. But always with style, old fashioned cocktails and once with calzone with a hint of fire department 😉

I would like to thank Alex Julier, Fabian Offensperger, Kathrin Götz and Franzi Müller for scientific and non-scientific discussions and for organizing and joining “Fabi’s Hütte”. It is always something to look forward to. Alex, thank you so much for your moral support during my writing block!

Thanks to all my friends at home and all over the place. Thank you for supporting me, especially during the writing period. This thesis would have not been possible without your support!

Last but not least, my biggest gratitude goes to my parents and my late grandmother who are always supporting me in any way possible. Thank you so much for always being there for me!